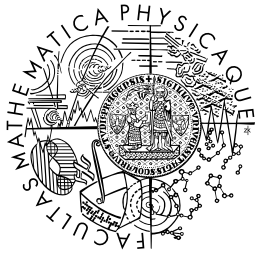

FACULTY
OF MATHEMATICS
AND PHYSICS
Charles University

MASTER THESIS

Kateřina Charvátová

Excited state dynamics in fluorescence-detected transient absorption

Institute of Physics of Charles University

Supervisor of the master thesis: RNDr. Pavel Malý, Ph.D.
Study programme: Biophysics and Chemical Physics
Study branch: FBCHPT

Prague 2024

I declare that I carried out this master thesis independently, and only with the cited sources, literature and other professional sources. It has not been used to obtain another or the same degree.

I understand that my work relates to the rights and obligations under the Act No. 121/2000 Sb., the Copyright Act, as amended, in particular the fact that the Charles University has the right to conclude a license agreement on the use of this work as a school work pursuant to Section 60 subsection 1 of the Copyright Act.

In ..... date ....

Author's signature

Foremost, I express my sincere appreciation to my supervisor, RNDr. Pavel Malý, Ph.D., for continual help and optimistic guidance. I would also like to extend my gratitude to doc. Mgr. Tomáš Mančal, Ph.D., for consultations and assistance with the Quantarhei library. I also wish to acknowledge the other teachers at the MFF UK, who prepared us perfectly for the master's studies.

Special thanks belong to my family and friends, who supported me through my ups and downs while writing this thesis.

Title: Excited state dynamics in fluorescence-detected transient absorption

Author: Kateřina Charvátová

Institute: Institute of Physics of Charles University

Supervisor: RNDr. Pavel Malý, Ph.D., Institute of Physics of Charles University

Abstract: The fluorescence-detected transient absorption (F-PP) technique has recently gained significant attention within the spectroscopic community for its numerous advantages. However, several aspects of these spectra remain unexplored. In this thesis, we investigated some of them, including the characterization of F-PP spectra for negative times. Our objective was to use these spectra to suppress incoherent mixing, a pursuit that ultimately proved almost impossible. Additionally, we examined the influence of pulse chirp on F-PP spectra. We proved that it does not change the main behaviour in longer times and only shifts the dynamic of a particular frequency according to the time delay caused by the chirp. Furthermore, we discussed its influence on the shape of the spectra for pulse overlap.

Keywords: fluorescence ultrafast spectroscopy nonlinear spectroscopy excitons

Contents

Introduction

Spectroscopic methods are invaluable for studying various properties of molecules, each providing slightly different information. Absorption measurements allow us to determine the energy levels of a molecule, while fluorescence excitation spectra show how different excitation frequencies contribute to fluorescence at a fixed frequency (this is described by Parson [2007] in detail). Conversely, fluorescence emission spectra involve fixing the excitation frequency and measuring fluorescence intensity at various frequencies. To determine the structure of vibration levels, we can measure infrared spectra. We can use IR spectra catalogues and further techniques to process the data to reveal which functional groups are represented in the sample and estimate which molecule it is. This already gives us a good idea of our sample but does not allow us to capture fast processes taking place in it.

To observe quick dynamics in excited states, we have to study the response of higher order and find out change in linear spectra. For instance, the pump-probe is a very often used transient absorption spectroscopy method. There, we are isolating the 3rd-order response. At first, we let our sample interact with the excitation pulse (pump), and then after waiting time T, we detect a change in absorption of the probe pulse caused by system's interaction with the pump and subsequent dynamics. To obtain the change in absorption, we subtract the unpumped spectrum for each time T from the pumped spectrum measured by the probe. Spectral resolution is provided by detection using a spectrophotometer, which records the intensity of the individual frequencies contained in the probe, which has passed through the sample.

Molecules are excited by the pump, and absorption of the probe is reduced due to the reduced ground state population. On the other hand, excited state absorption appears. In waiting time T, populations of excited states are decaying at some rate into the ground state, which reduces the difference between the pumped and unpumped spectrum. Transport from one excited state into another will be reflected as an increase in absorption of the first one and a decrease in absorption of the other. Further description of experimental design and signal characteristics of pump-probe could be found, for example, in my bachelor's thesis Charvátová [2022].

Fluorescence-detected pump-probe spectroscopy (F-PP) is a new method introduced by Malý and Brixner [2021], which modifies the conventional pump-probe technique. Instead of using a probe to measure the absorption change, we let the pump and probe interact with the sample and observe the fluorescence. The sample interacts with the pump and after waiting time T_{Pu}, two probe pulses with time delay T_{Pr} between them are used to determine the change in the fluorescence excitation spectrum (see picture 1). The fluorescence signal is then collected by a detector for a long time after the last pulse. Thus, we lose information about the time dependence of the signal intensity and its spectral properties. The time dependence can be obtained, for example, by using time-correlated single photon counting.

Subsequently, we perform a (discrete) Fourier transform over the variable T_{Pr},

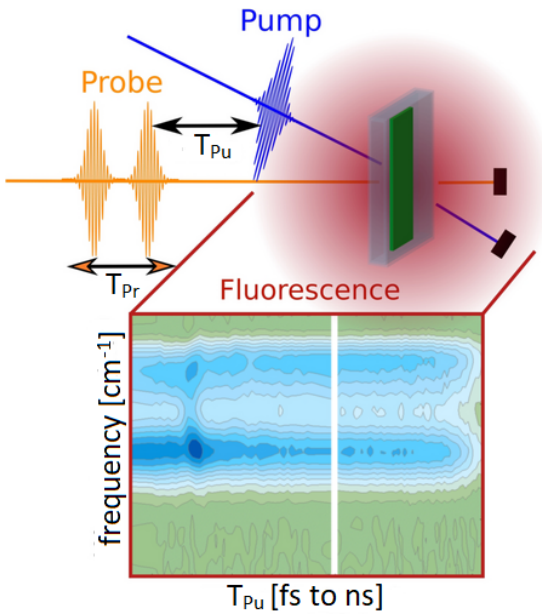

Figure 1: Fluorescence-detected pump-probe spectroscopy diagram (edited image was taken from an article by Malý and Brixner [2021]). Sample (green rectangle) interacts with one pump pulse (blue) and after time T_{Pu} with two probes (orange) distant from each other T_{Pr}. We measure a change in fluorescence signal (red glow in the picture) caused by various T_{Pu} and T_{Pr}. Fourier transform over time T_{Pr} gives us the F-PP spectrum.

which gives us F-PP spectrum dependent on frequency ω (retrieved from the Fourier transform) and on time T_{Pu} between pump and probe. Again, we must subtract the unpumped spectrum from the pumped one to obtain the change.

This approach offers many advantages and options. It is convenient to use this method for highly scattering samples, for which there is a problem with scattering the pulses and losing signal in the pump-probe. Moreover, according to Malý and Brixner [2021], F-PP is more sensitive, enabling us to use fewer measuring points, which is beneficial for samples with low photostability. It is also possible to combine this method with a microscope, as Fersch et al. [2023] show, which provides images where each region has its own F-PP spectrum. This allows us to examine complex organic structures without more significant damage in detail.

In further advancing the F-PP method, this thesis aims to investigate the following properties:

- reduction in the visibility of dynamics due to exciton-exciton annihilation (see section 3.3 about incoherent mixing)
- behaviour of the signal for negative times T (the sample interacts at first with probes and then with pump, see section 3.2)
- use of the signal from negative times to improve visibility of dynamics, which is reduced due to exciton-exciton annihilation
- signal behaviour around zero - pulse overlap (section 3.4)
- effect of a pulse chirp on the spectrum (subsection 3.5.2)

1. Theoretical introduction to used methods

In this chapter, we will discuss the main methods we usually use to describe the molecular system's dynamics during its interaction with light.

1.1 Master equation

The evolution of the density matrix $\hat{W}(t)$ of the system can be described by the Liouville von Neumann equation

$$\frac{\partial \hat{W}(t)}{\partial t} = -\frac{i}{\hbar}[\hat{H}, \hat{W}(t)] - \frac{i}{\hbar}[\hat{H}_\perp, \hat{W}(t)] + \frac{i}{\hbar}[\hat{\vec{\mu}} \cdot \hat{\vec{E}}, \hat{W}(t)] \tag{1.1}$$

We have used dipole approximation, which allows us to use the matter-field interaction operator in a form $\hat{\vec{\mu}} \cdot \hat{\vec{E}}$ (this is derived, for example, in a book by Valkunas et al. [2013]). This approximation is justifiable because our systems are at most about $\sim 10\,\mathrm{nm}$ in size, and the wavelength of used light is on the order of the hundreds of nanometres.

$\hat{H}$ is Hamiltonian for the whole system, including the molecular system, its environment, further referred to as bath, and their interaction. System-bath interaction is responsible for system's dynamics and is crucial in the whole problematics. Properties of the bath, for example, determine absorption line shape, as will be shown in section 1.4.

$\hat{\vec{\mu}}$ denotes transition dipole moment operator, which mediates transition between initial and final state. For two level system, we have

$$\hat{\vec{\mu}} = \mu_{eg}|e\rangle\langle g| + \mu_{ge}|g\rangle\langle e|, \tag{1.2}$$

where μ_{eg} is oscillator strength of particular transition. This parameter determines how strong will be this transition and whether it is allowed or not (in this case, μ_{eg} is really small).

We will use semiclassical description with classical coherent electric field. Thus, equation 1.1 becomes

$$\frac{\partial \hat{W}(t)}{\partial t} = -\frac{i}{\hbar}[\hat{H}, \hat{W}(t)] + \frac{i}{\hbar}[\hat{\vec{\mu}}, \hat{W}(t)] \cdot \vec{E}(t) \tag{1.3}$$

1.2 Multiparticle basis

It is convenient to use exciton states (multiparticle basis) to describe a system with N weakly interacting molecules. Consider each molecule as a two-level system characterized by energies ϵ_g^i and ϵ_e^i. Here, there is one basis vector for the situation when all molecules are in the ground state

$$|g\rangle = |g_1 g_2 ... g_N\rangle = \Pi_{i=1}^N |g_i\rangle. \tag{1.4}$$

We have N states, where one molecule is excited $|e_1 g_2 ... g_N\rangle$,$|g_1 e_2 ... g_N\rangle$,... State, where the i-th molecule is excited, corresponds to the eigenvector

$$|e_i\rangle = |g_1 g_2 ... e_i .. g_N\rangle = \prod_{j(\neq i)}^{N} |g_j\rangle |e_i\rangle, \tag{1.5}$$

with energy

$$E_i = \sum_{j(\neq i)} \epsilon_g^j + \epsilon_e^i \tag{1.6}$$

There are $\binom{N}{k}$ unique k-excitonic states. Excitonic state, where l,...,m-th molecule is excited, could be described as:

$$|g_1 g_2 ... e_l ... e_m ... g_N\rangle = \prod_{j(\neq l ... \neq m)}^{N} |g_j\rangle |e_l\rangle ... |e_m\rangle \tag{1.7}$$

with energy

$$E_{l...m} = \sum_{j(\neq l, ... \neq m)} \epsilon_g^j + \epsilon_e^l + ... + \epsilon_e^m \tag{1.8}$$

1.3 Perturbative approach to the interaction of the molecular system with light

The Liouville-von Neumann equation (1.3) can be solved in the interaction picture with respect to the Hamiltonian $\hat{H}$ of the entire system, including bath (this was described in detail by Valkunas et al. [2013] or Malý [2012]):

$$\frac{d}{dt}\hat{W}^{(I)}(t) = i\check{U_0}^{\dagger}(t)\check{\mathcal{V}}\check{U_0}(t)\hat{W}^{(I)}E(t), \tag{1.9}$$

$\check{U_0}$ is evolution superoperator - operator, which acts on space of linear operators. It is defined as $\check{U_0} = e^{-i\check{\mathcal{L}}t}$, where $\check{\mathcal{L}}$ denotes another superoperator $\check{\mathcal{L}}\bullet = \frac{1}{\hbar}[\hat{H}, \bullet]$. There, $\bullet$ represents any operator. Consequently, $\check{U_0}^{\dagger}(t)$ is Hermitian conjugate of evolution superoperator. $\check{\mathcal{V}}$ is a superoperator, which could be defined as $\check{\mathcal{V}}\bullet = \frac{i}{\hbar}[\hat{\mu}, \bullet]$. $\hat{W}^{(I)} = \check{U_0}(t)\hat{W}$ is density matrix in interaction picture.

We can directly integrate the equation. The solution remains dependent on its own. Iteratively, we can obtain any order of the response (the order is determined by the number of interactions with the electric field). Subsequently, we need to revert from the interaction picture by applying the evolution superoperator of the system to the entire equation. Finally, the reduced density matrix is calculated by tracing the equation through all degrees of freedom of the bath $\hat{\rho}(t) = tr_B\left(\hat{W}(t)\right)$.

In fluorescence-detected pump-probe, we observe a 4th-order response

$$\begin{aligned}\hat{\rho}^{(4)}(t) = \iiiint dt_4 dt_3 dt_2 dt_1 R^{(4)}(t_1, t_2, t_3, t_4) E(t - t_4) \\ E(t - t_4 - t_3) E(t - t_4 - t_3 - t_2) E(t - t_4 - t_3 - t_2 - t_1)\end{aligned} \tag{1.10}$$

where

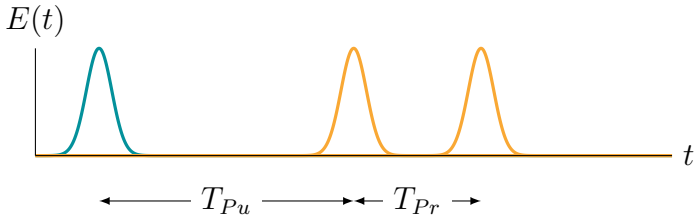

Figure 1.1: Pulses used in the experiment. We change time delay T_{Pu} between pump (blue) and probe (orange) and T_{Pr} between probes during F-PP experiment.

$$R^{(4)}(t_1, t_2, t_3, t_4) = tr_B\{\check{U}_0(t_4)\check{\mathcal{V}}\check{U}_0(t_3)\check{\mathcal{V}}\check{U}_0(t_2)\check{\mathcal{V}}\check{U}_0(t_1)\check{\mathcal{V}}\hat{\rho}_0\} \tag{1.11}$$

is a response function of the system. Time-dependent reduced density matrix could be thus shown as a convolution between electric field and the system's response function.

As was mentioned, superoperator $\check{\mathcal{V}}$ mediates the matter-field interaction $\check{\mathcal{V}}\hat{\rho} = \frac{i}{\hbar}[\hat{\mu}, \hat{\rho}]$. We have four superoperators of this kind, each producing two terms because of the commutator; thus, we get eight terms in total. Four of them are unique, and the other four are corresponding hermitian conjugations. We will later describe these terms using Feynman's diagrams.

We can see that we have somehow lost the scalar product, which was included in $\vec{\hat{\mu}} \cdot \vec{E}(t)$. Formally, according to Schott et al. [2014], we can get rid of this dependence on orientations of molecular transition dipole moments and electric fields polarization by orientational averaging. However, we can also measure under so-called magic angle between vectors of polarizations of pump and probe electric intensity, which removes the dependence too. This is not necessary in our simulations, because our transition dipole moments are almost parallel.

Now, we will describe the electric field we use in the equation 1.10. The sample interacts with the electric field of all used pulses. $E(t)$ can be, as is also mentioned in supporting information of article by Malý and Brixner [2021], written as

$$\begin{aligned} E(t) = {} & E_0^{Pu}(t)e^{i\Phi_{Pu} - i\omega_0^{Pu}t} + E_0^{Pr}(t - T_{Pu})e^{i\Phi_{Pr1} - i\omega_0^{Pr}(t - T_{Pu})} \\ & + E_0^{Pr}(t - T_{Pu} - T_{Pr})e^{i\Phi_{Pr2} - i\omega_0^{Pr}(t - T_{Pu} - T_{Pr})} + c.c. \end{aligned} \tag{1.12}$$

There, $E_0^i(t')$ denotes time dependent envelope of particular pulse with mean frequency ω_0^i and phase Φ_i. From there we can see that the centres of interacting pulses arrive to the sample location as follows: pump in time $t = 0$, first probe in time T_{Pu} and the second probe at $T_{Pu} + T_{Pr}$ as is shown in the picture 1.1. For sufficiently small values of T_{Pu} (depending on the pulse width), pulse overlap occurs. Hence, within the perturbation theory, we can get interactions in the wrong order that contribute to a very complicated signal shape around time zero. We did not write any dependence on wave vectors of the incident lights $\vec{k}$. This is because we observe the fluorescence signal, which is omnidirectional by its nature.

Spatial dependence is, thus, not important for us now. By inserting the equation 1.1 into equation 1.10, we will receive many terms oscillating on frequencies

$$\omega = \sum_i \pm\omega_i. \tag{1.13}$$

If the pulse frequencies are added with a positive sign, we get a fast oscillating term, which will contribute very little to the signal after integration and can therefore be neglected, as was described e.g. by Malý [2012]. This is called rotating wave approximation (RWA).

In similar way, each term has a phase as

$$\Phi_s = \sum_i \pm\Phi_i. \tag{1.14}$$

In F-PP, we observe signals with phase

$$\Phi_s = -\Phi_{Pu} + \Phi_{Pu} - \Phi_{Pr1} + \Phi_{Pr2}. \tag{1.15}$$

This option also corresponds to the subtraction of frequencies in equation 1.13 to zero. By appropriately choosing the phases, we can select detected signals. We can do a batch of measurements with different phases of the pulses and finally sum the signals. Some pathways will be cancelled, and this leads to isolating the desired signals. This method is called phase cycling and is often used. We will discuss this further in the section 1.6.

For very short pulses, we can eliminate convolutions in equation 1.10 (approximating the pulse envelope with a delta function), which greatly simplifies the calculation.

Fluorescence signal depends on population of first excited state n and its radiative rate K_{Fl_n}. We can calculate F-PP signal as

$$\text{F-PP}(t) = Tr\left(\sum_n |n\rangle K_{Fl_n}\langle n|\rho^{(4)}(t)\right) \tag{1.16}$$

As is described by Mukamel [1995], we have a special diagram for each term from the response function (see picture 1.2). Each row represents some state of the system, which has been evolving for some time t_x; between each of any two neighbouring rows, there is interaction with one of the pulses depicted by an arrow. If the arrow is on the left side, the interaction with the field also comes from the left and vice versa. Interaction from the right has a negative sign due to the commutator. Consequently, a diagram with an odd number of interactions/arrows from the right will have a negative sign.

In the picture 1.2, arrows for pump interaction are blue. The time between both interactions is $\tau = 0$. In T_{Pu} after pump comes first probe (orange arrow), after time T_{Pr} second probe pulse arrives. Only diagrams that end in an excited state are part of the detected signal. Two wavy red arrows at the top of each diagram represent fluorescence emission into the ground state in time t.

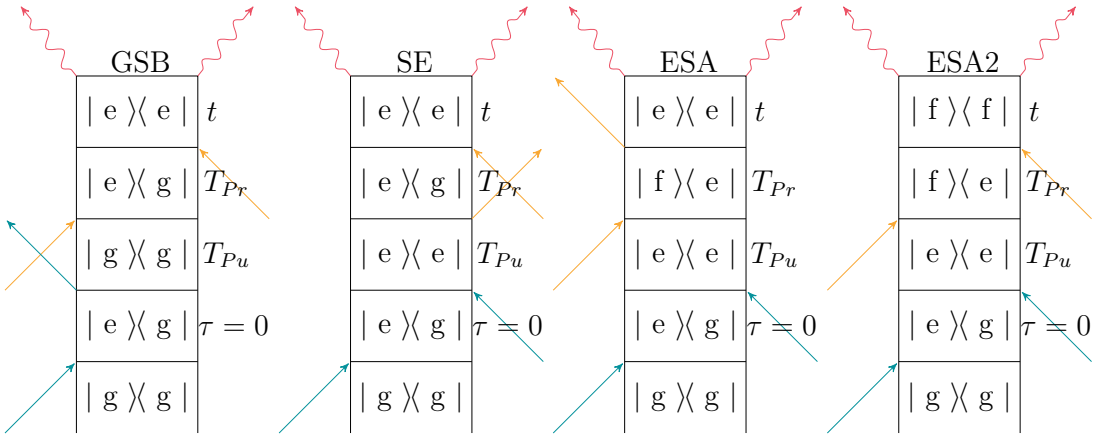

Figure 1.2: Main Liouville pathways for F-PP in Feynman diagrams (taken from Malý and Brixner [2021]) depict four types of contributions to the signal in the perturbative description of the system's interaction with the pump pulse (blue arrows) and probes (orange arrows). Red arrows feature fluorescence signal. The system is at the beginning in the ground state $|g\rangle\langle g|$. The letter e denotes an excited state of the system, and f is a higher excited state (two-excitonic state or single-excitonic state of higher energy). We can see diagrams for ground-state bleach (GSB), stimulated emission (SE), excited-state absorption (ESA and ESA 2).

There are four special types of these diagrams, as mentioned above. The first one, ground state bleach (GSB), is in the ground state in time T_{Pu} between interaction with the pump and the first probe. Other diagrams have all excited states during this waiting time. In the case of stimulated emission (SE), the first probe stimulates emission from the excited state, which leads to coherence between the ground and the excited state. There are two excited state absorption diagrams. The first probe excites the system into a higher excited state f in both of them. For ESA, the system is returned to the first excited state by its interaction with the second probe. ESA 2 pathway ends in a higher excited state; therefore, it could contribute with two photons instead of only one, as do other pathways (see section 1.5). Furthermore, it is the only diagram with a positive sign.

The diagrams could be divided into two groups - self-population pathways, where there is interaction with only one molecule and cross-population diagrams, where the field interact with two different molecules.

1.4 Line-shape function

In order to get the F-PP spectrum, we need to calculate the response function in equation 1.11. For this, we need to know the exact shape of evolution superoperator of the system, which we can obtain by solving the following Liouville von Neumann equation:

$$\frac{\partial \hat{W}(t)}{\partial t} = -\frac{i}{\hbar}[\hat{H}_S, \hat{W}(t)] - \frac{i}{\hbar}[\hat{H}_B, \hat{W}(t)] - \frac{i}{\hbar}[H_{S-B}, \hat{W}(t)] \tag{1.17}$$

where H_{S-B} is interaction between system (our molecule or molecular system

with hamiltonian H_S) and bath (environment of the system, here approximated by harmonic oscillators).

Hamiltonian for two level system and its bath could be written as

$$H = \underbrace{\epsilon_g|g\rangle\langle g| + (\epsilon_e + \lambda)|e\rangle\langle e|}_{H_S} + \underbrace{\sum_{n=1}^{N} \frac{\hbar\omega_n}{2}\left(p_n^2 + q_n^2\right)}_{H_B} - \underbrace{\sum_{n=1}^{N} \hbar\omega_n d_n q_n |e\rangle\langle e|}_{H_{S-B}} \tag{1.18}$$

λ is reorganization energy, corresponding to the difference between the absorption energy and the energy difference of the e and g levels. This difference arises because the motion of the nuclei is too slow compared to the absorption process. Thus, the excitation occurs in a higher vibrational state corresponding to the excited state (vertical absorption). The same situation occurs for relaxation, which gives us the value of Stokes shift as 2λ. q and p are in order canonical coordinate and momentum. d is distance of minima of potentials of ground and excited states in configurational coordinate q.

As in the case of interaction with the field, we will use the interaction picture to solve the equation. According to Mukamel [1995], after some approximations we will obtain an expression for time dependent element of reduced density matrix between excited and ground state, using evolution superoperator $\check{U}_0(t)$ of the system defined above, as follows

$$\rho_{eg}(t) = \langle e|\check{U}_0(t)\hat{\rho}(0)|g\rangle = e^{-g(t)-i\omega_{eg}t}\rho_{eg}(0). \tag{1.19}$$

$g(t)$ is so-called line shape function, which is defined as

$$g(t) = \frac{1}{\hbar^2}\int_0^t d\tau \int_0^\tau d\tau' C(\tau - \tau'), \tag{1.20}$$

where C(t) is correlation function of the bath

$$C(t) = tr_B\left(\hat{U}_B^\dagger(t)\Delta\hat{V}\hat{U}_B(t)\Delta\hat{V}\hat{\omega}_{eq}\right). \tag{1.21}$$

$\hat{\omega}_{eq}$ is density matrix for bath in equilibrium and $\hat{U}_B(t) = e^{\frac{i}{\hbar}\hat{H}_B}$ is its evolution operator. $\Delta\hat{V} = \sum_{n=1}^{N}\hbar\omega_n d_n q_n$ is part of the system-bath interaction Hamiltonian belonging to the bath. The correlation function describes the complex behaviour of the bath and how fast and how much the bath changes over time. Fortunately, the correlation function could be obtained experimentally, as was described by de Boeij et al. [1996]. For fast oscillations, as was mentioned by May and Kühn [2023], the correlation function could be approximated as $\Gamma_{eg}\delta(t)$, which gives us $g(t) = \Gamma_{eg}t$ and Lorentz line shape $G_{eg}(\omega) \sim \frac{\Gamma_{eg}}{\Gamma_{eg}^2 + (\omega - \omega eg)^2}$. Further, we will denote the line shape of the excitation spectrum as $G_{eg}(\omega)$.

1.5 Incoherent mixing

Exciton-exciton annihilation (EEA) denotes a phenomenon wherein two excitons coexisting within a sample interact, resulting in the elimination of all but one as described by Bruschi et al. [2023]. Excess energy released by the relaxation of

at least one of the excitons to the ground state is used to excite the remaining excited molecule into a higher excited state. According to Kasha [1950], the emitting level of a given multiplicity is the lowest excited level of that multiplicity. Consequently, the molecule in question will undergo radiationless de-excitation (internal conversion) to reach the lowest excited state, followed by radiative relaxation, resulting in a detected fluorescence signal. The fluorescence response is accumulated in the detector long after the final pulse. Therefore, the time delay caused by the internal conversion rate does not affect the detected signal. Unless we use time-correlated single photon counting or another method to obtain time-dependence of the events subsequent to the last interaction with the pulse, exciton-exciton annihilation could be described only as an additional, nonradiant, relaxation channel for the multi-excitonic states.

Unless fluorescence rate constant K_{recomb} is much quicker than the rate constant of EEA K_{annih}, exciton-exciton annihilation cannot be neglected. For a system where $K_{recomb} \gg K_{annih}$, both excited molecules in a two-excitonic state will relax radiatively and contribute with two photons to the signal. A decrease in the signal due to exciton-exciton annihilation could be neglected. On the other hand, for $K_{annih} \gg K_{recomb}$ for a vast majority of two-excitonic states, exciton-exciton annihilation will nonradiatively deexcitate one of the molecules, so only one of them contributes with one photon to the signal. Depending on the ratio between K_{recomb} and K_{annih}, a two-excitonic state contributes on average with $1 \leq N \leq 2$ photons.

Without EEA, ESA 2 pathways are eliminated with ESA and GSB^c cross-population pathways (pulses interact with two different molecules). Therefore, only SE and GSB^s self-populations (pulses interact with only one molecule) contribute to the signal. The signal of a sample with two different, non-interacting molecules A and B is, thus, the same as the sum of signals of those two molecules (see figure A.5). Conversely, if EEA is non-negligible, each ESA 2 pathway contributes with fewer than two photons; thus, the aforementioned cancellation of cross-population pathways remains incomplete, allowing their contribution to the signal. As a result, the EEA mixes signals from otherwise independent molecules according to Malý and Mančal [2018] or Bolzonello et al. [2023].

Provided that each ESA 2 pathway contributes with exactly one photon, ESA 2 and ESA pathways cancel each other. GSB signal is increased by cross-population GSB^c signal. Because of this, the GSB signal is much stronger than the signal belonging to SE. Bolzonello et al. [2023] also calculated, that the ratio between stimulated emission and ground state bleach signal decreases with growing number of molecules N in the sample as

$$\frac{SE}{GSB} = \frac{SE}{GSB^s + GSB^c} = \frac{N}{N + N(N-1)} = \frac{1}{N}. \tag{1.22}$$

For each molecule we have one SE diagram, the same holds for self-population GSB^s. But there are $N(N-1)$ cross-population GSB^c diagrams, because for each of N molecules, we have $N-1$ options to choose the second one to form the diagram.

To study SE properly, we should eliminate the additional GSB^c signal, which gives us a strong, unwanted background. It is also justified to use only one

exciton approach because two excitons' states are hardly observable. In F-PP spectroscopy, at most two excitons can be created because it is a 4-th order response theory (two interactions are needed to create one exciton).

1.6 Phase cycling

To isolate the desired nonlinear signal, we can cancel other pathways by cyclically changing the phases of used pulses (phase cycling) as was described in detail by Tan [2008].

The phase of the signal field is the linear combination of the phases of incident pulses. Thus, by changing them, we can change the phase of the signal field (see equation 1.15). In F-PP and F-2DES (see Figure 1.3), we are interested in pathways ending in populations, which means that there must be an equal number of interactions from left and right, which gives us the condition

$$\alpha + \beta + \gamma + \delta = 0. \tag{1.23}$$

There, the Greek symbol denotes the number of interactions with the respective pulse. A negative sign means interaction from the right, positive from the left. If we have one interaction with the first pump pulse from the left and one from the right, we get $\alpha = 0$.

From this, we can easily conclude that different pathways have different total phases $\Phi_S = \alpha\Phi_{Pu1} + \beta\Phi_{Pu2} + \gamma\Phi_{Pr1} + \delta\Phi_{Pr2}$. The signal is composed of responses with various $(\alpha, \beta, \gamma, \delta)$. To isolate the signal with the desired signature $(\alpha, \beta, \gamma, \delta)$, we will perform a discrete Fourier transform (our variables will be phases). According to Tan [2008] and Malý et al. [2020] we can obtain specific contribution $I'_{Fl}(\beta, \gamma, T_{Pu}, T_{Pr})$ from the total fluorescence signal $I_{Fl}(l \cdot \Delta\Phi_{21}, m \cdot \Delta\Phi_{31}, T_{Pu}, T_{Pr})$ as

$$\begin{aligned} &I'_{Fl}(\beta, \gamma, T_{Pu}, T_{Pr}) = \\ &= \frac{1}{LM} \sum_{m=0}^{M-1} \sum_{l=0}^{L-1} I_{Fl}(l \cdot \Delta\Phi_{21}, m \cdot \Delta\Phi_{31}, T_{Pu}, T_{Pr}) e^{-il\beta\Delta\Phi_{21}} e^{-im\gamma\Delta\Phi_{31}} \end{aligned} \tag{1.24}$$

where $\Delta\Phi_{21} = \frac{2\pi}{L}$ and $\Delta\Phi_{31} = \frac{2\pi}{M}$. So in the l-th step we have $\Phi_2 - \Phi_1 = l \cdot \frac{2\pi}{L}$. We can choose phase of the pump as $\Phi_1 = 0$, so $\Phi_{21} = \Phi_2$.

For example, by using the following sequence $(\Phi_{Pu_1}, \Phi_{Pu_2}, \Phi_1, \Phi_2) = (0, 0, 0, 0)$ and $(0, \pi, 0, 0)$ the 4-th order response will disappear, because we get 1 and -1 from the phase factor for different phases and the contributions cancel each other. Also, the pathways describing second-order response for the interaction with the pump pulse will cancel due to phase cycling. Only interaction with probes will remain unchanged, and we will obtain the excitation spectrum.

1.7 Fluorescence-detected two-dimensional electronic spectroscopy

Fluorescence-detected two-dimensional electronic spectroscopy (F-2DES) is another method using fluorescence signal. The main difference between F-PP and

F-2DES is that for F-2DES, we have two pump pulses with time delay τ. For F-PP the system interacted twice with the same pump (practically we set $\tau = 0$). Feynman diagrams are the same for F-2DES as for F-PP (see figure 1.2) with an exception to mentioned τ, which takes on different values (not only $\tau = 0$). In the F-2DES experiment, we measure signal for not only different T_{Pr} and T_{Pu}, but also for τ. The Fourier transform from time to frequency variable is now performed for T_{Pr} and τ. Kühn et al. [2019] described that this provides us excitation frequency axis, in the thesis denoted as ω_τ, and probing frequency axis (for 2DES detection frequency axis), further denoted as $\omega_{T_{Pu}}$.

Significantly simplified, for a system of two molecules A and B with different energies, we can divide the F-2DES diagram into four quadrants. One axis shows with which molecule (A or B) the pump pulses interacted, and the second axis with which molecule probes interacted (see figure 1.3). The contribution is called self-population if all pulses interact with only one molecule. On the other hand, cross-population contributions correspond to pathways, where pulses interact with both A and B molecules. Of course, because the excitation spectrum has some width, there are not only points but circles, whose intensity decreases with increasing radius (as the intensity in the excitation spectrum decreases for frequencies far from the mean frequency). Moreover, the shape of the peaks in F-2DES is often elongated and change in time, as described by Bruschi et al. [2022]. This is clearly visible in the simulated and experimentally obtained F-2DES spectra by Kunsel et al. [2018].

For each time T_{Pu}, we have a different diagram (the amplitude of the circles is evolving in time). To obtain some time-dependent curve, we must compare corresponding points in all diagrams of different T_{Pu}. Because we are primarily interested in, for example, the dynamics of a population of the excited state of molecule A, not in particular frequencies, it is common to integrate signals from the whole quadrant and determine the time evolution of this quantity.

F-PP spectrum could be obtained from F-2DES by integrating over variable ω_τ. We can see in figures A.2, A.1, A.3 and A.4 that the difference between F-PP and F-2DES spectra is only excess term $G_{eg}(\omega_\tau)$ which gives us additional information about interaction with pump pulses.

1.8 Sign convention

Like Malý and Brixner [2021], in the whole thesis, we are using the transient absorption convention of negative signals, which corresponds to reduce in fluorescence signal caused by the probe pulse. This means that GSB, SE and ESA contributions have negative sign and ESA 2 has positive sign. This is opposite to the sign convention used by the F-2DES community.

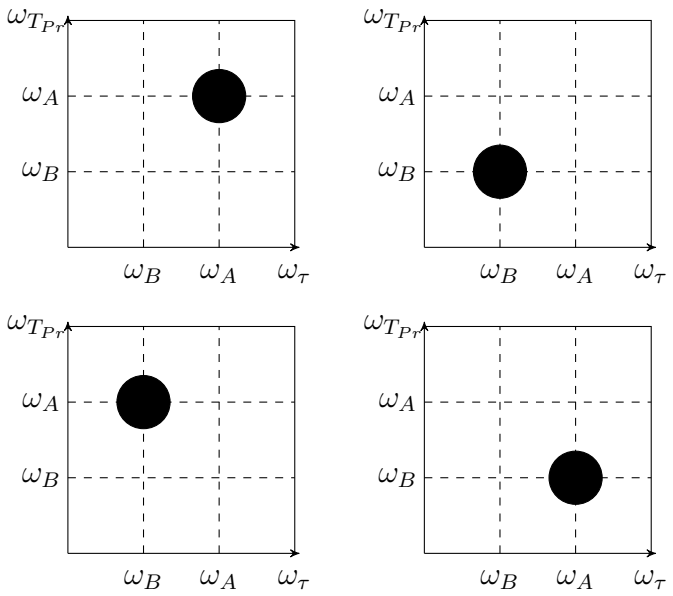

Figure 1.3: Illustration of four basic contributions to F-2DES spectra. The first row contains self-population contributions. In the first one, all pulses interact with molecule A. On the contrary, the second diagram in the first row corresponds to interaction with only molecule B. In the second row, cross-population contributions can be found. In the first diagram in the second row, pumps interact with molecule B and probes with molecule A. For the last picture, the situation is opposite - pumps interact with molecule A and probes with molecule B. F-PP spectra could be obtained by integration over ω_τ, diagrams in the left column corresponds thus to F-PP signal from molecule A, the right column contributes to F-PP signal from molecule B.

2. Computational methods

2.1 Numerical approach in Quantarhei

Part of the master thesis involved integrating the fluorescence-detected transient absorption spectroscopy method into the Quantarhei library in Python programming language, a tool designed by Mančal [2020] for simulating spectroscopic experiments on molecular quantum systems.

All simulations presented in this work were performed in this new program, which uses a numerical approach based on the direct solution of a special form of the Liouville von Neumann equation:

$$\frac{\partial \rho}{\partial t} = -\frac{i}{\hbar}[H_s, \rho(t)] - \mathcal{R}\rho(t) + \frac{i}{\hbar}[\hat{\vec{\mu}} \cdot \vec{E}, \rho(t)], \tag{2.1}$$

where $\mathcal{R}$ is relaxation tensor in Lindblad form (see Valkunas et al. [2013]). This tensor was constructed from input data such as rates of all transitions and dephasing constants. Nevertheless, Quantarhei enables the use of pre-defined Redfield or Förster tensor.

The concept of a multiparticle basis is used (see section 1.2). Solving the equation 2.1, we obtain a time-dependent reduced density matrix $\rho(t, T_{Pr}, T_{Pu})$, with which we can calculate fluorescence signal using equation 1.16. Consequently, to obtain F-PP spectrum, we perform a discrete Fourier transform ($T_{Pr} \longrightarrow \omega_{Pr}$) and subtract unpumped spectrum. For further research, we will always take signal on particular frequencies, so-called traces, to describe the dynamics (see picture 2.1).

Similarly to Malý and Brixner [2021], we do not consider Stokes shift in our calculations. This is alright, because we do not distinguish the frequency of the F-PP signal.

In this numerical approach, we can easily choose any experimental setup we want - for example, pulses with a finite length, which would, in the perturbative approach presented in section 1.3, lead to a very lengthy calculation of convolutions. But for these benefits, we pay some price. Choosing the right parameters for the numerical calculation - such as the time step - is very important. So we can obtain accurate results in the shortest computing time possible. We can change the time step in dynamics computation, watch if the correct dynamics change, and subsequently choose the longest step to obtain the correct dynamics (the same as for some very short time steps).

Evolution matrix is propagated using function propagate, there we can set all necessary things needed for the propagation, such as time axis, hamiltonian of the system, relaxation tensor, electric field and of course also transition dipole moment. In all simulations, we have used a Taylor expansion of the propagator exponential into second order with time step in propagation $dt = 0.5\,\text{fs}$, time step for T_{Pr}: 4 fs and for T_{Pu} time step 5 fs. We have used a partially rotating frame, which allowed us to use a larger time step. Exactly as described by Malý and Brixner [2021], our second probe has additional phase $-(1-\gamma)\omega_0 t$, where ω_0 is the mean frequency of the pulse. We have set $\gamma = 0.2$. Meanwhile, $\gamma = 1$

corresponds to the laboratory frame, and $\gamma = 0$ is a fully rotating frame. Because of this, as Malý and Brixner [2021] state, the phase between the probes is $\gamma\omega_0$. This decreases the frequency of the coherent oscillations by $(1-\gamma)\omega_0$, and with slower oscillations, we can make larger time steps.

Detail comparison between perturbative and non-perturbative approaches was written by Malý [2012].

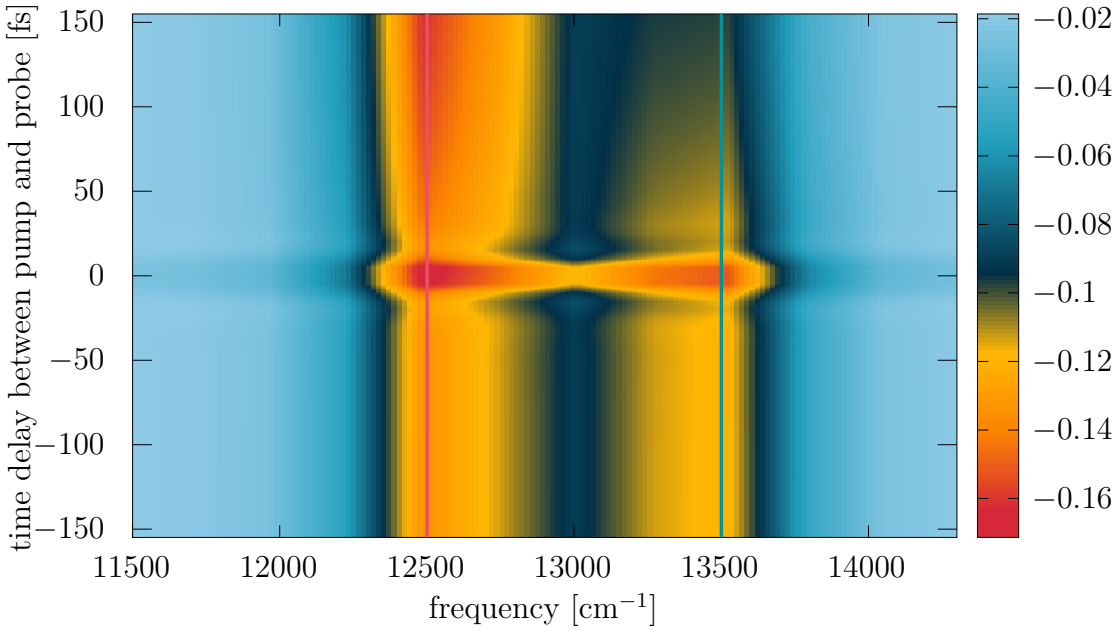

Figure 2.1: F-PP spectrum for heterodimer of two-level molecules AB. For further research, we will always take signal on particular frequencies, so-called traces, to describe the dynamics. Here, there are highlighted traces for frequencies $\epsilon_A = 13500\,\mathrm{cm}^{-1}$ (blue) and $\epsilon_B = 12500\,\mathrm{cm}^{-1}$ (pink). Signal was multiplied by 10^5.

2.2 Pulse properties

In this thesis, we use only Gaussian pulses. The negative-frequency part of the electric intensity of these pulses could be described as follows (leaving out the spatial dependence):

$$E^-(t) = Ae^{-4\cdot log(2)\left(\frac{t-t_0}{FWHM}\right)^2} e^{i\omega_0 t} e^{i\phi} \tag{2.2}$$

where A is the amplitude, chosen in such a way that after integration, we get the pulse energy. $FWHM$ is an abbreviation for full weight half maximum, which is a parameter of the Gaussian-shaped envelope — it says how wide the peak is in its half height. The whole wave packet is moving through space with group velocity v_g, while individual waves forming the packet each have their phase velocity.

In the frequency domain, which we can obtain from the time domain using the Fourier transform, we can write (for $t_0 = 0$)

$$E(\omega) = A' e^{-\frac{(\omega-\omega_0)^2}{16log(2)}(FWHM)^2} e^{i\phi} \tag{2.3}$$

We have used for all pulses $FWHM = 15\,\mathrm{fs}$ except for chirped pulses, which have special properties.

To remove unwanted contributions, we have used 3×3 phase cycling (three different phases for both probes) isolating signals with signature $(-1, 1, -1, 1)$. The simulated signal was processed using the equation 1.24 and the phase was cyclically changed as follows

$$(\Phi_{Pr1}, \Phi_{Pr2}) = (0,0)\,;\left(0, \tfrac{2}{3}\pi\right);\left(0, \tfrac{4}{3}\pi\right);\left(\tfrac{2}{3}\pi, 0\right);\left(\tfrac{2}{3}\pi, \tfrac{2}{3}\pi\right); \tag{2.4}$$

$$\left(\tfrac{2}{3}\pi, \tfrac{4}{3}\pi\right);\left(\tfrac{4}{3}\pi, 0\right);\left(\tfrac{4}{3}\pi, \tfrac{2}{3}\pi\right);\left(\tfrac{4}{3}\pi, \tfrac{4}{3}\pi\right) \tag{2.5}$$

2.3 Chirp

Because the refraction index is dependent on the frequency of radiation, the laser beam that went through a material with refractive index n(ω) gets a time-dependent phase (see, for example, book by Trebino [2000]). This phenomenon is called group-velocity dispersion because the group-velocity differs with frequency in this material. The colours separate, and the wave packed gets wider with the time it spends in this dispersive medium.

As a wave, the electric intensity depends on time and space coordinates.

$$E^-(\vec{r}, t) = A(\vec{r}, t) e^{-i\vec{k}_0 \cdot \vec{r} + i\omega_0 t}, \tag{2.6}$$

where $A(\vec{r}, t)$ is a slow envelope of the pulse with mean frequency ω_0. The absolute value of wave vector $\vec{k}$ depends on the frequency and refractive index (which is frequency dependent too), according to Boyd et al. [2008], we can write

$$k(\omega) = \sqrt{\epsilon(\omega)}\frac{\omega}{c}. \tag{2.7}$$

After leaving the optical component with refractive index $n(\omega)$ and permittivity $\epsilon(\omega)$, where the light travelled the path d, it gained additional phase

$$\Phi(\omega) = k(\omega) d. \tag{2.8}$$

The wave vector could be approximated using the second order of the Taylor series (neglecting any nonlinearities) as

$$k(\omega) = k(\omega_0) + \frac{\partial}{\partial\omega} k(\omega)|_{\omega=\omega_0}(\omega - \omega_0) + \frac{1}{2}\frac{\partial^2}{\partial\omega^2} k(\omega)|_{\omega=\omega_0}(\omega - \omega_0)^2. \tag{2.9}$$

Using the definition of group velocity, we get

$$k(\omega) = k(\omega_0) + k_1(\omega - \omega_0) + \frac{1}{2}k_2(\omega - \omega_0)^2 = k(\omega_0) + \frac{1}{v_g}(\omega - \omega_0) + \frac{1}{2}\frac{\partial}{\partial\omega}\left(\frac{1}{v_g}\right)(\omega - \omega_0)^2. \tag{2.10}$$

k_2 is also called the group-velocity dispersion parameter (GVD).

Now, we will use the inverse Fourier transform to obtain electric intensity in the time domain after it leaves the optical component.

$$E(t) = \frac{1}{2\pi}\int_{-\infty}^{+\infty} E(\omega)e^{i\omega t}d\omega \tag{2.11}$$

We are interested mainly in the change of $FWHM$ of the pulse and the time-dependent phase change. This means that we can ignore the terms which contribute only to the amplitude or constant phase. We will include them in the changed amplitude (see, for example, the third term in the second row of the following calculation). From equations 2.10, 2.8 and 2.3 we can write (using $c_0 = k_0 d$, $c_1 = k_1 d$, $c_2 = k_2 d$ and $\Delta^2 = \frac{FWHM^2}{4log(2)}$):

$$\begin{aligned}
E(t) &= \int_{-\infty}^{+\infty} \widetilde{A}e^{-\frac{(\omega-\omega_0)^2}{4}\Delta^2} e^{ic_0+ic_1(\omega-\omega_0)+\frac{1}{2}ic_2(\omega-\omega_0)^2} e^{i\omega t}d\omega = \\
&= \int_{-\infty}^{+\infty} \widetilde{A}e^{-\omega^2\left(\frac{\Delta^2}{4}-\frac{1}{2}ic_2\right)+i\omega\left(-i\frac{\Delta^2}{2}\omega_0+c_1-c_2\omega_0+t\right)+\left(-\frac{\Delta^2}{4}\omega_0^2+ic_0-ic_1\omega_0+\frac{1}{2}ic_2\omega_0^2\right)}d\omega = \\
&= |R = \frac{\Delta^2}{4}-\frac{1}{2}ic_2, B = -i\frac{\Delta^2}{2}\omega_0 + c_1 - c_2\omega_0 + t| = \\
&= \int_{-\infty}^{+\infty} \widetilde{\widetilde{A}}e^{-\omega^2 R}e^{i\omega B}d\omega = \\
&= |\mathcal{F}^{-1}[\widetilde{\widetilde{A}}e^{-R\omega^2}](B) = \widetilde{\widetilde{A}}\frac{1}{\sqrt{2}\sqrt{R}}e^{-\frac{B^2}{4R}}| = \\
&= A'e^{-\frac{t^2+2t\left(-c_2\omega_0+c_1-i\frac{\Delta^2\omega_0}{2}\right)+\left(-c_2\omega_0+c_1-i\frac{\Delta^2\omega_0}{2}\right)^2}{4R}} = A''e^{-\frac{t^2+2t\left(-c_2\omega_0+c_1-i\frac{\Delta^2\omega_0}{2}\right)}{4R}} = \\
&= A''e^{-\frac{t^2+2t\left(-c_2\omega_0+c_1-i\frac{\Delta^2\omega_0}{2}\right)}{4\left(\frac{\Delta^2}{4}-\frac{1}{2}ic_2\right)}\frac{\left(\frac{\Delta^2}{4}+\frac{1}{2}ic_2\right)}{\left(\frac{\Delta^2}{4}+\frac{1}{2}ic_2\right)}} = \\
&= A''e^{-\frac{t^2\frac{\Delta^2}{4}+2t[\frac{\Delta^2}{4}(-c_2\omega_0+c_1)+\frac{\Delta^2}{4}\omega_0 c_2]-i\frac{\Delta^2}{4}\omega_0 t+ic_2t(-c_2\omega_0+c_1)+\frac{1}{2}ic_2t^2}{4\left(\frac{\Delta^4}{16}+\frac{1}{4}c_2^2\right)}} = \\
&= A'''e^{-\frac{[t-c_1]^2\frac{\Delta^2}{4}-i[\frac{\Delta^2}{4}\omega_0+c_2^2\omega_0-c_1c_2]t-\frac{1}{2}ic_2t^2}{4\left(\frac{\Delta^4}{16}+\frac{1}{4}c_2^2\right)}} = \\
&= A'''e^{-\frac{[t-c_1]^2\frac{\Delta^2}{4}}{\left(\frac{\Delta^4}{4}+c_2^2\right)}}e^{i\omega_0 t}e^{\frac{-ic_1c_2t}{\left(\frac{\Delta^4}{4}+c_2^2\right)}}e^{\frac{-\frac{1}{2}ic_2t^2}{\left(\frac{\Delta^4}{4}+c_2^2\right)}} = \\
&\approx A'''e^{-\frac{[t-c_1]^2}{\Delta'^2}}e^{i\omega_0 t}e^{-\frac{1}{2}ic_2't^2}
\end{aligned} \tag{2.12}$$

By comparison with the expected result

$$E(t) = E_0 e^{-\frac{(t-t_0)^2}{\Delta'^2}}e^{i\omega(t-t_0)+i\phi(t)}, \tag{2.13}$$

where for the linearly chirped pulse is

$$\phi(t) = \phi_0 + \frac{1}{2}c_2'(t-t_0)^2 \tag{2.14}$$

we get $FWHM$ in the time domain for chirped pulse

$$\Delta' = \sqrt{\left(\Delta^2 + \frac{4c_2^2}{\Delta^2}\right)} \tag{2.15}$$

and GVD in time domain

$$c_2' = c_2 \frac{1}{\left(\frac{\Delta^4}{4} + c_2^2\right)}. \tag{2.16}$$

Expressed in original variables, we get

$$\begin{aligned} FWHM' &= \Delta'\sqrt{4ln(2)} = \\ &= \sqrt{\left(\Delta^2 + \frac{4c_2^2}{\Delta^2}\right)}\sqrt{4ln(2)} = \\ &= \sqrt{\left(\frac{FWHM^2}{4ln(2)} + \frac{4c_2^2}{\frac{FWHM^2}{4ln(2)}}\right)}\sqrt{4ln(2)} = \\ &= \sqrt{\left(FWHM^2 + \frac{64ln(2)^2c_2^2}{FWHM^2})\right)} \end{aligned} \tag{2.17}$$

$$c_2' = c_2 \frac{1}{\left(\frac{FWHM^4}{64log(2)^2} + c_2^2\right)} \tag{2.18}$$

Time dependence of the frequency could be obtained as

$$\omega(t) = \frac{d}{dt}\left(\omega_0(t - t_0) + \phi_0 + \frac{1}{2}c_2'(t - t_0)^2\right) = \omega_0 + c_2'(t - t_0). \tag{2.19}$$

This means that lower frequencies will arrive earlier than higher frequencies.

The time delay between centres of Gaussians of two different frequencies in chirped pulse

$$t_1 - t_2 = \frac{1}{v_{g_1}} - \frac{1}{v_{g_2}} = c_2(\omega_2 - \omega_1) \tag{2.20}$$

This looks like $c_2 = \frac{1}{c_2'}$, which is not true. However, we have to be careful that there is a difference between those two approaches. $\omega(t)$ gives us the average frequency of the pulse in time t. On the other hand, from equation 2.20, we can compute a time in which a given frequency has its maximum. $\omega(t_i) = \epsilon_A$ does not necessarily mean that in time t_i, frequency ϵ_A has its maximum in pulse spectrum if we decompose the spectrum into different frequencies. We are interested in the maximum of the particular frequencies, so we will start from the equation 2.20, based on the wanted time shift between ϵ_A and ϵ_B compute c_2. From this constant, we will compute c_2', which directly appears in our code in the phase definition (see equation 2.14). However, the difference between $\omega(t)$ and maxima for particular frequencies from equation 2.20 is minimal. In the case we would use equation 2.19, the time delay between $\epsilon_A = 13500\,\mathrm{cm}^{-1}$ and $\epsilon_B = 12500\,\mathrm{cm}^{-1}$ would change from 100 fs to 100.6 fs, which is under our detection resolution.

3. Theoretical results

3.1 Used model

To examine the behaviour of F-PP spectra, we have used a model as basic as possible - two two-level systems with different excited energies $\epsilon_A = 13500\,\mathrm{cm}^{-1}$ and $\epsilon_B = 12500\,\mathrm{cm}^{-1}$ creating weakly coupled heterodimer (see figure 3.1 and 3.2) with energy transfer from the higher to the lower energy level with rate constant $K_{AB} = \frac{1}{100}\,\mathrm{fs}^{-1}$. All used parameters are summarized in section A.1.

For that heterodimer, we can write down all possible Liouville pathways (see figures A.2,A.1, A.3, A.4). Each pulse can interact either with molecule A or with molecule B. In our model, we use quick dephasing of the coherence between the two excitons on the different molecules $|A\rangle\langle B|$ (see section A.1). Because of this, we do not observe them in longer times. In this section, we will consider only the pathways with populations in waiting time T_{Pu} before the pump and probe. (The other pathways play a crucial role in the appearance of the spectra near time zero, which will be further discussed in section 3.4.)

In the thesis, we consider relaxation to the ground state (with rate constant K_{recomb}) to be much slower than all the other excitation dynamics. It thus doesn't have to be considered explicitly, allowing us to use only transport from molecule A to molecule B with rate constant K_{AB} and dephasing of the coherences as dynamics in the waiting time T_{Pu} in Feynman diagrams.

Populations of $|\mathrm{g}\rangle\langle\mathrm{g}|$ and $|\mathrm{B}\rangle\langle\mathrm{B}|$ don't thus evolve in time in comparison to the rapid evolvement of population of $|\mathrm{A}\rangle\langle\mathrm{A}|$, which is decaying with evolution operator $e^{-K_{AB}T_{Pu}}$. Consequently, the pathway containing transport from A to B will evolve with the factor $1 - e^{-K_{AB}T_{Pu}}$.

For the system-bath interaction, we are using an approximation of quick oscillations, where the bath's correlation function is approximated with $\Gamma\delta(t)$, which gives us an evolution operator for coherence $|\mathrm{g}\rangle\langle\mathrm{e}|$ as $e^{i\omega_{eg}t-\Gamma_{eg}t}$ and provides us with Lorentz line-shape (see section 1.4). In the computations, we will denote the line-shape for excitation spectra of molecule A as $G_{Ag}(\omega)$.

Energy transfer from A to B is very distinct in F-PP spectra. A signal on a frequency corresponding to the transition from the ground state to the excited state of molecule A is decreasing exponentially with the rate factor K_{AB}. On the other hand, the signal from molecule B is increasing at the same rate (see equation 3.1). If we include exciton-exciton annihilation (EEA), which is necessary unless $K_{annih} \ll K_{recomb}$, both A and B signals are increased by adding a constant signal (according to equation 3.2). All simulations of F-PP spectra in this chapter are for the above-mentioned system with EEA. Spectra for a system with negligible EEA are presented in section A.6.

$$
\begin{aligned}
\text{F-PP} \sim & -|\mu_A|^4 G_{Ag}(\omega_{T_{Pr}}) - |\mu_A|^2|\mu_B|^2 G_{Ag}(\omega_{T_{Pr}}) \\
& - |\mu_B|^4 G_{Bg}(\omega_{T_{Pr}}) - |\mu_A|^2|\mu_B|^2 G_{Bg}(\omega_{T_{Pr}}) \\
& - |\mu_A|^2|\mu_B|^2 G_{Bg}(\omega_{T_{Pr}}) \left(1 - e^{-K_{AB}T_{Pu}}\right) - |\mu_A|^4 G_{Bg}(\omega_{T_{Pr}}) \\
& - |\mu_A|^4 G_{Ag}(\omega_{T_{Pr}}) e^{-K_{AB}T_{Pu}} - |\mu_A|^2|\mu_B|^2 G_{Bg}(\omega_{T_{Pr}}) e^{-K_{AB}T_{Pu}} \\
& - |\mu_A|^2|\mu_B|^2 G_{Ag}(\omega_{T_{Pr}}) - |\mu_A|^4 G_{Ag}(\omega_{T_{Pr}}) \left(1 - e^{-K_{AB}T_{Pu}}\right) \\
& + 2 \cdot |\mu_A|^2|\mu_B|^2 G_{Bg}(\omega_{T_{Pr}}) e^{-K_{AB}T_{Pu}} + 2 \cdot |\mu_A|^2|\mu_B|^2 G_{Ag}(\omega_{T_{Pr}}) \\
& + 2 \cdot |\mu_A|^4 G_{Ag}(\omega_{T_{Pr}}) \left(1 - e^{-K_{AB}T_{Pu}}\right) = \\
= & -2 \cdot |\mu_A|^4 G_{Ag}(\omega_{T_{Pr}}) e^{-K_{AB}T_{Pu}} \\
& - 2 \cdot \left(|\mu_B|^4 + |\mu_A|^2|\mu_B|^2 (1 - e^{-K_{AB}T_{Pu}})\right) G_{Bg}(\omega_{T_{Pr}})
\end{aligned} \tag{3.1}
$$

The same way for $K_{recomb} \ll K_{annih}$, where ESA 2 pathways contribute with only one photon each, we get

$$
\begin{aligned}
F - PP \sim & - \left(|\mu_A|^4 + |\mu_A|^2|\mu_B|^2 + |\mu_A|^4 e^{-K_{AB}T_{Pu}}\right) G_{Ag}(\omega_{T_{Pr}}) \\
& - \left(2 \cdot |\mu_B|^4 + |\mu_A|^2|\mu_B|^2 (2 - e^{-K_{AB}T_{Pu}})\right) G_{Bg}(\omega_{T_{Pr}})
\end{aligned} \tag{3.2}
$$

For $T_{Pu} = 0\,\text{fs}$, the cross peaks in F-2DES will cancel each other (in the absence of coupling) - see picture A.5 and equation 3.3. For weak coupling, ESA 2 pathways are influenced by exciton-exciton annihilation; they contribute with only one photon instead of two, the cancellation is incomplete, and cross peaks will appear (see equation 3.4), which was mentioned, for example, by Malý and Mančal [2018]. The consequences are described in section 1.5 and section 3.3.

A diagonal peak depicting the transfer from A to B will appear in longer times

$$
\begin{aligned}
\text{F-2DES} \sim & -|\mu_A|^4 G_{Ag}(\omega_{T_{Pr}}) G_{Ag}(\omega_\tau) - |\mu_A|^2|\mu_B|^2 G_{Ag}(\omega_{T_{Pr}}) G_{Bg}(\omega_\tau) \\
& - |\mu_B|^4 G_{Bg}(\omega_{T_{Pr}}) G_{Bg}(\omega_\tau) - |\mu_A|^2|\mu_B|^2 G_{Bg}(\omega_{T_{Pr}}) G_{Ag}(\omega_\tau) \\
& - |\mu_A|^2|\mu_B|^2 G_{Bg}(\omega_{T_{Pr}}) \left(1 - e^{-K_{AB}T_{Pu}}\right) G_{Ag}(\omega_\tau) - |\mu_B|^4 G_{Bg}(\omega_{T_{Pr}}) G_{Bg}(\omega_\tau) \\
& - |\mu_A|^4 G_{Ag}(\omega_{T_{Pr}}) e^{-K_{AB}T_{Pu}} G_{Ag}(\omega_\tau) - |\mu_A|^2|\mu_B|^2 G_{Bg}(\omega_{T_{Pr}}) e^{-K_{AB}T_{Pu}} G_{Ag}(\omega_\tau) \\
& - |\mu_A|^2|\mu_B|^2 G_{Ag}(\omega_{T_{Pr}}) G_{Bg}(\omega_\tau) - |\mu_A|^4 G_{Ag}(\omega_{T_{Pr}}) \left(1 - e^{-K_{AB}T_{Pu}}\right) G_{Ag}(\omega_\tau) \\
& + 2 \cdot |\mu_A|^2|\mu_B|^2 G_{Bg}(\omega_{T_{Pr}}) e^{-K_{AB}T_{Pu}} G_{Ag}(\omega_\tau) + 2 \cdot |\mu_A|^2|\mu_B|^2 G_{Ag}(\omega_{T_{Pr}}) G_{Bg}(\omega_\tau) \\
& + 2 \cdot |\mu_A|^4 G_{Ag}(\omega_{T_{Pr}}) \left(1 - e^{-K_{AB}T_{Pu}}\right) G_{Ag}(\omega_\tau) \\
= & - 2 \cdot |\mu_A|^4 e^{-K_{AB}T_{Pu}} G_{Ag}(\omega_{T_{Pr}}) G_{Ag}(\omega_\tau) + \\
& + 0 \cdot G_{Ag}(\omega_{T_{Pr}}) G_{Bg}(\omega_\tau) \\
& - 2 \cdot |\mu_B|^4 G_{Bg}(\omega_{T_{Pr}}) G_{Bg}(\omega_\tau) \\
& - 2|\mu_A|^2|\mu_B|^2 \left(1 - e^{-K_{AB}T_{Pu}}\right) G_{Bg}(\omega_{T_{Pr}}) G_{Ag}(\omega_\tau)
\end{aligned} \tag{3.3}
$$

For $K_{recomb} \ll K_{annih}$ we get

$$\begin{aligned}\text{F-2DES} \sim & - |\mu_A|^4 \left(1 + e^{-K_{AB}T_{Pu}}\right) G_{Ag}(\omega_{T_{Pr}}) G_{Ag}(\omega_\tau) + \\ & - |\mu_A|^2 |\mu_B|^2 G_{Ag}(\omega_{T_{Pr}}) G_{Bg}(\omega_\tau) + \\ & - 2 \cdot |\mu_B|^4 G_{Bg}(\omega_{T_{Pr}}) G_{Bg}(\omega_\tau) + \\ & - |\mu_A|^2 |\mu_B|^2 \left(2 - e^{-K_{AB}T_{Pu}}\right) G_{Bg}(\omega_{T_{Pr}}) G_{Ag}(\omega_\tau) \end{aligned} \tag{3.4}$$

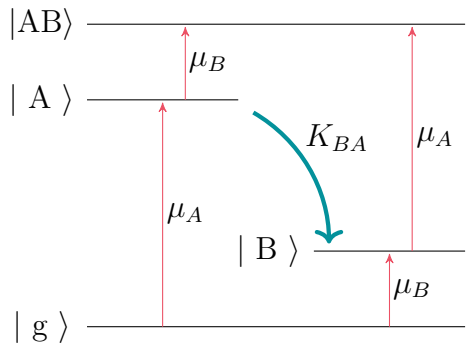

Figure 3.1: Heterodimer AB with energies $\epsilon_A > \epsilon_B$, transition dipole moments μ_A and μ_B, and with transmission rate constant from system A to system B K_{AB}.

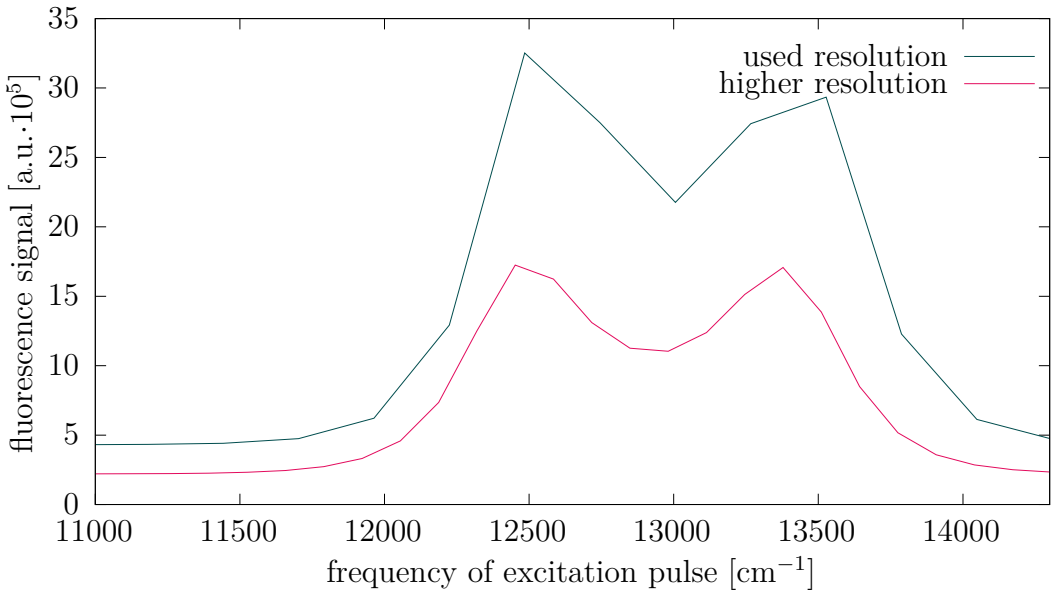

Figure 3.2: Excitation spectrum of heterodimer AB with energies ϵ_A=13500 cm^{-1} and ϵ_B=12500 cm^{-1} (see picture 3.1). For comparison, there is spectrum with used resolution (maximal $T_{Pr} = 124\,\mathrm{fs}$) and twice the resolution (maximal $T_{Pr} = 248\,\mathrm{fs}$).

3.2 Negative time signal

In negative waiting times, the system first interacts with both probes and then with the pump. For $K_{annih} \ll K_{recomb}$ we can neglect the exciton-exciton annihilation; the time evolution is then (according to figures A.7,A.6, A.8, A.9):

$$\begin{aligned}
&\text{F-PP} \sim \\
&- |\mu_A|^4 G_{Ag}(\omega_{T_{Pr}}) - |\mu_A|^2|\mu_B|^2 G_{Bg}(\omega_{T_{Pr}}) - |\mu_B|^4 G_{Bg}(\omega_{T_{Pr}}) + \\
&- |\mu_A|^2|\mu_B|^2 G_{Ag}(\omega_{T_{Pr}}) - |\mu_A|^2|\mu_B|^2 G_{Ag}(\omega_{T_{Pr}}) \left(1 - e^{-K_{AB}|T_{Pu}|}\right) + \\
&- |\mu_B|^4 G_{Bg}(\omega_{T_{Pr}}) - |\mu_A|^4 G_{Ag}(\omega_{T_{Pr}}) e^{-K_{AB}|T_{Pu}|} + \\
&- |\mu_A|^2|\mu_B|^2 G_{Ag}(\omega_{T_{Pr}}) e^{-K_{AB}|T_{Pu}|} - |\mu_A|^2|\mu_B|^2 G_{Bg}(\omega_{T_{Pr}}) + \\
&- |\mu_A|^4 G_{Ag}(\omega_{T_{Pr}}) \left(1 - e^{-K_{AB}|T_{Pu}|}\right) + 2 \cdot |\mu_A|^2|\mu_B|^2 G_{Ag}(\omega_{T_{Pr}}) e^{-K_{AB}|T_{Pu}|} + \\
&+ 2 \cdot |\mu_A|^2|\mu_B|^2 G_{Bg}(\omega_{T_{Pr}}) + 2 \cdot |\mu_A|^4 G_{Ag}(\omega_{T_{Pr}}) \left(1 - e^{-K_{AB}|T_{Pu}|}\right) = \\
&= \left(-2 \cdot |\mu_A|^2|\mu_B|^2 + 2\left(|\mu_A|^2|\mu_B|^2 - |\mu_A|^4\right) e^{-K_{AB}|T_{Pu}|}\right) G_{Ag}(\omega_{T_{Pr}}) + \\
&- 2 \cdot |\mu_B|^4 G_{Bg}(\omega_{T_{Pr}})
\end{aligned} \tag{3.5}$$

For $|\mu_A| = |\mu_B| = |\mu|$, we get

$$\text{F-PP} \sim -2 \cdot |\mu|^4 G_{Ag}(\omega_{T_{Pr}}) - 2 \cdot |\mu|^4 G_{Bg}(\omega_{T_{Pr}}) \tag{3.6}$$

Analogously for $K_{recomb} \ll K_{annih}$, where ESA2 pathways contribute with only one photon each, we get

$$\begin{aligned}
\text{F-PP} \sim &\left(-2 \cdot |\mu_A|^2|\mu_B|^2 - |\mu_A|^4 + \left(|\mu_A|^2|\mu_B|^2 - |\mu_A|^4\right) e^{-K_{AB}|T_{Pu}|}\right) G_{Ag}(\omega_{T_{Pr}}) \\
&+ \left(-|\mu_A|^2|\mu_B|^2 - 2 \cdot |\mu_B|^4\right) G_{Bg}(\omega_{T_{Pr}})
\end{aligned} \tag{3.7}$$

For $|\mu_A| = |\mu_B| = |\mu|$, we get

$$\text{F-PP} \sim -3 \cdot |\mu|^4 G_{Ag}(\omega_{T_{Pr}}) - 3 \cdot |\mu|^4 G_{Bg}(\omega_{T_{Pr}}) \tag{3.8}$$

From this, it is easy to conclude that only if the oscillatory strengths of both transitions are comparable, there is no time evolution in F-PP spectra in negative times (when we neglect fluorescence rate). Moreover, the signal is the same for both A and B. Nevertheless, in other cases, there is visible time dependence for the signal from molecule A. If $|\mu_A| > |\mu_B|$, the second term in $-2 \cdot |\mu_A|^2|\mu_B|^2 - |\mu_A|^4 + (|\mu_A|^2|\mu_B|^2 - |\mu_A|^4)\, e^{-K_{AB}|T_{Pu}|}$ is negative and with increasing $|T_{Pu}|$ the signal is (in absolute value) decreasing. This corresponds with our simulations in graph 3.3. On the contrary, the second term is positive for $|\mu_A| < |\mu_B|$, and the overall signal from A increases with $|T_{Pu}|$ (see graph 3.4).

$$
\begin{aligned}
&\text{F-2DES} \sim \\
&- |\mu_A|^2|\mu_B|^2 G_{Ag}(\omega_{T_{Pr}}) G_{Bg}(\omega_\tau) - |\mu_A|^4 G_{Ag}(\omega_{T_{Pr}}) G_{Ag}(\omega_\tau) \\
&- |\mu_A|^2|\mu_B|^2 G_{Bg}(\omega_{T_{Pr}}) G_{Ag}(\omega_\tau) - |\mu_B|^4 G_{Bg}(\omega_{T_{Pr}}) G_{Bg}(\omega_\tau) \\
&- |\mu_A|^2|\mu_B|^2 G_{Ag}(\omega_{T_{Pr}}) \left(1 - e^{-K_{AB}|T_{Pu}|}\right) G_{Bg}(\omega_\tau) - |\mu_B|^4 G_{Bg}(\omega_{T_{Pr}}) G_{Bg}(\omega_\tau) \\
&- |\mu_A|^4 G_{Ag}(\omega_{T_{Pr}}) e^{-K_{AB}|T_{Pu}|} G_{Ag}(\omega_\tau) - |\mu_A|^2|\mu_B|^2 G_{Ag}(\omega_{T_{Pr}}) e^{-K_{AB}|T_{Pu}|} G_{Bg}(\omega_\tau) \\
&- |\mu_A|^2|\mu_B|^2 G_{Bg}(\omega_{T_{Pr}}) G_{Ag}(\omega_\tau) - |\mu_A|^4 G_{Ag}(\omega_{T_{Pr}}) \left(1 - e^{-K_{AB}|T_{Pu}|}\right) G_{Ag}(\omega_\tau) \\
&+ 2 \cdot |\mu_A|^2|\mu_B|^2 G_{Ag}(\omega_{T_{Pr}}) e^{-K_{AB}|T_{Pu}|} G_{Bg}(\omega_\tau) + 2 \cdot |\mu_A|^2|\mu_B|^2 G_{Bg}(\omega_{T_{Pr}}) G_{Ag}(\omega_\tau) \\
&+ 2 \cdot |\mu_A|^4 G_{Ag}(\omega_{T_{Pr}}) \left(1 - e^{-K_{AB}|T_{Pu}|}\right) G_{Ag}(\omega_\tau) = \\
&= -2 \cdot |\mu_A|^4 e^{-K_{AB}|T_{Pu}|} G_{Ag}(\omega_{T_{Pr}}) G_{Ag}(\omega_\tau) + \\
&- 2 \cdot |\mu_A|^2|\mu_B|^2 \left(1 - e^{-K_{AB}|T_{Pu}|}\right) G_{Ag}(\omega_{T_{Pr}}) G_{Bg}(\omega_\tau) + \\
&+ 0 \cdot G_{Bg}(\omega_{T_{Pr}}) G_{Ag}(\omega_\tau) - 2 \cdot |\mu_B|^4 G_{Bg}(\omega_{T_{Pr}}) G_{Bg}(\omega_\tau)
\end{aligned} \tag{3.9}
$$

For $K_{recomb} \ll K_{annih}$ again:

$$
\begin{aligned}
\text{F-2DES} \sim &- |\mu_A|^4 \left(1 + e^{-K_{AB}|T_{Pu}|}\right) G_{Ag}(\omega_{T_{Pr}}) G_{Ag}(\omega_\tau) + \\
&- |\mu_A|^2|\mu_B|^2 \left(2 - e^{-K_{AB}|T_{Pu}|}\right) G_{Ag}(\omega_{T_{Pr}}) G_{Bg}(\omega_\tau) + \\
&- |\mu_A|^2|\mu_B|^2 G_{Bg}(\omega_{T_{Pr}}) G_{Ag}(\omega_\tau) + \\
&- 2 \cdot |\mu_B|^4 G_{Bg}(\omega_{T_{Pr}}) G_{Bg}(\omega_\tau)
\end{aligned} \tag{3.10}
$$

With or without EEA, F-2DES spectra in negative times are only Hermitian conjugate of corresponding F-2DES spectra in positive times (see picture A.13).

Our goal was to find out how the F-PP signal behaves in negative times in various conditions. For heterodimer AB with energy transfer from molecule A to molecule B, there is visible dynamics in negative times, unless special situation $\mu_A = \mu_B$ applies. Then we have to distinguish between cases where $\mu_A > \mu_B$ and the signal from A is decreasing, the signal from B is constant and cases where $\mu_A < \mu_B$. There, the signal from A is weak but increasing with $|T_{Pu}|$ and the signal from B is again constant. This holds for both cases, with or without EEA.

For F-2DES is the signal from negative times, regardless of μ_A and μ_B, Hermitian conjugate of F-2DES spectrum in positive times for particular T_{Pu}. Again, this is true regardless of whether we include EEA or not, but both for negative and positive times, the situation must be, of course, the same.

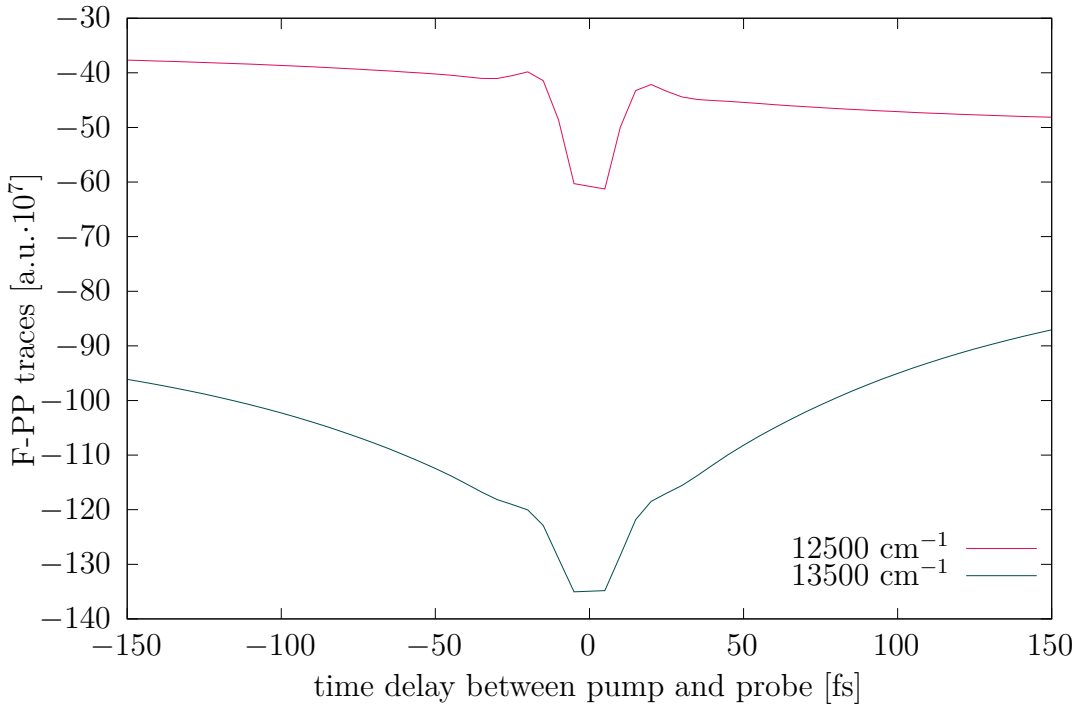

Figure 3.3: F-PP traces for frequencies ϵ_A and ϵ_B, $\mu_A = 2\mu_B$. We can see time dependence for the signal from molecule A in negative times, because $\mu_A > \mu_B$, signal from molecule A is (in absolute value) decreasing. Signal from molecule B is constant.

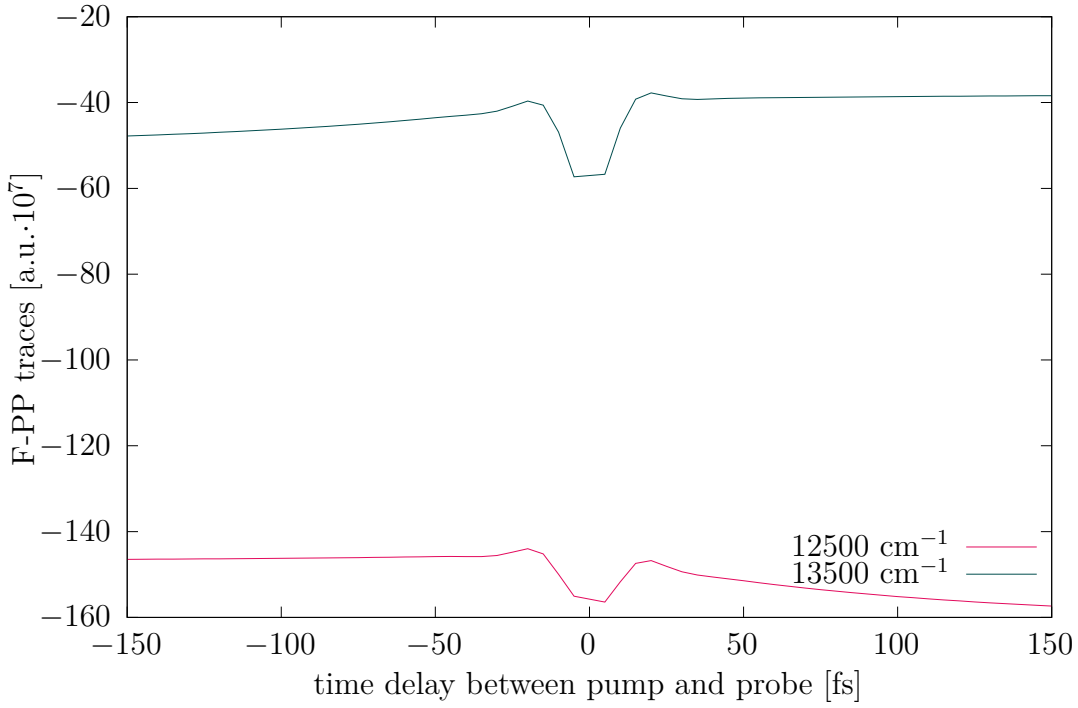

Figure 3.4: F-PP traces for frequencies ϵ_A and ϵ_B, $\mu_B = 2\mu_A$. Signal from molecule A, although weak, is in negative times increasing with $|T_{Pu}|$. Signal from molecule B is constant in negative times.

3.3 Incoherent mixing

As was mentioned in section 1.5, exciton-exciton annihilation causes in F-PP cancellation of ESA and ESA 2 pathways. Thus, cross-population GSB remains intact, decreasing the ratio between SE and GSB to $\frac{1}{N}$. With an increasing number of molecules, the dynamics became less and less visible, which could be demonstrated by comparison of graph 3.5 for two molecules (A and B) and graph 3.6 for six molecules - three molecules A and three molecules B.

The idea of subtracting signal from negative times to obtain the right dynamics as it would be without exciton-exciton annihilation was suggested at first by Malý and Brixner [2021]. This concept is understandable and tempting because, for many measurements (see, for example, chapter 4), the signal from negative times seems to be constant, and also, the contribution of cross-population GSB is time-independent. We can see now that the negative-time signal is constant in time only for $\mu_A = \mu_B$. But there is still a chance that the dynamics would be in such a form that it would be possible.

To confirm or refute this hypothesis, we need to find the correct constants C and S, when we will subtract the signal from negative times multiplied by the mentioned constant C from the signal from positive times multiplied by constant S.

$$\text{signal}_{T_{Pu}>0,\text{without EEA}} = S \cdot \text{signal}_{T_{Pu}>0,\text{with EEA}} - C \cdot \text{signal}_{T_{Pu}<0,\text{with EEA}} \tag{3.11}$$

Now we will insert the results of the calculations 3.1, 3.2, 3.7 into the equation 3.11 and compare the terms.

$$\begin{aligned}
&F - PP \sim -S \cdot \left(|\mu_A|^4 + |\mu_A|^2|\mu_B|^2 + |\mu_A|^4 e^{-K_{AB}T_{Pu}}\right) G_{Ag}(\omega_{T_{Pr}}) \\
&- S \cdot \left(2 \cdot |\mu_B|^4 + |\mu_A|^2|\mu_B|^2(2 - e^{-K_{AB}T_{Pu}})\right) G_{Bg}(\omega_{T_{Pr}}) \\
&- C \cdot \left(-2 \cdot |\mu_A|^2|\mu_B|^2 - |\mu_A|^4 + \left(|\mu_A|^2|\mu_B|^2 - |\mu_A|^4\right) e^{-K_{AB}|T_{Pu}|}\right) G_{Ag}(\omega_{T_{Pr}}) \\
&- C \cdot \left(-|\mu_A|^2|\mu_B|^2 - 2 \cdot |\mu_B|^4\right) G_{Bg}(\omega_{T_{Pr}}) = \\
&= -2 \cdot |\mu_A|^4 e^{-K_{AB}T_{Pu}} G_{Ag}(\omega_{T_{Pr}}) \\
&- 2 \cdot \left(|\mu_B|^4 + |\mu_A|^2|\mu_B|^2(1 - e^{-K_{AB}T_{Pu}})\right) G_{Bg}(\omega_{T_{Pr}})
\end{aligned} \tag{3.12}$$

Because this must hold for each time T_{Pu}, we have to compare the coefficients between terms with $e^{-K_{AB}T_{Pu}}$ and constant terms separately.

For signal from molecule A, we get:

$$C = \frac{2\mu_A^2}{\mu_A^2 + \mu_B^2} \tag{3.13}$$

$$S = 2 - 2 \cdot \frac{\mu_B^2 - \mu_A^2}{\mu_A^2 + \mu_B^2}. \tag{3.14}$$

For $\mu_A = \mu_B$, we get $C = 1$ and $S = 2$.

Solution for signal from molecule B is

$$C = \frac{2\left(\mu_A^2 + \mu_B^2\right)}{\mu_A^2 + 2\mu_B^2} \tag{3.15}$$

$$S = 2. \tag{3.16}$$

And for $\mu_A = \mu_B$ we get $C = \frac{4}{3}$ and $S = 2$.

We can see that the coefficients S and C are different for traces for ϵ_A and for ϵ_B (even for $\mu_A = \mu_B$ when traces are constant in negative times). We must subtract negative times from positive times for each frequency in the spectrum separately. This does not make sense for more complex systems. Furthermore, the spectrum is more or less continuous, depending on the resolution. Finally, expressions for coefficients depend on the oscillatory strengths of participating transitions, making it even more complicated.

We wanted to investigate if it is possible to obtain PP spectra (or F-PP spectra without EEA) simply by subtracting F-PP spectra in negative times from F-PP spectra in positive times with quick exciton-exciton annihilation. This would significantly improve the visibility of dynamics, which is now worsened due to incoherent mixing. In this section, we have shown that even for the special situation $\mu_A = \mu_B$, it is almost impossible to subtract the signal from negative times to obtain the signal from positive times without EEA. However, the dynamics are still visible, and therefore, the advantages of F-PP still outweigh its disadvantages.

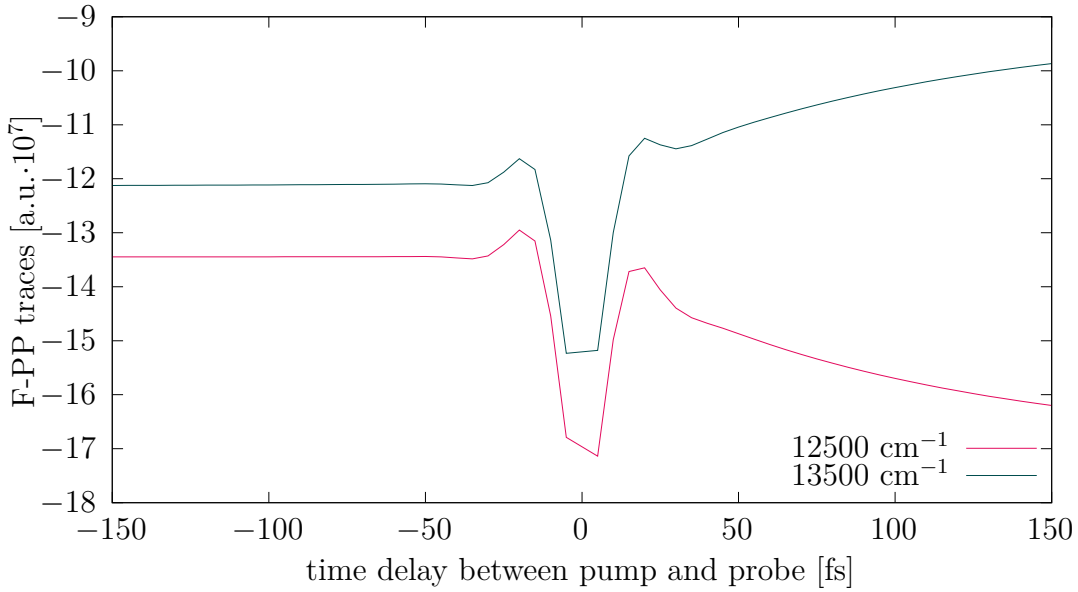

Figure 3.5: F-PP traces for frequencies ϵ_A and ϵ_B, two molecules (one molecule A and one molecule B, $\mu_A = \mu_B$). The signal from molecule A is decreasing in time, and the signal from molecule B is increasing. Signal in negative times is constant both for A and B.

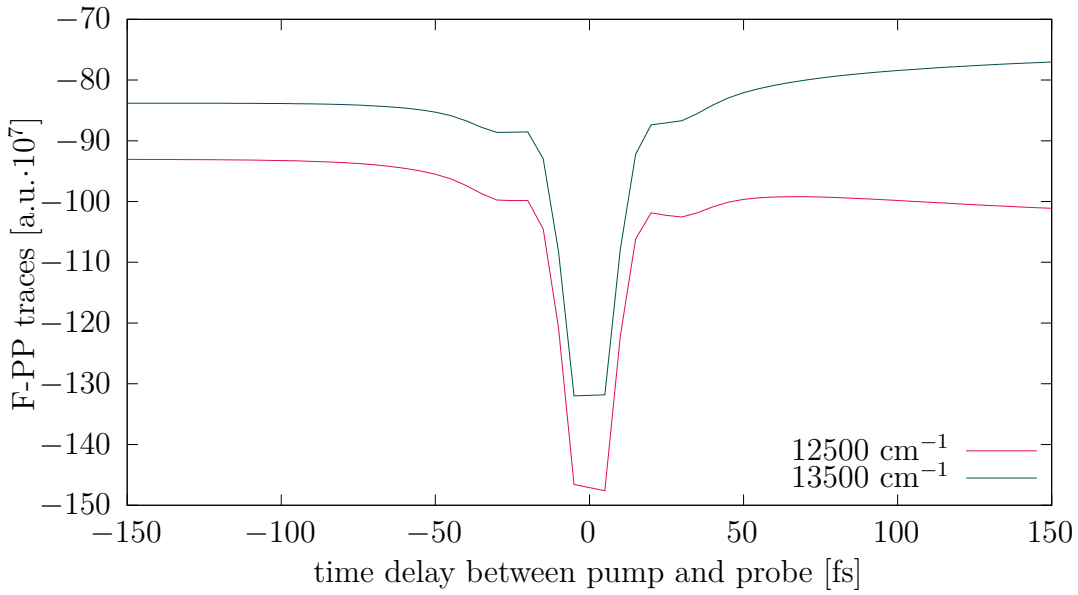

Figure 3.6: F-PP traces for frequencies ϵ_A and ϵ_B for six molecules (three molecules A and three molecules B, $\mu_A = \mu_B$). Although the dynamics is less visible due to EEA, the signal from molecule A is still decreasing in time, and the signal from molecule B is increasing. Signal in negative times remains constant both for A and B.

3.4 Time zero

If the waiting time between the pump and the first of the probes is around zero, we can see two more types of contribution to the signal in addition to the later times. The first one is, naturally, pulse overlap. If $T = 0$, there is no restriction on which pulse the system should interact first. This leads to pathways depicting all possible combinations of the order of interactions, including, for example, one where it interacts at first with the pump, then with both probes, and then again with the pump.

Moreover, pathways with coherences in the waiting time, previously dampened by quick dephasing, became visible. All main contributions for the overlapping pump and probe are shown in picture 3.7. $|1\rangle$ is either $|A\rangle$ or $|B\rangle$, $|2\rangle$ is the excited state of the other molecule than in $|1\rangle$. x in $|x\rangle$ could stand both for A and B, independent of what molecule 1 is. $G_{yg}(\omega)$ then denotes absorption line shape centred in the frequency of molecule y, which is complementary to x (if x is A, then y is B and vice versa). Because of interaction with the bath, we have a line broadening of molecules A and B's absorption/excitation spectrum. From the excitation spectrum in graph 3.2, we can see that the spectrum of both A and B contains, for example, frequency $13000\,\mathrm{cm}^{-1}$. Because of this, coherences such as $|A\rangle\langle 13000|$ contribute to the spectrum.

The shape of the peak of the traces around $T_{Pu} = 0$ is complicated because we need to perform the time convolutions in the perturbative picture used for the interpretation of influence of the pulse spectra shape. Moreover, we can see that it drastically changes if we neglect EEA (see graphs in section A.6). Besides, the pulse's shape heavily influences the peak's shape in time zero. As was mentioned by Malý and Brixner [2021], in fluorescence-detected pump-probe spectroscopy, we are not able to remove the dependence of the pulse shape as is easily done by division in pump-probe spectra. Thus, it is impossible to predict the resulting shape easily based only on computations with delta pulses. As a result, many scientists (for example, Paleček et al. [2019]) avoid time zero and start measuring spectra for times after the pulse-overlap peak.

The purpose of this section was to show that behaviour around time zero is complicated and reflects properties of not only the investigated system but also of used pulses. We have shown that the peak in time zero is caused by pulse overlap and oscillations; all possible contributions are summarised in figure 3.7. Although it is hard to conclude the shape of the traces during pulse overlap, these diagrams will be helpful in subsection 3.5.2.

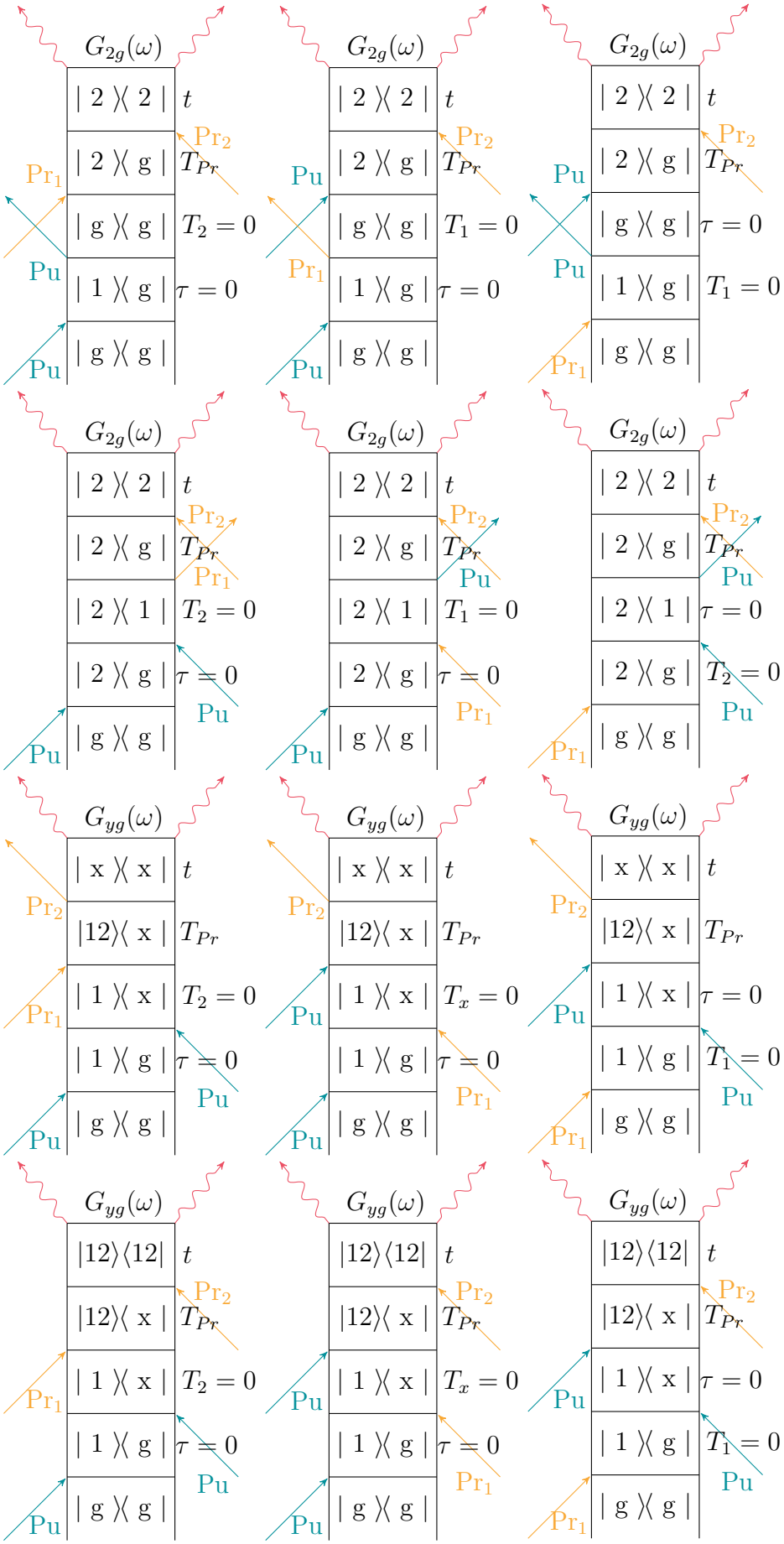

Figure 3.7: Contributions to the signal for $T = 0\,\mathrm{fs}$.

3.5 Chirped pulses and selective excitation

3.5.1 Selective excitation

To verify that our simulations are correct, we can test them on selective excitation, the outcome of which could be easily deduced from Feynman diagrams.

In experiments, we tend to use broad-spectrum pulses for probes. This means for transform-limited pulses that the $FWHM$ is about 15 fs in the time domain. In reality, the pulse duration can sometimes be even 1 ps due to the chirp of the pulse (see section 2.3 and subsection 3.5.2). On the other hand, if we want, for example, to selectively excite with the pump only one of two molecules in the dimer, the pump must be as narrow in the frequency domain as possible. Because of the time-energy uncertainty relation (described, for example, by Busch [2002]), $FWHM$ in the time domain must be broader. We cannot afford to lose the time distinction, therefore we should find some compromise.

In our computation, we have again used pulses with $FWHM = 15\,\mathrm{fs}$, and even for that, the change in dynamics was clearly visible. The only change was, thus, different excitation frequency. Until now, we have used the mean frequency of the pulse $13000\,\mathrm{cm}^{-1}$, which is the average of energies $\epsilon_A = 13500\,\mathrm{cm}^{-1}$ and $\epsilon_B = 12500\,\mathrm{cm}^{-1}$. For the selective excitation, we will now use a pump with a mean frequency corresponding to the energy of the excited state of one of the molecules.

When we selectively excite with pump molecule B only, in waiting time T_{Pu} there is only $|\mathrm{B}\rangle\langle\mathrm{B}|$ population or ground state until the probe pulses arrive. These populations do not, in our approximation, evolve in time. Consequently, there will be no visible time evolution. The signal of molecule A will practically disappear because the negative contribution of GSB and ESA to A signal is cancelled with a positive contribution of ESA 2 for $K_{recomb} \ll K_{annih}$ (see equation 3.18). On the other hand, if we selectively excite molecule A, there will be visible transport from A to B, which causes (in absolute value) a decrease of signal from A and an increase of signal from B (see equations 3.26 and 3.28).

In the negative times, we can observe some dynamics, contrary to the F-PP spectra for $13000\,\mathrm{cm}^{-1}$ pump frequency (and, of course, again $\mu_A = \mu_B$). For the selective excitation of molecule B, the signal from molecule A should be increasing, and the signal from molecule B is constant (see equations 3.22 and 3.24). For the ideal case of selective excitation of molecule B, we can observe the dynamics only in negative times on frequency corresponding to molecule A, which is obvious because in negative times are pump and probe reversed in time; probes interact first, creating a population of A (probe pulse has broad-spectrum) which is decaying with time $|T_{Pu}|$. In all other cases, there could be only a population of molecule B in waiting time T_{Pu} or ground state.

For the selective excitation of molecule A, the F-PP signal of molecule A is in negative times decreasing, the signal from B is constant (see equation 3.30) and disappears in the absence of EEA (equation 3.32).

This is consistent with the simulations in the graphs 3.8 and 3.9.

Coherences between A and B will also be strongly suppressed because to obtain a coherence pathway that contributes to the signal, we need the pump to interact once with molecule A and once with molecule B. This is, of course, only possible if the frequencies of the other molecule absorption spectrum are included in the pump spectrum.

It is important to note that the spectrum of the pulses we used for the simulation contained both absorption frequencies of molecules A and B (although one was always weak). Because of this, we can still see faint signals from other pathways. This causes, for example, slight time evolution in positive times for selective excitation of molecule B in graph 3.8, which should be constant based on our theoretical predictions. Although we are not supposed to see oscillations in the spectra, they are present precisely because of the above-mentioned reason. All these deviations from the calculations were significantly reduced when choosing a pump with FWHM 30 fs as could be seen in graphs A.14 and A.15.

To complement the above considerations, we can write the results of the calculations for selective excitation with a pump with frequency ϵ_B in positive times (for the case where we neglect the EEA):

$$\text{F-PP} \sim 0 \cdot G_{Ag}(\omega_{T_{Pr}}) - 2 \cdot \mu_B^4 G_{Bg}(\omega_{T_{Pr}}) \tag{3.17}$$

$$\text{F-2DES} \sim 0 \cdot G_{Ag}(\omega_{T_{Pr}}) G_{Bg}(\omega_\tau) - 2 \cdot \mu_B^4 G_{Bg}(\omega_{T_{Pr}}) G_{Bg}(\omega_\tau) \tag{3.18}$$

For $K_{annih} \ll K_{recomb}$, $\omega_{Pu} \sim \epsilon_B$, $T_{Pu} > 0$ we get

$$\text{F-PP} \sim -\mu_A^2 \mu_B^2 \cdot G_{Ag}(\omega_{T_{Pr}}) - 2 \cdot \mu_B^4 G_{Bg}(\omega_{T_{Pr}}) \tag{3.19}$$

$$\text{F-2DES} \sim -\mu_A^2 \mu_B^2 \cdot G_{Ag}(\omega_{T_{Pr}}) G_{Bg}(\omega_\tau) - 2 \cdot \mu_B^4 G_{Bg}(\omega_{T_{Pr}}) G_{Bg}(\omega_\tau) \tag{3.20}$$

For the negative times $T_{Pu} < 0$, we get for $\omega_{Pu} \sim \epsilon_B$ and $K_{recomb} \ll K_{annih}$:

$$\text{F-PP} \sim -2 \cdot \mu_A^2 \mu_B^2 \left(1 - e^{-K_{AB}|T_{Pu}|}\right) G_{Ag}(\omega_{T_{Pr}}) - 2 \cdot \mu_B^4 G_{Bg}(\omega_{T_{Pr}}) \tag{3.21}$$

$$\begin{aligned}\text{F-2DES} \sim &-2 \cdot \mu_A^2 \mu_B^2 \left(1 - e^{-K_{AB}|T_{Pu}|}\right) G_{Ag}(\omega_{T_{Pr}}) G_{Bg}(\omega_\tau) \\ &- 2 \cdot \mu_B^4 G_{Bg}(\omega_{T_{Pr}}) G_{Bg}(\omega_\tau)\end{aligned} \tag{3.22}$$

and for $K_{annih} \ll K_{recomb}$, $\omega_{Pu} \sim \epsilon_B$, $T_{Pu} < 0$:

$$\text{F-PP} \sim -\mu_A^2 \mu_B^2 \left(2 - e^{-K_{AB}|T_{Pu}|}\right) G_{Ag}(\omega_{T_{Pr}}) - 2 \cdot \mu_B^4 G_{Bg}(\omega_{T_{Pr}}) \tag{3.23}$$

$$\begin{aligned}\text{F-2DES} \sim &-\mu_A^2 \mu_B^2 \left(2 - e^{-K_{AB}|T_{Pu}|}\right) G_{Ag}(\omega_{T_{Pr}}) G_{Bg}(\omega_\tau) \\ &- 2 \cdot \mu_B^4 G_{Bg}(\omega_{T_{Pr}}) G_{Bg}(\omega_\tau)\end{aligned} \tag{3.24}$$

Now we will write results of the same calculations, now for selective excitation with pump with frequency ϵ_A.

$T_{Pu} > 0$, $\omega_{Pu} \sim \epsilon_A$, and $K_{recomb} \ll K_{annih}$:

$$\text{F-PP} \sim -2 \cdot \mu_A^4 e^{-K_{AB}T_{Pu}} G_{Ag}(\omega_{T_{Pr}}) - 2 \cdot \mu_A^2 \mu_B^2 \left(1 - e^{-K_{AB}T_{Pu}}\right) G_{Bg}(\omega_{T_{Pr}}) \tag{3.25}$$

$$\begin{aligned}\text{F-2DES} \sim &-2 \cdot \mu_A^4 e^{-K_{AB}T_{Pu}} G_{Ag}(\omega_{T_{Pr}}) G_{ag}(\omega_\tau) \\ &- 2 \cdot \mu_A^2 \mu_B^2 \left(1 - e^{-K_{AB}T_{Pu}}\right) G_{Bg}(\omega_{T_{Pr}}) G_{Ag}(\omega_\tau)\end{aligned} \tag{3.26}$$

$T_{Pu} > 0$, $\omega_{Pu} \sim \epsilon_A$ and $K_{annih} \ll K_{recomb}$:

$$\text{F-PP} \sim -\mu_A^4 \left(1 + e^{-K_{AB}T_{Pu}}\right) G_{Ag}(\omega_{T_{Pr}}) - \mu_A^2\mu_B^2 \left(2 - e^{-K_{AB}T_{Pu}}\right) G_{Bg}(\omega_{T_{Pr}}) \tag{3.27}$$

$$\begin{aligned}\text{F-2DES} \sim &-\mu_a^4 \left(1 + e^{-K_{AB}T_{Pu}}\right) G_{Ag}(\omega_{T_{Pr}})G_{Ag}(\omega_\tau) \\ &-\mu_A^2\mu_B^2 \left(2 - e^{-K_{AB}T_{Pu}}\right) G_{Bg}(\omega_{T_{Pr}})G_{Ag}(\omega_\tau)\end{aligned} \tag{3.28}$$

$T_{Pu} < 0$, $\omega_{Pu} \sim \epsilon_A$ and $K_{recomb} \ll K_{annih}$:

$$\text{F-PP} \sim -2 \cdot \mu_a^4 e^{-K_{AB}|T_{Pu}|} G_{Ag}(\omega_{T_{Pr}}) - 0 \cdot G_{Bg}(\omega_{T_{Pr}}) \tag{3.29}$$

$$\text{F-2DES} \sim -2 \cdot \mu_A^4 e^{-k_{AB}|T_{Pu}|} G_{Ag}(\omega_{T_{Pr}})G_{Ag}(\omega_\tau) - 0 \cdot G_{Bg}(\omega_{T_{Pr}})G_{Ag}(\omega_\tau) \tag{3.30}$$

$T_{Pu} < 0$, $\omega_{Pu} \sim \epsilon_A$ and $K_{annih} \ll K_{recomb}$:

$$\text{F-PP} \sim -\mu_A^4 \left(1 + e^{-K_{AB}|T_{Pu}|}\right) G_{Ag}(\omega_{T_{Pr}}) - \mu_A^2\mu_B^2 G_{bg}(\omega_{T_{Pr}}) \tag{3.31}$$

$$\begin{aligned}\text{F-2DES} \sim &-\mu_A^4 \left(1 + e^{-K_{AB}|T_{Pu}|}\right) G_{Ag}(\omega_{T_{Pr}})G_{Ag}(\omega_\tau) \\ &-\mu_A^2\mu_B^2 G_{Ag}(\omega_{T_{Pr}})G_{Ag}(\omega_\tau)\end{aligned} \tag{3.32}$$

In this section, we wanted to verify that our program in Quantarhei and, thus, our simulations are correct. We have predicted F-PP dynamics for selective excitation with a pump of only one molecule, A or B, and compared them to the simulations. The agreement is sufficiently satisfactory to say that the calculations and simulations are correct.

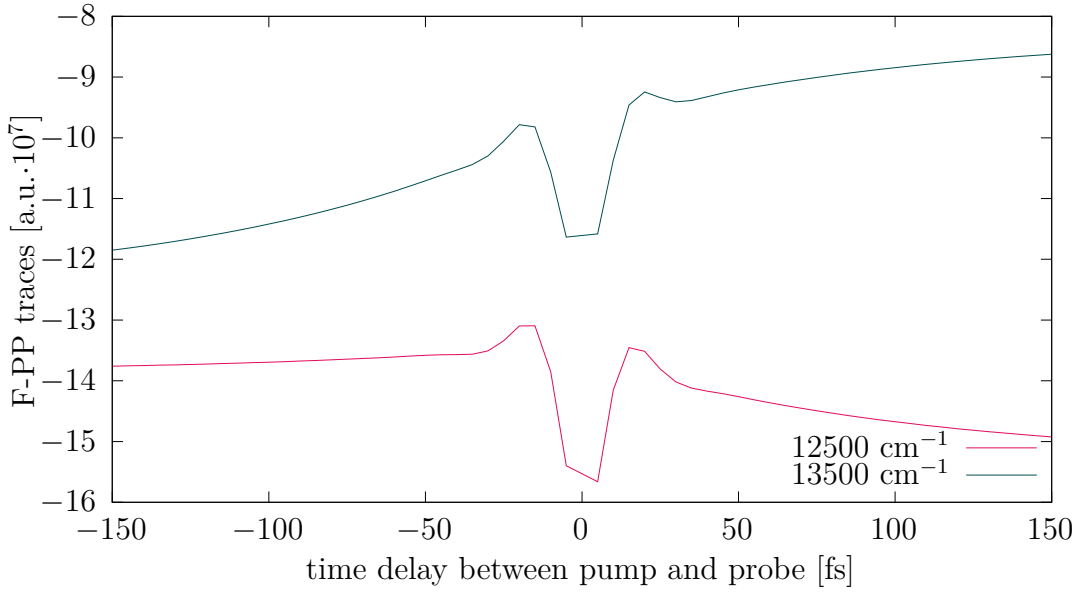

Figure 3.8: F-PP traces for frequencies ϵ_A and ϵ_B, pump frequency 12500 cm^{-1} (selective excitation of molecule B). For positive times, the signal from molecule A is decreasing and signal from B is increasing. Even for $\mu_A = \mu_B$, molecule A's signal is not constant in negative times, it is increasing with $|T_{Pu}|$.

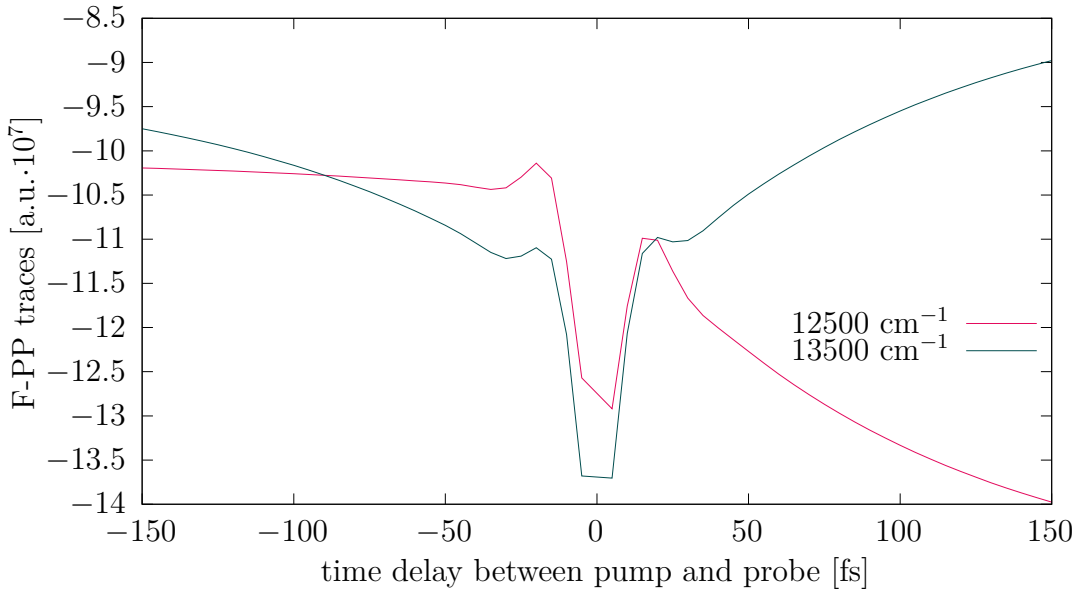

Figure 3.9: F-PP traces for frequencies ϵ_A and ϵ_B, pump frequency 13500 cm^{-1} (selective excitation of molecule A). For positive times, the signal from molecule A is decreasing and signal from B is increasing. Even for $\mu_A = \mu_B$, signal from molecule A is not constant in negative times, it is decreasing with increasing $|T_{Pu}|$, signal from B is again constant.

3.5.2 Chirped pulses

Chirped pulses find frequent application in spectroscopy laboratories, as elucidated by Nuernberger et al. [2007], among others. Therefore, it would be beneficial to find out how the chirped probes influence F-PP spectra. Furthermore, chirp represents an inherent characteristic of all pulses in laboratory settings, stemming from their path through various optical components in the aperture. The refractive index of these components varies with the frequency of light, causing a positive chirp (see section 2.3). This means the pulse frequency increases with time (longer wavelengths arrive earlier). In our simulations, we produce a chirped pulse using a time-dependent phase shift (equation 2.14), which gives us a linearly time-dependent frequency (equation 2.19).

For 100 fs time delay between maxima of frequencies $\epsilon_B = 12500\,\mathrm{cm}^{-1}$ and $\epsilon_A = 13500\,\mathrm{cm}^{-1}$ we have set these parameters:

$c_2 = 530.9\,\mathrm{fs}^2{\cdot}\mathrm{rad}^{-1}$
$c_2' = 0.00187\,\mathrm{fs}^{-2}{\cdot}\mathrm{rad}$
$FWHM' = 197\,\mathrm{fs}$

To check, that the program and above-mentioned parameters are correct, we can analyse time dependence of excited state populations after excitation with chirped pulse. In graph 3.12 we can see excited state populations time evolution for heterodimer AB, which interact with two positively chirped pulses (defined as above, with centres in $t = 0\,\mathrm{fs}$ and $t = 10\,\mathrm{fs}$). At first, we can observe rise of population $|\mathrm{B}\rangle\langle\mathrm{B}|$, reaching half of its first local maximum at $t \approx -50\,\mathrm{fs}$, which corresponds to time, when frequency ϵ_B reaches its maximum in pulse. Later we can see increase in the population of $|\mathrm{A}\rangle\langle\mathrm{A}|$, which reaches half of its maximum for $t \approx 50\,\mathrm{fs}$. After reaching its global maximum in $t \approx 100\,\mathrm{fs}$, it starts decreasing due to energy transfer to molecule B, which excited state population is on the contrary increasing. We can see that not only times when population of excited state of A respective B reaches half of its first maximum, but also times in which they have its first local or global maximum are distant from each other 100 fs, which is the time difference we set between maxima of frequencies ϵ_A and ϵ_B. This is strong evidence that calculations in section 2.3 are correct.

At first glance, based on the Feynman diagrams, it looks like there will be only shift for traces of different frequencies. To predict, how would the traces behave, we can at first deduce from figures 3.10 and 3.11 the direction of the shift for particular frequencies. For the chirped probe (see picture 3.10), T_B denotes time delay between the centre of the pump and the maxima of lower energy frequency ϵ_B in the probe (red colour on the picture), T_0 is time delay between centres of the pump and probe, and finally, T_A states for time delay between the centre of the pump and the maxima of higher energy frequency ϵ_A in the probe. The pulse overlap of the pump and probe for the examined frequency occurs, when $T_x = 0\,\mathrm{fs}$.

We can deduce from the figure that

$$T_0 = T_B + \frac{1}{2}\Delta T = T_A - \frac{1}{2}\Delta T, \tag{3.33}$$

where ΔT is time delay between frequencies ϵ_A and ϵ_B in the chirped probe. The time delay between pulse overlap of centres of pulses ($T_0 = 0$) and of energies ϵ_B ($T_B = 0$) is $+\frac{1}{2}\Delta T$, for energy ϵ_A ($T_A = 0$), it is $-\frac{1}{2}\Delta T$. So the trace of lower energy will be shifted to the right and for higher energy to the left for the chirped probe. This partially corresponds with simulation in graph 3.13, nevertheless, the shift is only about $-20\,\mathrm{fs}$ and $+20\,\mathrm{fs}$ instead of $-50\,\mathrm{fs}$ and $+50\,\mathrm{fs}$ as calculated above. We will discuss this later.

For the chirped pump, the situation is quite the opposite (again, consistent with graph 3.15, except that the shift is smaller than predicted).

However, for the chirped pump and probe, the time delay between the pump and probe is the same for different frequencies. There should not be any shift in time zero for any of the traces, which, again, is in accordance with the simulation (see graph 3.14).

Nevertheless, the situation is not that simple; as we can see from the graphs (3.13,3.15, 3.14), there are also oscillations. Compared with the traces for non-chirped pulses, these waves are stretched in time. We will now explain why. See second row in the table 3.7 of Feynman diagrams depicting the pulse overlap. There is coherence $|2\rangle\langle 1|$ in the waiting time $|T_{Pu}|$. This pathway will contribute to the trace of either A or B if and only if 2 corresponds to the exact frequency $13500\,\mathrm{cm}^{-1}$ or $12500\,\mathrm{cm}^{-1}$. In this row, the first diagram from the left significantly contributes only if the T_2 time delay between the maxima of frequency 2 in the pump and probe is zero. This means that these oscillations have their centre in $\pm\frac{1}{2}\Delta T$. If 1=2, we get a non-oscillating signal, which even more contributes to the peak.

In the table, there are diagrams that contribute to the signal for $T_2 = 0$ for both 1 and 2 molecules, but there are, on the contrary, contributions to the time $T_1 = 0$ again for both 1 and 2. This means that for both traces A and B, there is some peak for $\pm\frac{1}{2}\Delta T$.

Fascinating is the second diagram in the second row. There is again coherence $|2\rangle\langle 1|$, now it will contribute to the signal from 2 if $T_1 = 0$. We will see this contribution even if 1 is neither A nor B. This gives us an oscillating signal for each frequency in the excitation spectrum of A or B with the centre in T_1=0. Because of this, the main shifted peak with the centre in $\pm\frac{1}{2}\Delta T$ is widened, as well as the oscillation peak from coherence contribution. Because frequency $13000\,\mathrm{cm}^{-1}$ is represented in the pulse spectrum with the largest amplitude - as it is mean frequency, contributions including this frequency will be strongly influencing the signal and reducing the shift of traces (because $T_0 = 0$ corresponds to zero shift of time-zero gap). This phenomenon is further enhanced by the fact that frequencies between 12500 and $13500\,\mathrm{cm}^{-1}$, which reduce the shift of zero-time peak, contribute strongly to the excitation spectrum of heterodimer AB (see figure 3.2). On the other hand, excitation spectrum is rapidly decreasing for frequencies lower than $12500\,\mathrm{cm}^{-1}$ or higher than $13500\,\mathrm{cm}^{-1}$. Moreover, these frequencies have also a weak amplitude in our Gaussian-shaped pulses. This suggests that the contribution of frequencies $12500\,\mathrm{cm}^{-1} < \omega < 13500\,\mathrm{cm}^{-1}$, which reduce time-shift from zero for traces, is higher than contributions of frequencies $\omega < 12500\,\mathrm{cm}^{-1}$ or $\omega > 13500\,\mathrm{cm}^{-1}$, which enlarge the shift.

We can see that more than half of possible Feynman diagrams in figure 3.7 contribute to this shift for correct frequencies (not only the one mentioned).

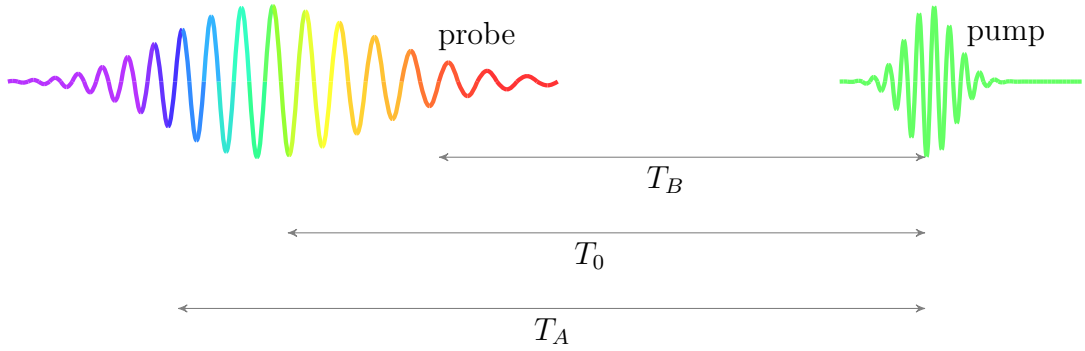

Figure 3.10: Time delays between pump and chirped probe for maxima of different frequencies. T_B is the time delay between maximal amplitude of frequency ϵ_B in pump and probe. T_A corresponds to frequency ϵ_A and T_0 is time delay between pulse centres of pump and probe (corresponds to frequency 13000 cm^{-1}).

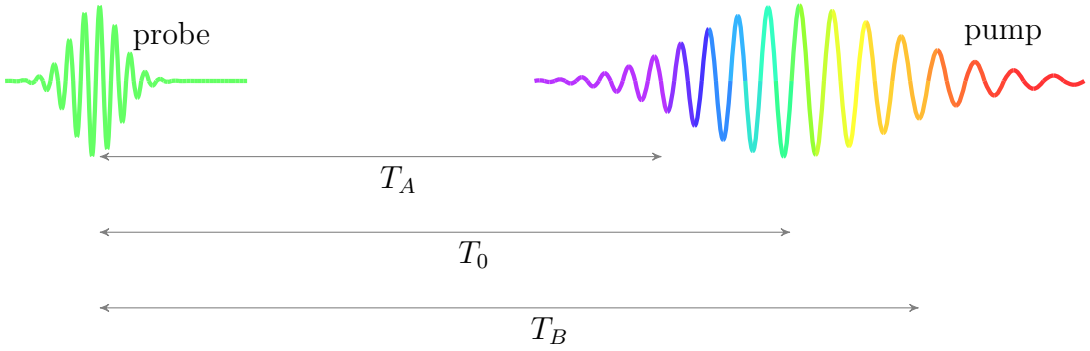

Figure 3.11: Time delays between probe and chirped pump for maxima of different frequencies.

In this section, we wanted to investigate the effect of a pulse chirp on the F-PP spectrum. We have implemented the pulse chirp into the Quantarhei and verified its correctness by calculating the dynamics of excited state populations of heterodimer AB, which corresponds with the expectations. Further, we have shown that the pulse chirp does not change the dynamics of F-PP spectra at later times. Around zero, in the case of a chirped probe, there is a shift of traces to the right for lower frequencies and to the left for higher frequencies. For the pump chirp, the situation is opposite. The distance of zero-time peaks for frequencies ϵ_A and ϵ_B is lower than the distance of their maxima in chirped pulse due to contributions of other frequencies.

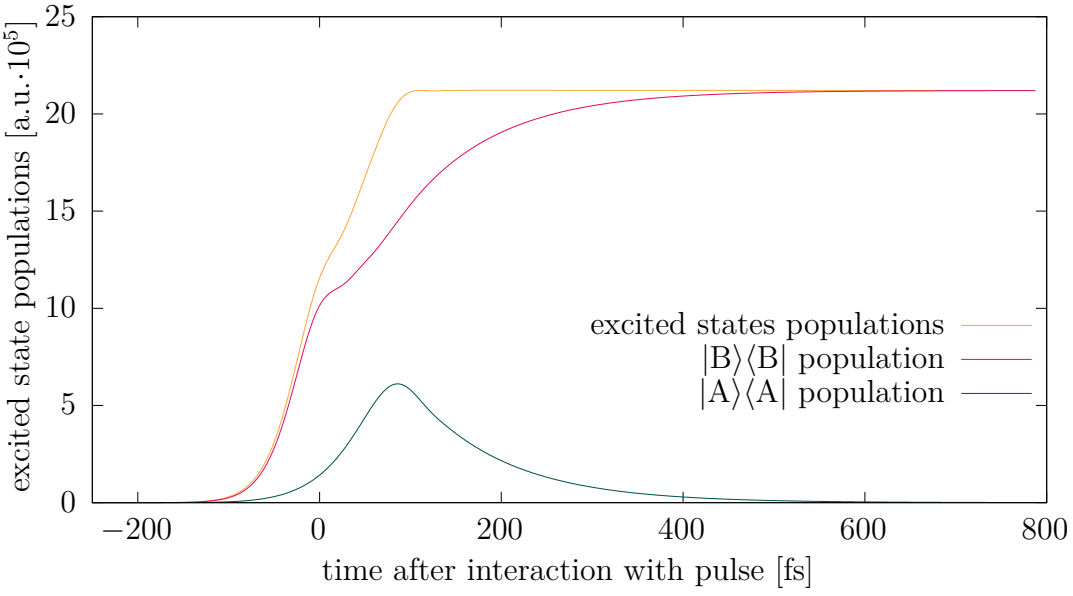

Figure 3.12: Dynamics of heterodimer AB after excitation with a chirped pulse. Frequency ϵ_B arrives first, increasing the population of $|\mathrm{B}\rangle\langle\mathrm{B}|$. Later, population $|\mathrm{A}\rangle\langle\mathrm{A}|$ increases (reaches its maximum in $t = 100\,\mathrm{fs}$). Nevertheless, after a while, it starts decreasing due to energy transfer to molecule B.

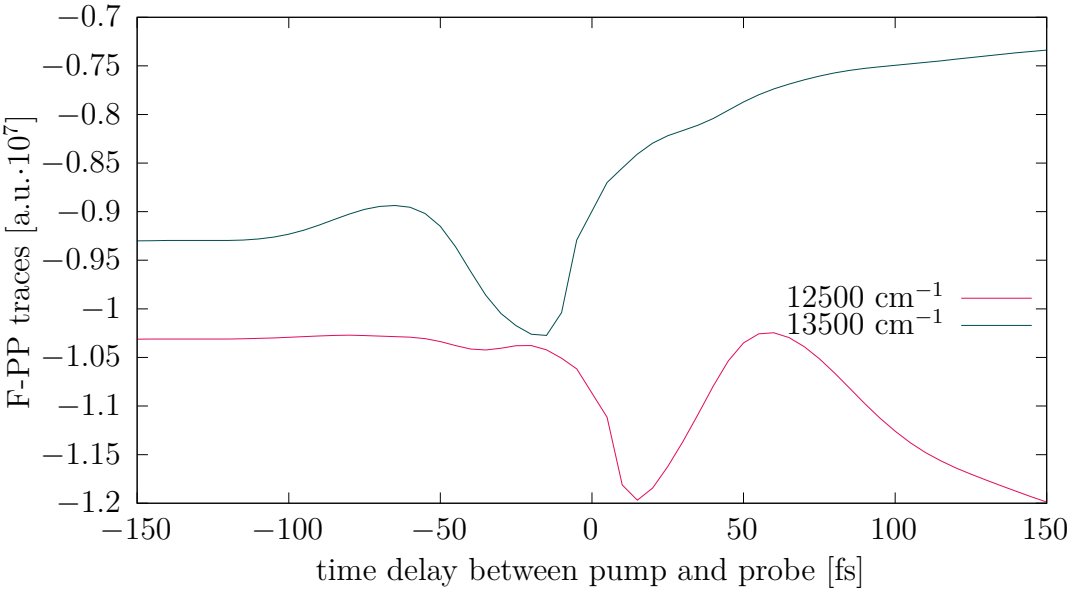

Figure 3.13: F-PP traces for frequencies ϵ_A and ϵ_B for chirped probe. The signal from molecule A is shifted to negative times; on the contrary, the signal from B is shifted to the right to positive times. A peak around zero for a particular frequency is broadened. Except for the behaviour around time zero, the dynamics is similar to the situation without chirp - in positive times, the signal from A decreases, and the signal from molecule B increases. In negative times, the signal remains constant (for longer times, see graph A.25).

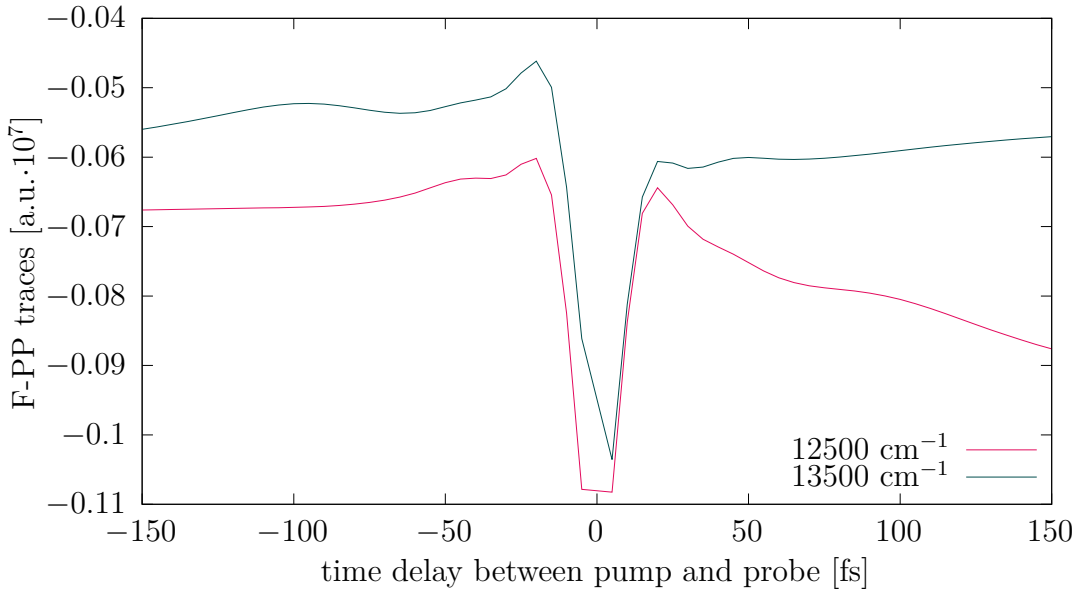

Figure 3.14: F-PP traces for frequencies ϵ_A and ϵ_B, chirped probe and chirped pump. There is no shift of time zero for any of the traces.

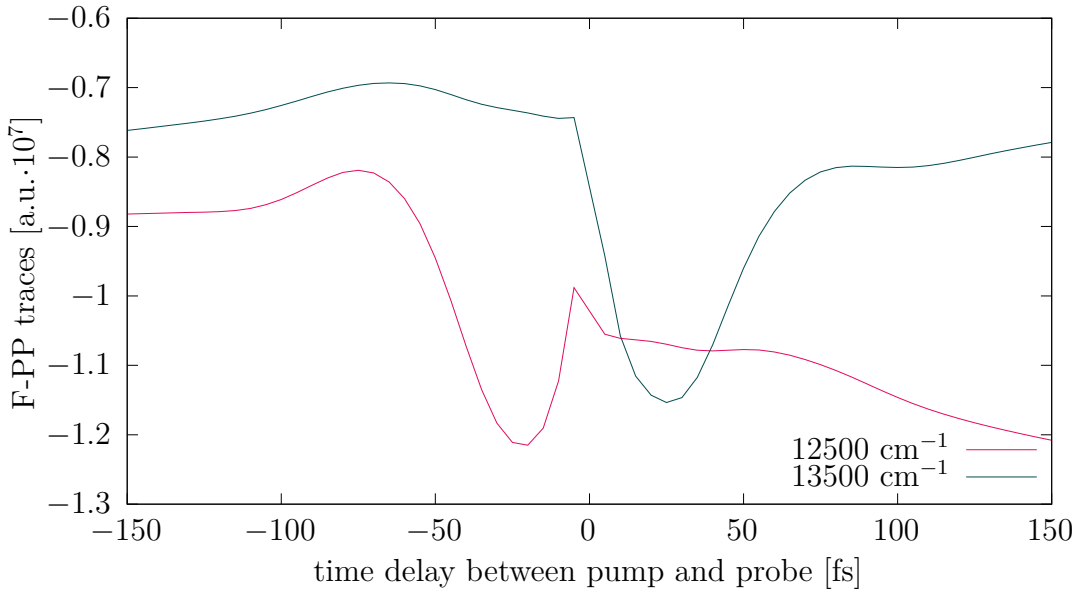

Figure 3.15: F-PP traces for frequencies ϵ_A and ϵ_B, chirped pump. The signal from molecule A is shifted to the right and the signal from B to the left (opposite situation to the one with chirped probe in graph 3.13). A peak around zero for a particular frequency is broadened. Except for the behaviour around time zero, the dynamics is similar to the situation without chirp - in positive times, the signal from A decreases, and the signal from molecule B increases. In negative times, the signal remains constant.

4. Comparison to experimental data

The results were compared to experimental data obtained from the article by Malý and Brixner [2021]. For the measurement, Malý et al. used a squarine heterodimer sample (see picture 4.1), which has two prominent absorption peaks at 1.73 eV (13953.4 cm^{-1}) and 1.88 eV (15163.2 cm^{-1}). Like in our model, there is an energy transfer from the higher to the lower energy state, with a transition rate constant $K_{SQA \to SQB} \approx 30$ fs.

In accordance with our computation, experimental data show a decrease in signal from the higher energy level, and in addition to that, signal from the lower energy level increases with the time delay between pump and probe. For the negative time, the signal is relatively constant for both energies. This suggests that the oscillator strength of SQA is almost the same as that of SQB. The data were measured with chirp-compensated, near-transform-limited pulses. In the data (see graph 4.2), there is a little but visible displacement from zero, which could be caused by an almost negligible chirp of pulses but could also be only a mere accident caused by a limited accuracy of real-life measurement.

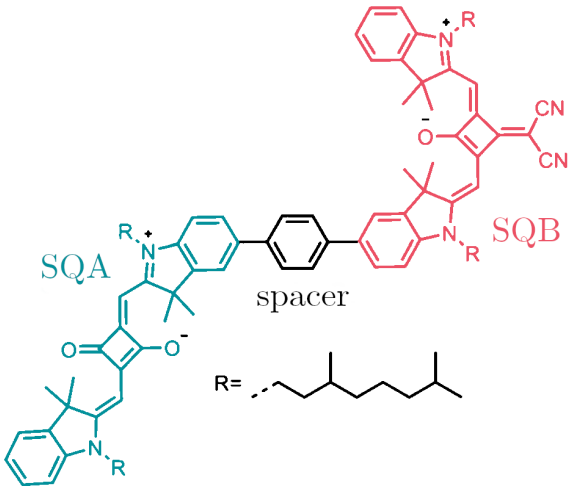

Figure 4.1: Squaraine heterodimer with two prominent absorption peaks at 1.73 eV (13953.4 cm^{-1}) corresponding to SQB and 1.88 eV (15163.2 cm^{-1}) related to SQA. There is also a photophysically inactive spacer which provides weak coupling of SQA and SQB. Figure provided by Malý and Brixner [2021].

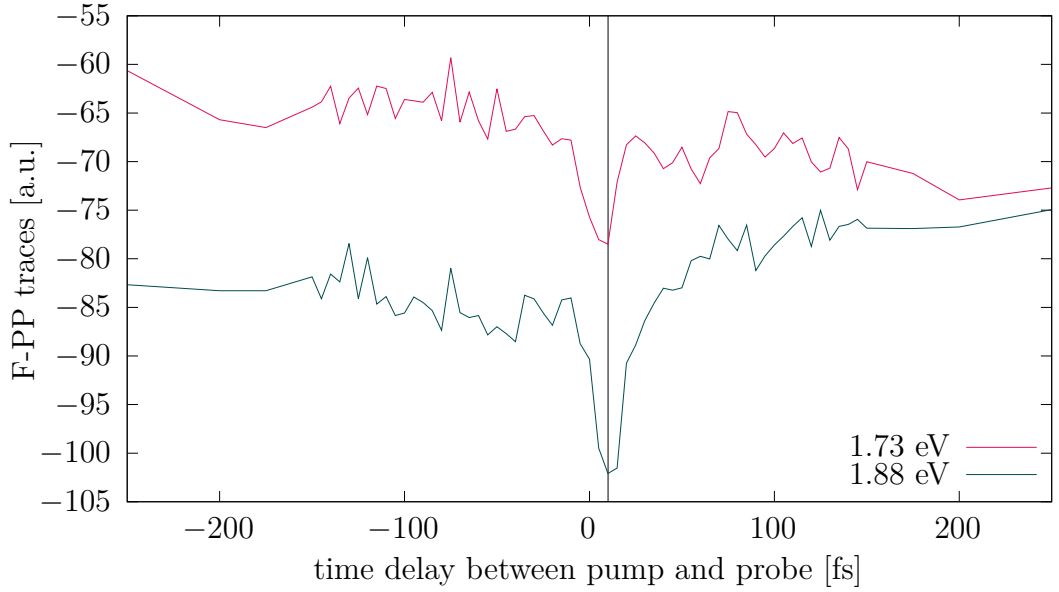

Figure 4.2: F-PP traces for frequencies ϵ_{SQA} and ϵ_{SQB}, measurement of squaraine heterodimer provided by Malý and Brixner [2021]. The signal from SQA is decreasing in time due to energy transfer from SQA to SQB. The signal from SQB is thus increasing with T_{Pu}. In negative times, the signal of both molecules is almost constant.

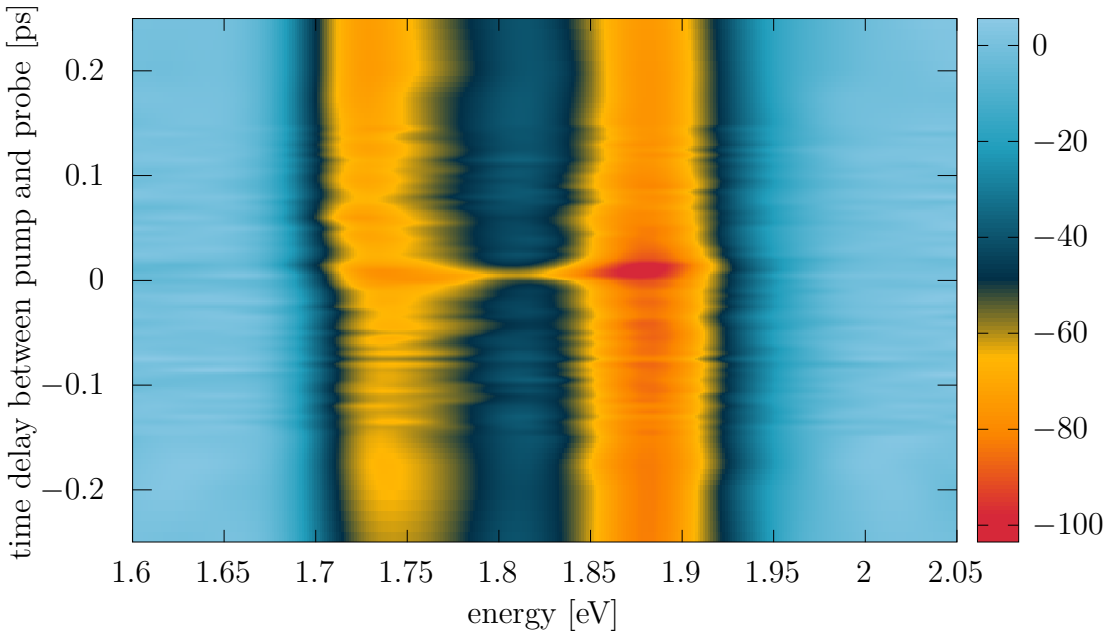

Figure 4.3: F-PP spectrum of squaraine heterodimer, measured by Malý and Brixner [2021].

5. Summary

The main aim of this work was to get acquainted with the fluorescence-detected transient absorption spectroscopy method and to investigate the behaviour of its spectra under different conditions.

Foremost, we successfully implemented this method into Quantarhei, a molecular open quantum systems simulator developed by Mančal [2020]. This simulator enables the creation of complex molecules and offers many possibilities, such as a predefined Förster or Redfield relaxation tensor. It is now possible to simulate F-PP spectra even for such complicated structures as light-harvesting complex II (LHC II, described, for example, by Kühlbrandt [1994]) in interaction with pulses with parameters which we can choose to fit our investigated situation or experiment best. This option could be helpful for further research.

One of our primary concerns was the problem of incoherent mixing, where because of exciton-exciton annihilation, the ground-state bleach signal increases compared to the signal of stimulated emission. The ratio between SE and GSB decreases as $\frac{1}{N}$ (see equation 1.22) which reduces the visibility of dynamics as shown by Bolzonello et al. [2023] (see section 1.5 and section 3.3). Because of this, we have investigated the behaviour of F-PP spectra in negative times and the possibility of subtracting them from F-PP spectra in positive times to remove the consequences of incoherent mixing.

By writing out all unique Feynman diagrams for heterodimer of two-level molecules A and B and summing their contributions, we have calculated the signal dynamics from molecules A and B both in positive and negative times. For positive times, the sample interacts at first with the pump, and after the time T_{Pu}, twin probe pulses measure a change in the excitation spectrum. The dynamics of the signal is straightforward (see graph 3.5 or equations 3.1 and 3.2); the signal from molecule A is decreasing with increasing time delay between pump and probe T_{Pu}. On the contrary, the signal from B is increasing, which corresponds to the energy transfer from the molecule A to the molecule B.

In negative times, the situation is more complicated. The system first interacts with probes and, consequently, with the pump. The fluorescence response depends heavily on a mutual relation between the oscillatory strengths of the transition from the ground state to the excited state of molecule A and molecule B. For $\mu_A > \mu_B$, the signal from molecule A is decreasing (see graph 3.3 and equations 3.5 and 3.7). On the contrary, for $\mu_A < \mu_B$, the signal from the molecule A increases with rate K_{AB}. The signal from molecule B is constant for both cases (see graph 3.4). For special condition $\mu_A = \mu_B$, traces for both A and B are constant in negative waiting time T_{Pu}.

Consequently, we have tried to find the coefficients with which we must multiply the F-PP spectrum with EEA in positive times and the F-PP spectrum with EEA in negative times to obtain by their subtraction the F-PP spectrum without EEA in positive times. The coefficients are different for trace from molecule A (see equations 3.14) and for B (equations 3.16) even for $\mu_A = \mu_B$, which provides constant F-PP spectrum in negative times. The subtraction would have to be

done separately for each trace corresponding to a different frequency. Moreover, the coefficients depend on μ_A and μ_B. This makes the subtraction complicated even for the most straightforward system, like a heterodimer of two two-level molecules we used. This suggests that it would not be possible to convert F-PP spectra with EEA to F-PP spectra without EEA (which correspond to PP spectra), even for other molecules.

Subsequently, we have analysed F-PP spectra behaviour during pulse overlap ($T_{Pu} = 0$). Although the spectral shape around time zero is very complicated because it is influenced not only by the system but also by the shape of the pulses, we can draw some conclusions. We have written out all possible Feynman diagrams (see figure 3.7), which were used for further research.

To verify that our simulations are correct, we have compared them with our theoretical results for a model situation of selective excitation. In this, we selectively excited only one molecule (A or B) with the pump and consequently observed its F-PP spectra. For selective excitation of molecule B, we can see dynamics only in negative times, where the signal from molecule A is increasing with $|T_{Pu}|$ (see graph 3.8 equations 3.18,3.20,3.22 and 3.24). If we selectively excite only molecule A with the pump, there is still visible dynamics. The signal from A decreases with $|T_{Pu}|$ both in positive and negative times (see graph 3.9 equations 3.26,3.28,3.30 and 3.32). The signal from B is constant in negative and increases in positive times. We can see reduced oscillations, especially for excitation with a narrower pump pulse ($FWHM = 30\,\mathrm{fs}$, see graphs A.14 and A.15). All this is in accordance with theoretical predictions.

Finally, we were interested in how a pulse chirp affects the F-PP spectrum. From the Feynman diagrams, we have concluded that there will be a shift in time for traces dependent on their frequency and whether the pump or probe is chirped. We will now describe the situation for probe chirp. For the chirped pump, the situation will be quite the opposite. Traces corresponding to frequencies higher than the mean frequency of the chirped probe (for example, ϵ_A) will be shifted to the left to negative times. On the contrary, traces for lower frequencies (for example, ϵ_B) will shift to the right to positive times. As could be concluded from Feynman diagrams for pulse overlap (see figure 3.7), around time zero, various coherence contributions influence the spectrum, which leads to an extension of the zero-time peak and oscillation. Further, the influence of Feynman diagrams with other frequencies in the excitation spectrum leads to a reduction of a shift for traces that was predicted by Feynman diagrams for longer times. We thought the shift would be precisely the time delay between a particular frequency and the middle of the pulse chirp (for our calculations, 50 fs). Nevertheless, the shift is reduced, as could be seen in graphs 3.13 and 3.15. This is due to the influence of pathways, which describes interaction with a pulse with frequencies between ϵ_B and ϵ_A.

All theoretical predictions were calculated using a perturbation approach with an approximation of delta pulses. In the meantime, all simulations were obtained by numerical solution of the Liouville von Neumann equation with Gaussian-shaped pulses. Despite the different approaches, the primary behaviour of the dynamics is the same in both results.

Additionally, we have compared our results with experimentally measured data by Malý and Brixner [2021]. In the experiment, squaraine heterodimer molecules (see figure 4.1) were used as a sample. This molecule is very similar to our model system. It has two main absorption peaks, and the heterodimer is weakly coupled, which leads to energy transport from SQA to SQB molecule in the dimer. Identical properties of the simulations and experimental F-PP spectra further prove our calculations' accuracy (see graphs 3.5 and 4.2).

For these reasons, we believe that both computations were correct and that the implementation of F-PP in Quantarhei could be used for further research without any problems.

Conclusion

In this thesis, we have investigated various properties of the F-PP signal and implemented this method in the Quantarhei simulator. Theoretical computations agreed with simulations, which were obtained using different approaches. Some of the properties were successfully compared with the experiment.

In F-PP spectra for an exemplary heterodimer, the energy transfer dynamics is present for negative waiting times between pump and probe, and it disappears only for a special choice of oscillatory strengths. Therefore, we can conclude that the dynamics will be visible even for more complicated systems. Furthermore, the presented evidence illustrates that it is, in general, not possible to use the negative-waiting-time data to suppress incoherent mixing and highlight excited-state dynamics.

Finally, our computations suggest that pulse chirp does not change dynamics in longer times. Thus, it is not necessary to use chirp-compensated pulses to obtain results consistent with theory, of course, excluding pulse overlap.

The next step in this research could be to experimentally verify our conclusions about negative time behaviour for different oscillatory strengths of participating transitions and pulse chirp influence on F-PP spectra. For this, it would be ideal to use squaraine heterodimer again because of its useful properties and similarities to our theoretical model.

Another improvement would be modifying the program for the simulations of F-PP and F-2DES spectra so that some calculations can be performed parallelly. This would allow us to calculate spectra for more complex systems, such as the previously mentioned LHC II, in a reasonable time.

Bibliography

Luca Bolzonello, Matteo Bruschi, Barbara Fresch, and Niek F van Hulst. Nonlinear optical spectroscopy of molecular assemblies: What is gained and lost in action detection? *The Journal of Physical Chemistry Letters*, 14(50):11438–11446, 2023.

Robert W Boyd, Alexander L Gaeta, and Enno Giese. Nonlinear optics. In *Springer Handbook of Atomic, Molecular, and Optical Physics*, pages 1097–1110. Springer, 2008.

Matteo Bruschi, Federico Gallina, and Barbara Fresch. Simulating action-2d electronic spectroscopy of quantum dots: insights on the exciton and biexciton interplay from detection-mode and time-gating. *Physical Chemistry Chemical Physics*, 24(45):27645–27659, 2022.

Matteo Bruschi, Luca Bolzonello, Federico Gallina, and Barbara Fresch. Unifying nonlinear response and incoherent mixing in action-2d electronic spectroscopy. *The Journal of Physical Chemistry Letters*, 14(30):6872–6879, 2023.

Paul Busch. *The Time-Energy Uncertainty Relation*, pages 69–98. Springer Berlin Heidelberg, Berlin, Heidelberg, 2002. ISBN 978-3-540-45846-3. doi: 10.1007/3-540-45846-8_3. URL `https://doi.org/10.1007/3-540-45846-8_3`.

Kateřina Charvátová. Optimization of the signal from pigment triplet states in photosystem i. *Bachelor thesis, Charles University, MFF UK*, 2022.

Wim P de Boeij, Maxim S Pshenichnikov, and Douwe A Wiersma. System- bath correlation function probed by conventional and time-gated stimulated photon echo. *The Journal of Physical Chemistry*, 100(29):11806–11823, 1996.

Daniel Fersch, Pavel Malý, Jessica Rühe, Victor Lisinetskii, Matthias Hensen, Frank Würthner, and Tobias Brixner. Single-molecule ultrafast fluorescence-detected pump–probe microscopy. *The Journal of Physical Chemistry Letters*, 14(21):4923–4932, 2023.

Michael Kasha. Characterization of electronic transitions in complex molecules. *Discussions of the Faraday society*, 9:14–19, 1950.

Werner Kühlbrandt. Structure and function of the plant light-harvesting complex, lhc-ii. *Current Opinion in Structural Biology*, 4(4):519–528, 1994.

Oliver Kühn, Tomas Mancal, and Tõnu Pullerits. Interpreting fluorescence detected 2d electronic spectroscopy. *arXiv preprint arXiv:1912.09471*, 2019.

Tenzin Kunsel, Vivek Tiwari, Yassel Acosta Matutes, Alastair T Gardiner, Richard J Cogdell, Jennifer P Ogilvie, and Thomas LC Jansen. Simulating fluorescence-detected two-dimensional electronic spectroscopy of multichromophoric systems. *The Journal of Physical Chemistry B*, 123(2):394–406, 2018.

Pavel Malý. Comparison of perturbative and non-perturbative approaches to optical spectroscopy. *Bachelor thesis, Charles University, MFF UK*, 2012.

Pavel Malý and Tobias Brixner. Fluorescence-detected pump–probe spectroscopy. *Angewandte Chemie International Edition*, 60(34):18867–18875, 2021.

Pavel Malý and Tomáš Mančal. Signatures of exciton delocalization and exciton–exciton annihilation in fluorescence-detected two-dimensional coherent spectroscopy. *The Journal of Physical Chemistry Letters*, 9(19):5654–5659, 2018.

Pavel Malý, Stefan Mueller, Julian Lüttig, Christoph Lambert, and Tobias Brixner. Signatures of exciton dynamics and interaction in coherently and fluorescence-detected four-and six-wave-mixing two-dimensional electronic spectroscopy. *The Journal of Chemical Physics*, 153(14), 2020.

T Mančal. Quantarhei: Molecular open quantum systems package, 2020.

Volkhard May and Oliver Kühn. *Charge and energy transfer dynamics in molecular systems*. John Wiley & Sons, 2023.

Shaul Mukamel. Principles of nonlinear optical spectroscopy, 1995.

Patrick Nuernberger, Gerhard Vogt, Tobias Brixner, and Gustav Gerber. Femtosecond quantum control of molecular dynamics in the condensed phase. *Physical Chemistry Chemical Physics*, 9(20):2470–2497, 2007.

David Paleček, Petra Edlund, Emil Gustavsson, Sebastian Westenhoff, and Donatas Zigmantas. Potential pitfalls of the early-time dynamics in two-dimensional electronic spectroscopy. *The Journal of Chemical Physics*, 151 (2), 2019.

William W Parson. *Modern optical spectroscopy*, volume 2. Springer, 2007.

Sebastian Schott, Andreas Steinbacher, Johannes Buback, Patrick Nuernberger, and Tobias Brixner. Generalized magic angle for time-resolved spectroscopy with laser pulses of arbitrary ellipticity. *Journal of Physics B: Atomic, Molecular and Optical Physics*, 47(12):124014, 2014.

Howe-Siang Tan. Theory and phase-cycling scheme selection principles of collinear phase coherent multi-dimensional optical spectroscopy. *The Journal of chemical physics*, 129(12), 2008.

Rick Trebino. *Frequency-Resolved Optical Gating: The Measurement of Ultrashort Laser Pulses: The Measurement of Ultrashort Laser Pulses*. Springer Science & Business Media, 2000.

Leonas Valkunas, Darius Abramavicius, and Tomas Mancal. *Molecular excitation dynamics and relaxation: quantum theory and spectroscopy*. John Wiley & Sons, 2013.

List of Figures

List of Abbreviations

F-PP .... fluorescence-detected pump-probe spectroscopy
PP ..... pump-probe spectroscopy
F-2DES .. fluorescence-detected two-dimensional electronic spectroscopy
2DES .... two-dimensional electronic spectroscopy
GSB ..... ground state bleach (type of contribution to the signal)
SE ..... stimulated emission (type of contribution to the signal)
ESA ..... excited state absorption (type of contribution to the signal)
ESA 2 ... excited state absorption, which ends in higher excited state
EEA ..... exciton-exciton annihilation
RWA .... rotating wave approximation
a.u. ..... arbitrary units
SQA ..... squaraine molecule A in squaraine heterodimer
SQB ..... squaraine molecule B in squaraine heterodimer
GVD .... group-velocity dispersion

A. Attachments

A.1 Parameters used in simulations

$\epsilon_A = 13500\,\mathrm{cm}^{-1}$	frequency of energy transition between ground state and excited state of molecule A
$\epsilon_B = 12500\,\mathrm{cm}^{-1}$	frequency of energy transition between ground state and excited state of molecule B
$K_{AB} = \frac{1}{100}\,\mathrm{fs}^{-1}$	rate constant of the energy transfer from molecule A to molecule B
$\Gamma_{pd} = \frac{1}{20}\,\mathrm{fs}^{-1}$	rate constant of dephasing of the coherences
$\Gamma'_{AB} = \frac{1}{10}\,\mathrm{fs}^{-1}$	additional rate constant of dephasing of the coherences between excited states of molecules A and B
$K_{annih} = \frac{1}{20}\,\mathrm{fs}^{-1}$	rate constant of exciton-exciton annihilation (for the case when we neglect EEA, it was set extremely small: $10^{-34}\,\mathrm{s}^{-1}$)
$K_{recomb} = 1\,\mathrm{ns}^{-1}$	fluorescence rate constant
$FWHM = 15\,\mathrm{fs}$	full width half maximum for pump and probe pulses
ω_0=13000 cm^{-1}	mean frequency of the pulses
$c_2 = 530.9\,\mathrm{fs}^2{\cdot}\mathrm{rad}^{-1}$	pulse chirp parameter
$c'_2 = 0.00187\,\mathrm{fs}^{-2}{\cdot}\mathrm{rad}$	pulse chirp parameter
$FWHM' = 197\,\mathrm{fs}$	full width half maximum for chirped pump and probe pulses

A.2 Feynman diagrams for heterodimer AB for positive times

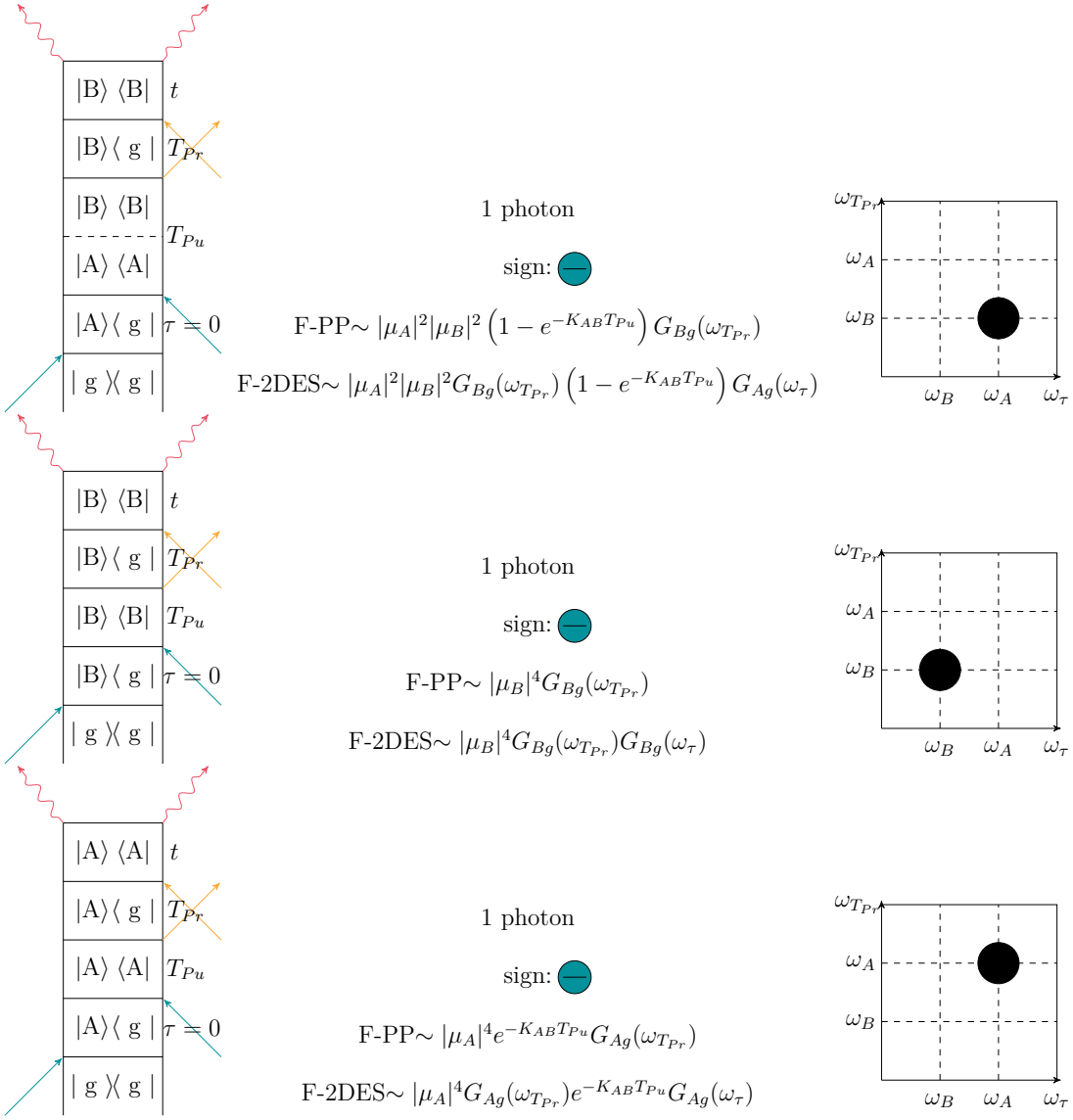

Figure A.1: Stimulated emission Liouville pathways for heterodimer (left column), corresponding FPP and F-2DES spectra equations (middle), F-2DES spectra visualization (right column).

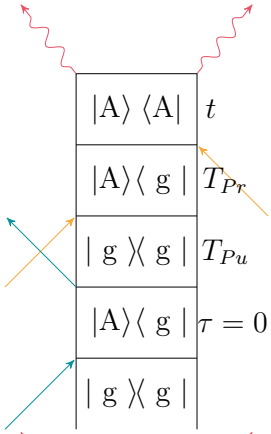

1 photon

sign: —

F-PP$\sim |\mu_A|^4 G_{Ag}(\omega_{T_{Pr}})$

F-2DES$\sim |\mu_a|^4 G_{Ag}(\omega_{T_{Pr}}) G_{Ag}(\omega_\tau)$

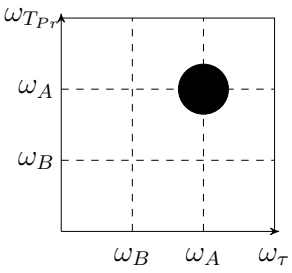

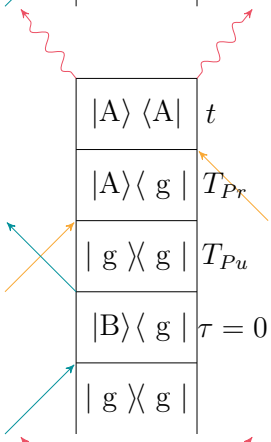

1 photon

sign: —

F-PP$\sim |\mu_A|^2 |\mu_B|^2 G_{Ag}(\omega_{T_{Pr}})$

F-2DES$\sim |\mu_A|^2 |\mu_B|^2 G_{Ag}(\omega_{T_{Pr}}) G_{Bg}(\omega_\tau)$

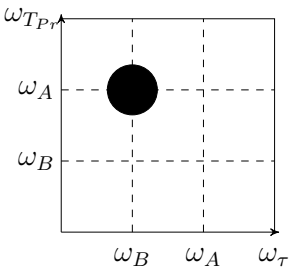

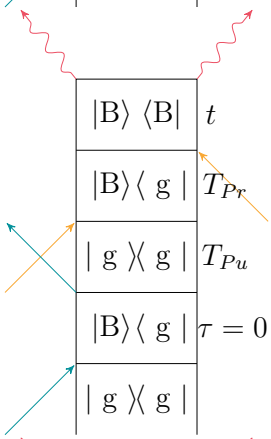

1 photon

sign: —

F-PP$\sim |\mu_B|^4 G_{Bg}(\omega_{T_{Pr}})$

F-2DES$\sim |\mu_B|^4 G_{Bg}(\omega_{T_{Pr}}) G_{Bg}(\omega_\tau)$

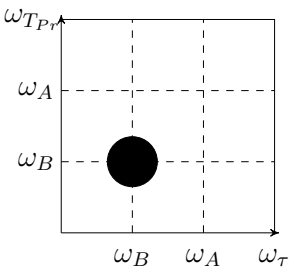

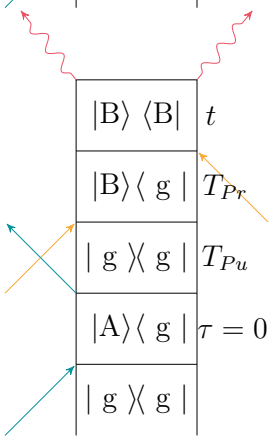

1 photon

sign: —

F-PP$\sim |\mu_A|^2 |\mu_B|^2 G_{Bg}(\omega_{T_{Pr}})$

F-2DES$\sim |\mu_A|^2 |\mu_B|^2 G_{Bg}(\omega_{T_{Pr}}) G_{Ag}(\omega_\tau)$

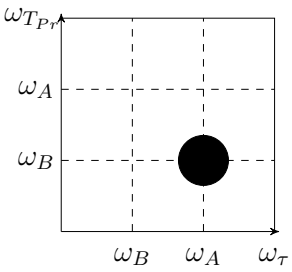

Figure A.2: Ground state bleach Liouville pathways for heterodimer (left column), corresponding FPP and F-2DES spectra equations (middle), F-2DES spectra visualization (right column).

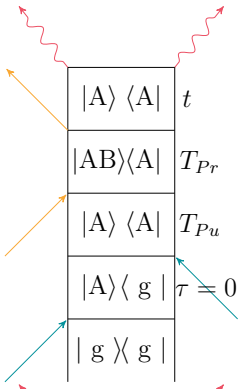

1 photon

sign: —

F-PP$\sim |\mu_A|^2|\mu_B|^2 e^{-K_{AB}T_{Pu}} G_{Bg}(\omega_{T_{Pr}})$

F-2DES$\sim |\mu_A|^2|\mu_B|^2 G_{Bg}(\omega_{T_{Pr}}) e^{-K_{AB}T_{Pu}} G_{Ag}(\omega_\tau)$

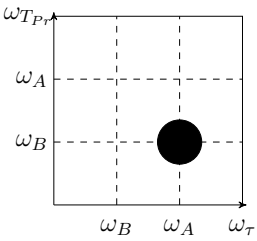

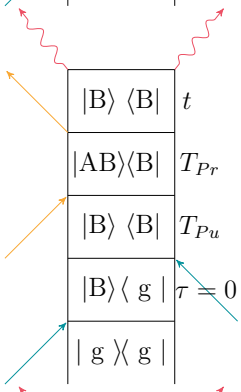

1 photon

sign: —

F-PP$\sim |\mu_A|^2|\mu_B|^2 G_{Ag}(\omega_{T_{Pr}})$

F-2DES$\sim |\mu_A|^2|\mu_B|^2 G_{Ag}(\omega_{T_{Pr}}) G_{Bg}(\omega_\tau)$

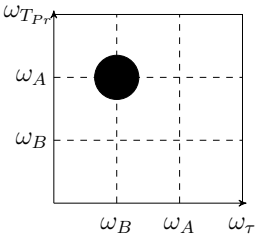

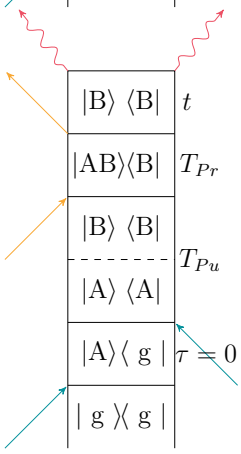

1 photon

sign: —

F-PP$\sim |\mu_A|^4 \left(1 - e^{-K_{AB}T_{Pu}}\right) G_{Ag}(\omega_{T_{Pr}})$

F-2DES$\sim |\mu_A|^4 G_{Ag}(\omega_{T_{Pr}}) \left(1 - e^{-K_{AB}T_{Pu}}\right) G_{Ag}(\omega_\tau)$

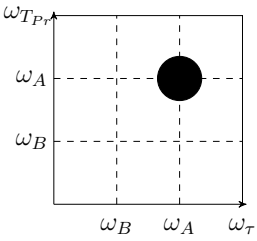

Figure A.3: Excited state absorption Liouville pathways for heterodimer (left column), corresponding FPP and F-2DES spectra equations (middle), F-2DES spectra visualization (right column).

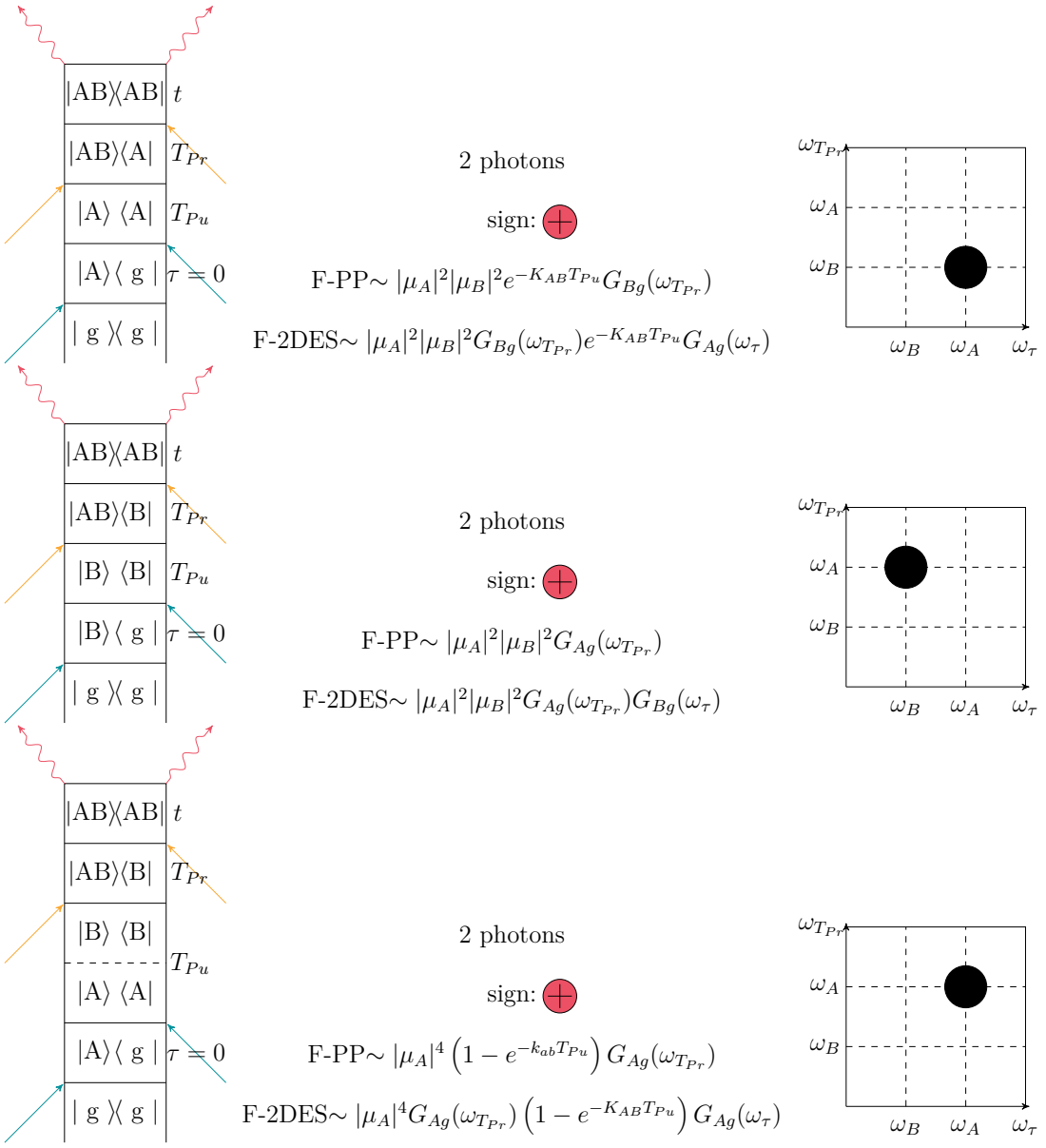

Figure A.4: Excited state absorption 2 Liouville pathways for heterodimer (left column), corresponding FPP and F-2DES spectra equations (middle), F-2DES spectra visualization (right column).

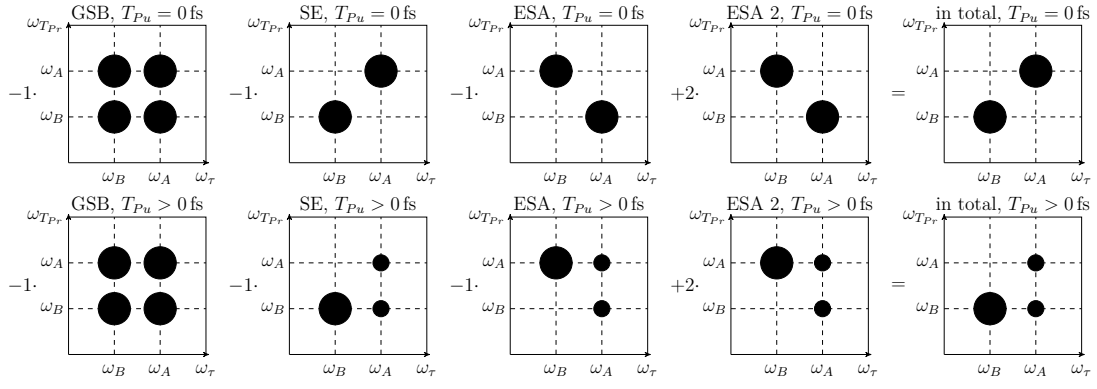

Figure A.5: F-2DES signal from all pathways for $T_{Pu} \geq 0$ fs, without EEA.

A.3 Feynman diagrams for heterodimer AB for negative times

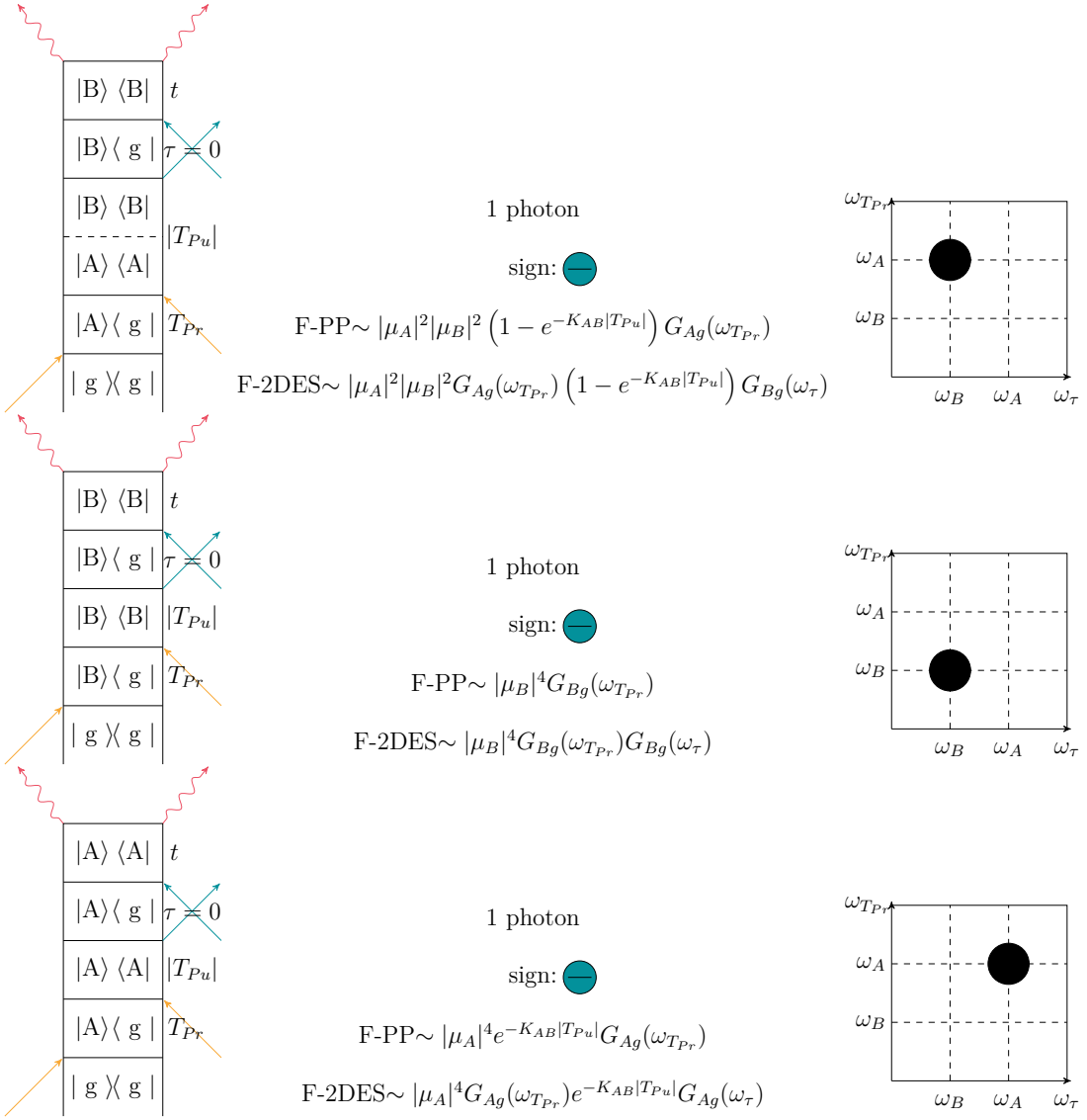

Figure A.6: Stimulated emission Liouville pathways for heterodimer (left column), corresponding FPP and F-2DES spectra equations (middle), F-2DES spectra visualization (right column) for negative time delay between pump and probe.

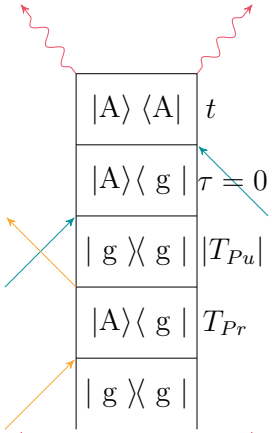

1 photon

sign: —

F-PP$\sim |\mu_A|^4 G_{Ag}(\omega_{T_{Pr}})$

F-2DES$\sim |\mu_A|^4 G_{Ag}(\omega_{T_{Pr}}) G_{Ag}(\omega_\tau)$

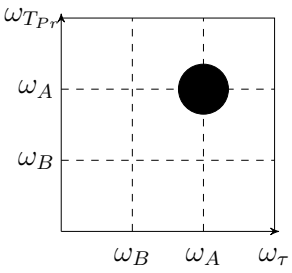

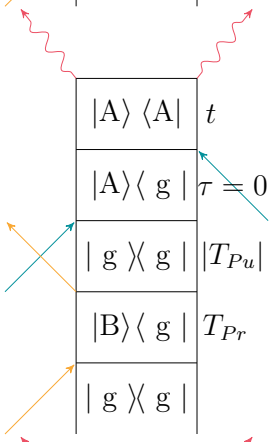

1 photon

sign: —

F-PP$\sim |\mu_A|^2 |\mu_B|^2 G_{Bg}(\omega_{T_{Pr}})$

F-2DES$\sim |\mu_A|^2 |\mu_B|^2 G_{Bg}(\omega_{T_{Pr}}) G_{Ag}(\omega_\tau)$

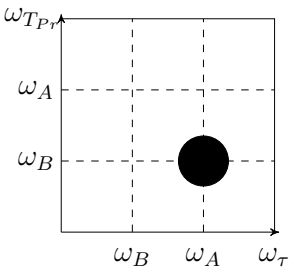

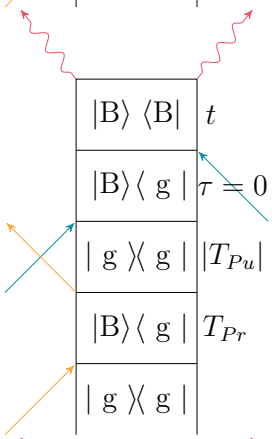

1 photon

sign: —

F-PP$\sim |\mu_B|^4 G_{Bg}(\omega_{T_{Pr}})$

F-2DES$\sim |\mu_B|^4 G_{Bg}(\omega_{T_{Pr}}) G_{Bg}(\omega_\tau)$

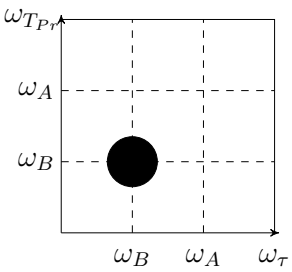

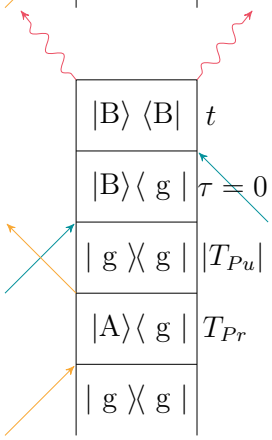

1 photon

sign: —

F-PP$\sim |\mu_A|^2 |\mu_B|^2 G_{Ag}(\omega_{T_{Pr}})$

F-2DES$\sim |\mu_A|^2 |\mu_B|^2 G_{Ag}(\omega_{T_{Pr}}) G_{Bg}(\omega_\tau)$

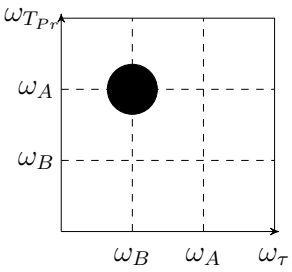

Figure A.7: Ground state bleach Liouville pathways for heterodimer (left column), corresponding FPP and F-2DES spectra equations (middle), F-2DES spectra visualization (right column) for negative time delay between pump and probe.

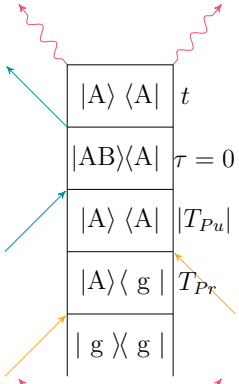

1 photon

sign: —

F-PP$\sim |\mu_A|^2|\mu_B|^2 e^{-K_{AB}|T_{Pu}|} G_{Ag}(\omega_{T_{Pr}})$

F-2DES$\sim |\mu_A|^2|\mu_B|^2 G_{Ag}(\omega_{T_{Pr}}) e^{-K_{AB}|T_{Pu}|} G_{Bg}(\omega_\tau)$

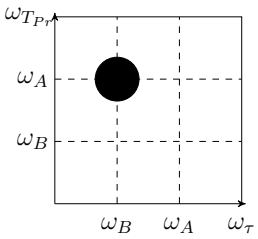

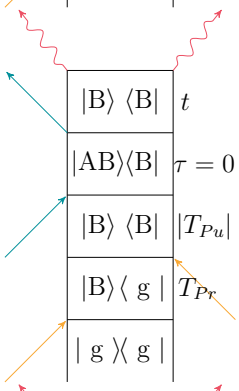

1 photon

sign: —

F-PP$\sim |\mu_A|^2|\mu_B|^2 G_{Bg}(\omega_{T_{Pr}})$

F-2DES$\sim |\mu_A|^2|\mu_B|^2 G_{Bg}(\omega_{T_{Pr}}) G_{Ag}(\omega_\tau)$

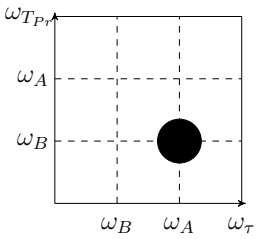

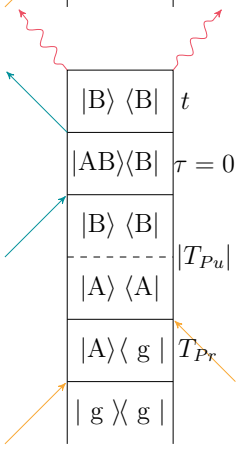

1 photon

sign: —

F-PP$\sim |\mu_A|^4 \left(1 - e^{-K_{AB}|T_{Pu}|}\right) G_{Ag}(\omega_{T_{Pr}})$

F-2DES$\sim |\mu_A|^4 G_{Ag}(\omega_{T_{Pr}}) \left(1 - e^{-K_{AB}|T_{Pu}|}\right) G_{Ag}(\omega_\tau)$

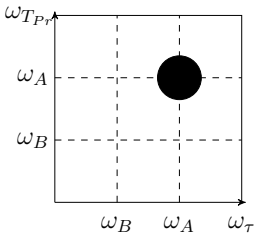

Figure A.8: Excited state absorption Liouville pathways for heterodimer (left column), corresponding FPP and F-2DES spectra equations (middle), F-2DES spectra visualization (right column) for negative time delay between pump and probe.

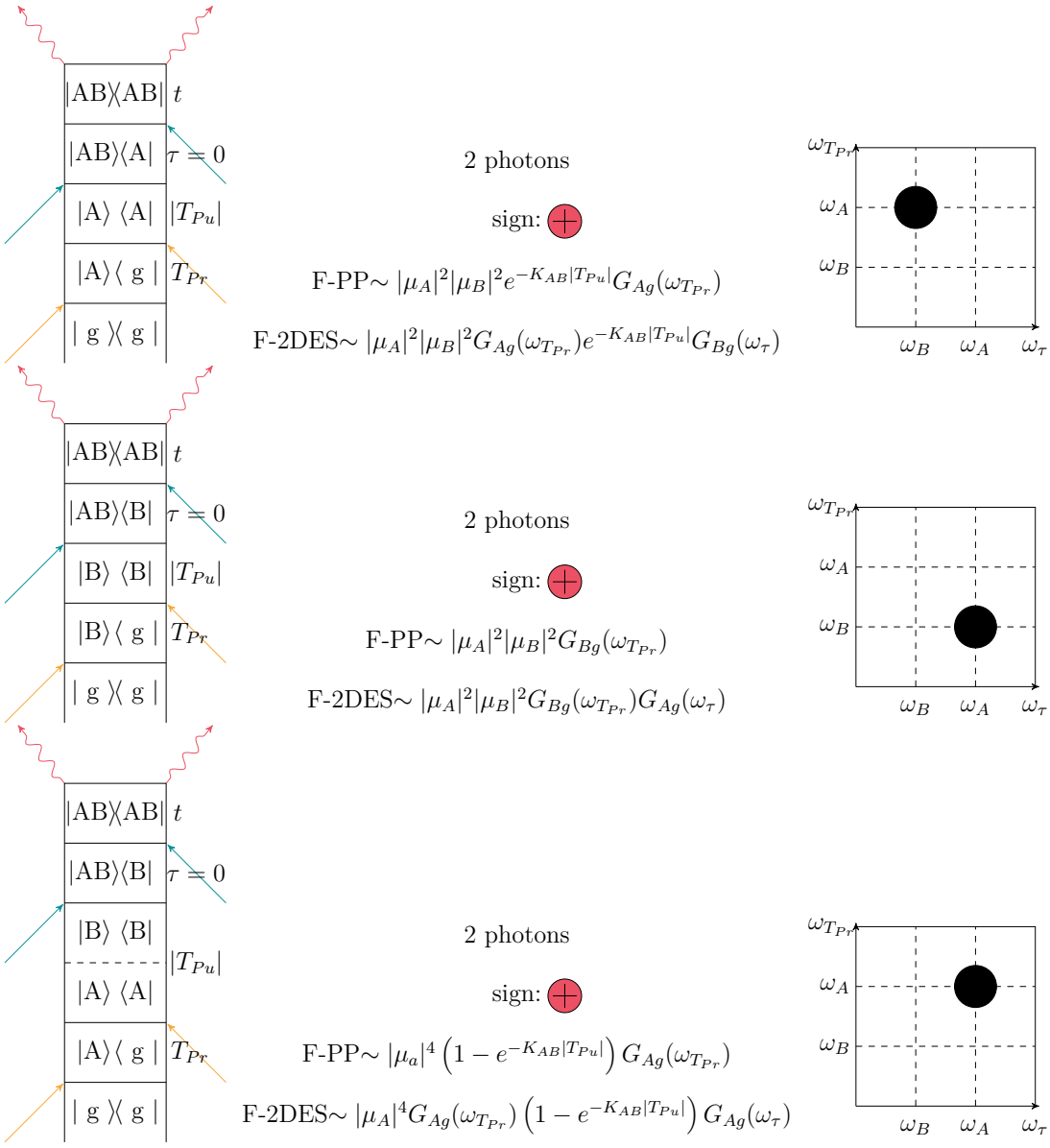

Figure A.9: Excited state absorption 2 Liouville pathways for heterodimer (left column), corresponding FPP and F-2DES spectra equations (middle), F-2DES spectra visualization (right column) for negative time $T_{Pu} < 0$.

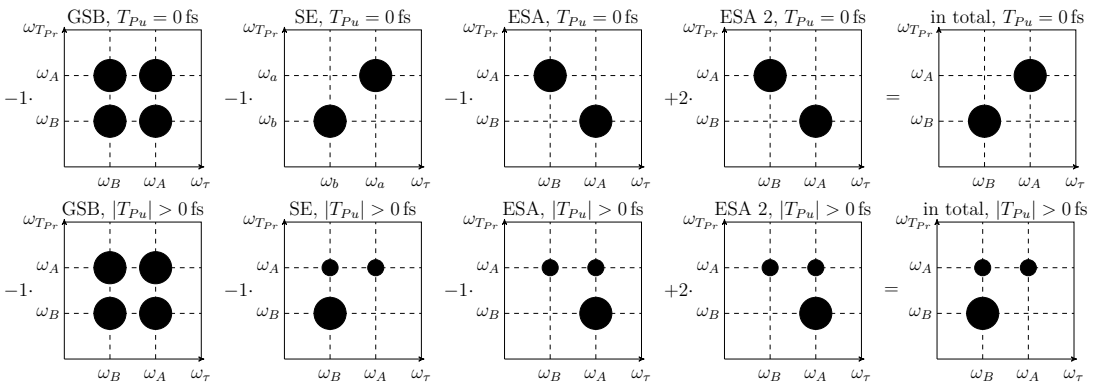

Figure A.10: F-2DES signal from all pathways for $T_{Pu} \leq 0$ fs, without EEA.

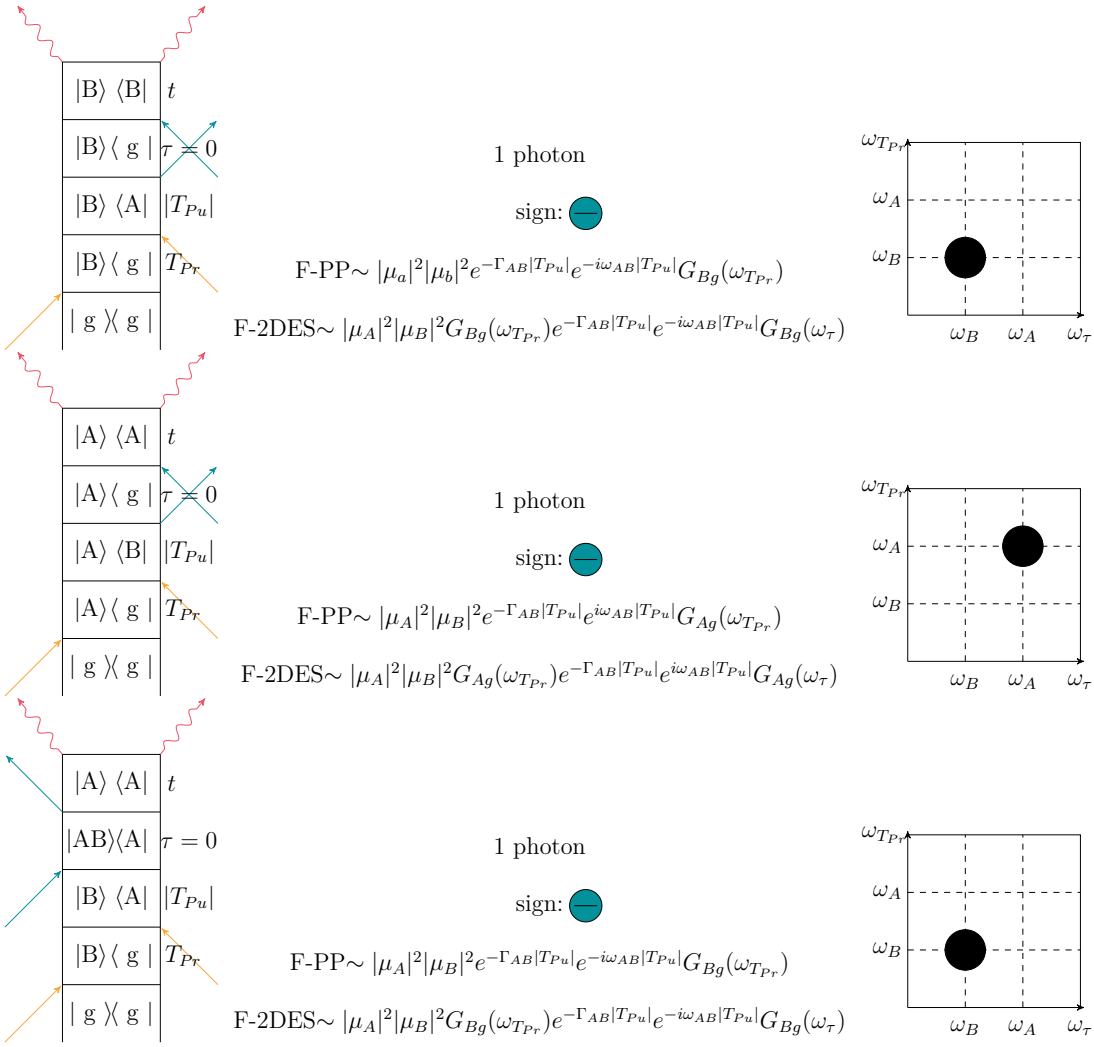

Figure A.11: Oscillation Liouville pathways for heterodimer (left column), corresponding FPP and F-2DES spectra equations (middle), F-2DES spectra visualization (right column) for negative time delay between pump and probe.

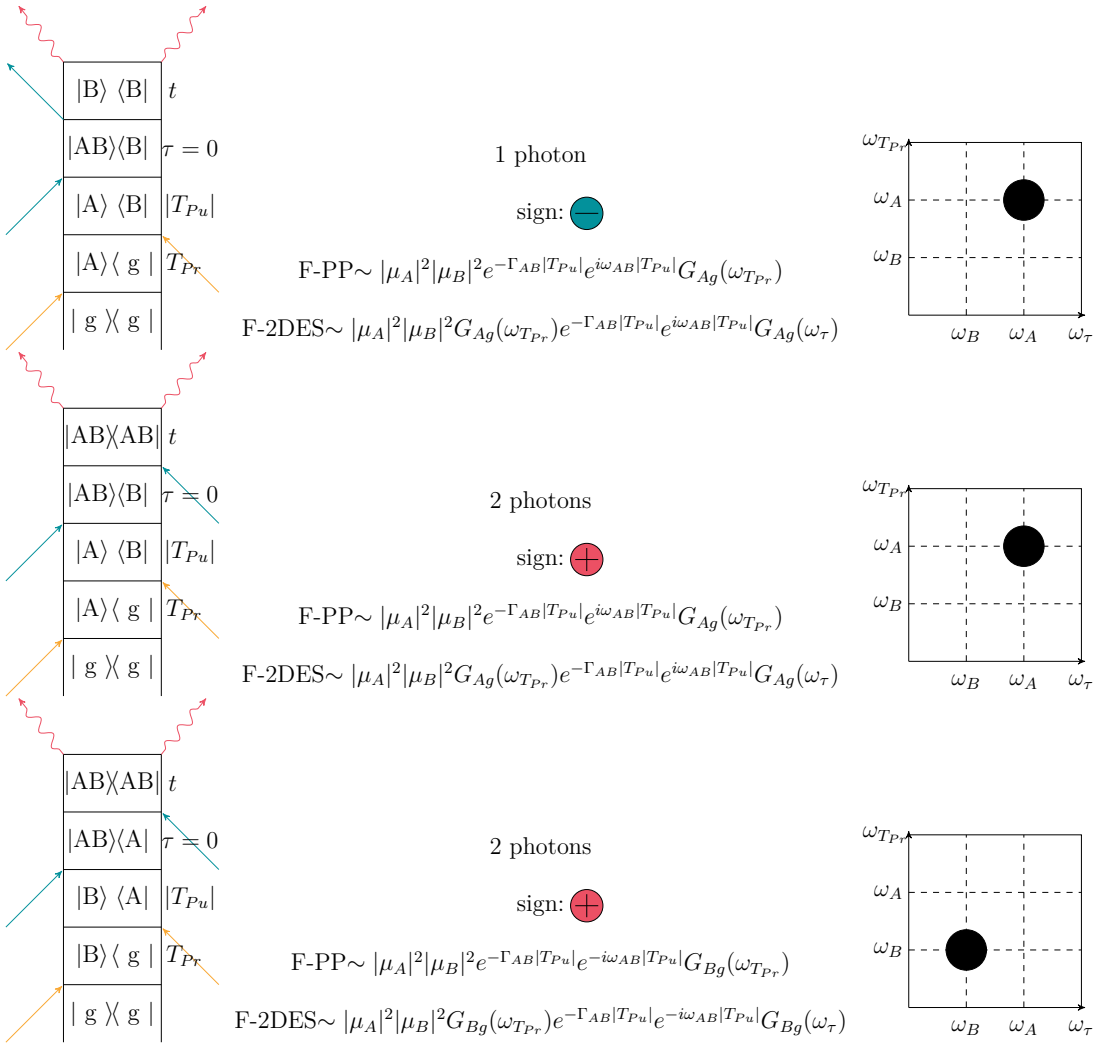

Figure A.12: Oscillation Liouville pathways for heterodimer (left column), corresponding FPP and F-2DES spectra equations (middle), F-2DES spectra visualization (right column) for negative time delay between pump and probe.

A.4 Comparison of F-2DES spectra for positive and negative times

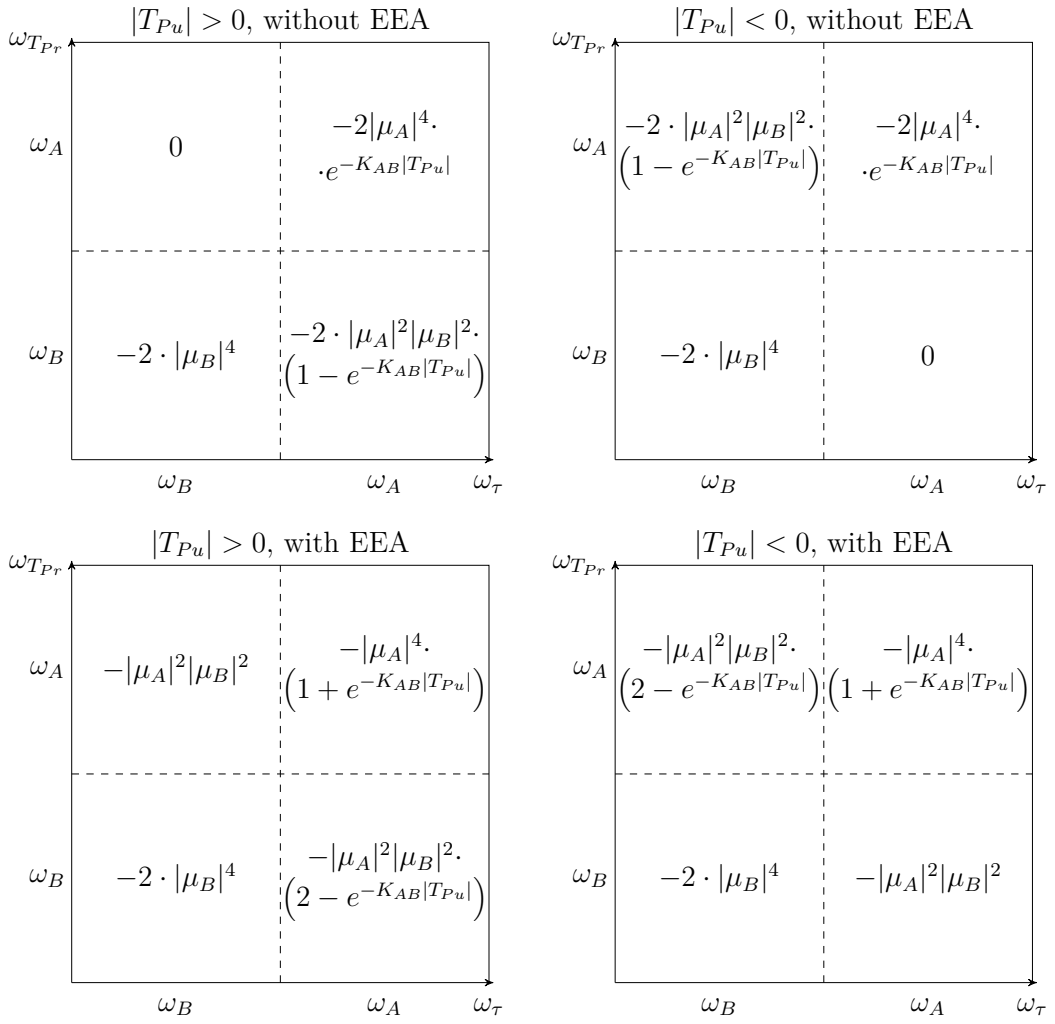

Figure A.13: 2-DES signal for time $T_{Pu} < 0\,\text{fs}$ and $T_{Pu} > 0\,\text{fs}$, with and without exciton-exciton annihilation (EEA).

A.5 Traces of F-PP spectra for selective excitation with narrower pump spectrum

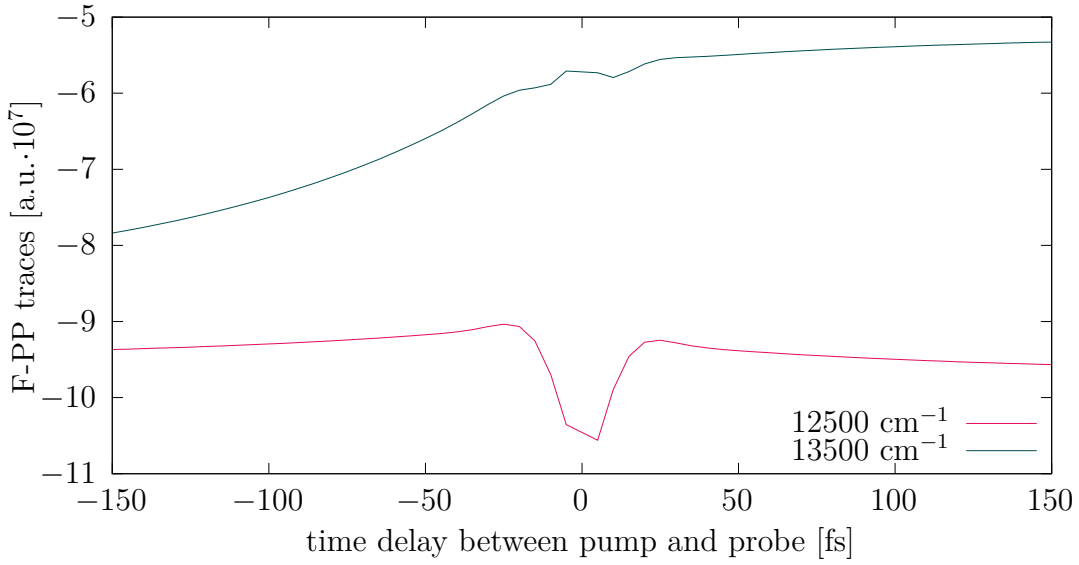

Figure A.14: F-PP traces for frequencies ϵ_A and ϵ_B, pump frequency 12500 cm^{-1}, $FWHM = 30\,\mathrm{fs}$. The signal from A is increasing in negative times, and the signal from B is constant in positive and negative times, as is a signal from A in positive times. Oscillations are suppressed.

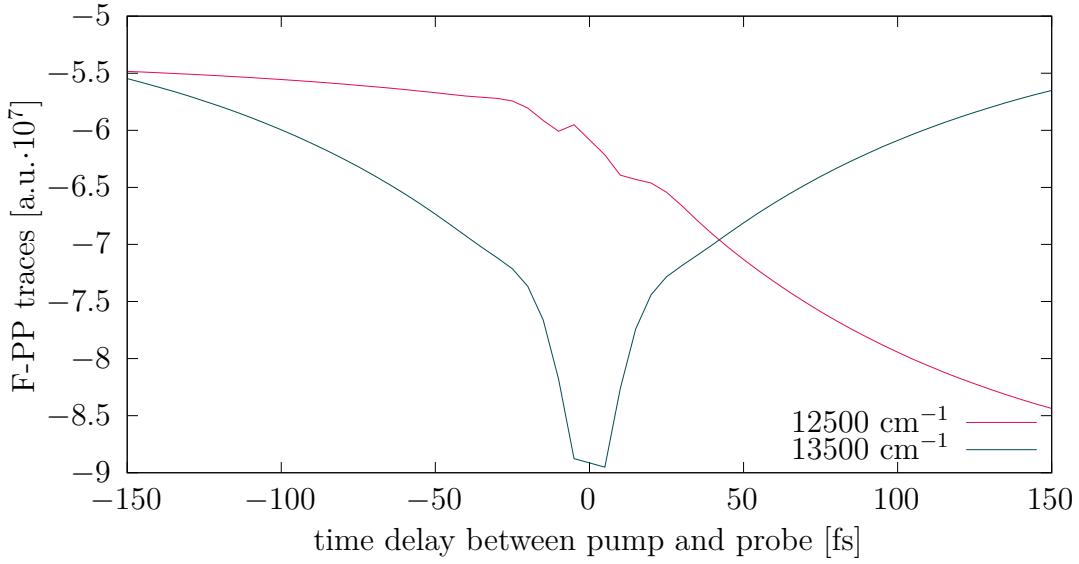

Figure A.15: F-PP traces for frequencies ϵ_A and ϵ_B, pump frequency 13500 cm^{-1}, $FWHM = 30\,\mathrm{fs}$. In positive times, we can see a decrease in signal from A and an increase in signal from B, corresponding to the energy transfer from A to B. In negative times, the signal from molecule B is constant, and the signal from molecule A is decreasing. Oscillations are suppressed.

A.6 Traces of F-PP spectra for heterodimer AB with negligible exciton-exciton annihilation

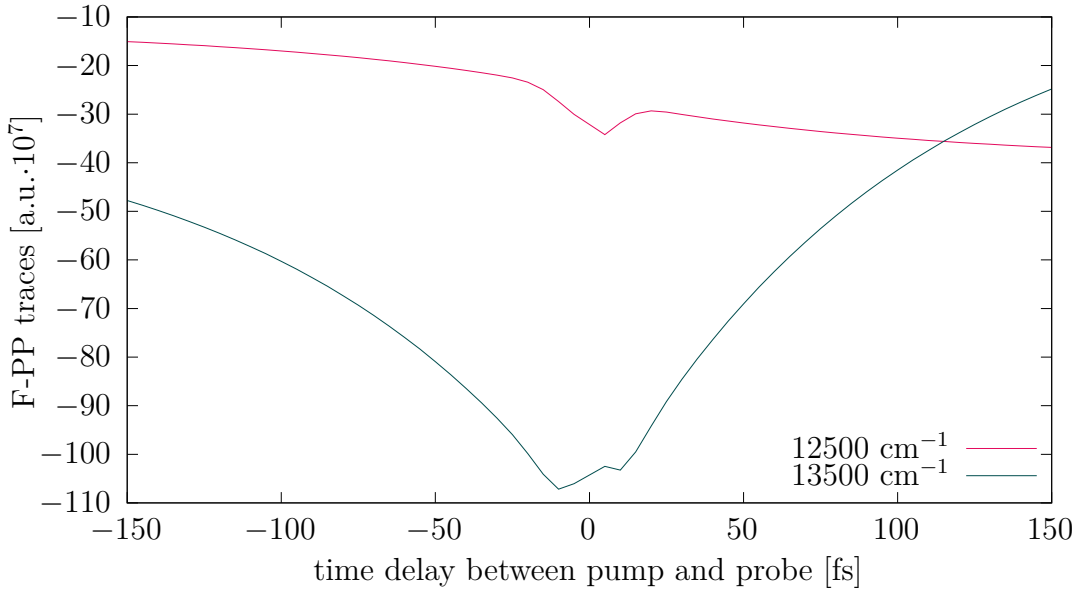

Figure A.16: F-PP traces for frequencies ϵ_A and ϵ_B, $\mu_A = 2\mu_B$, negligible EEA. We can see time dependence for the signal from molecule A in negative times, because $\mu_A > \mu_B$, signal from molecule A is (in absolute value) decreasing. Signal from molecule B is constant.

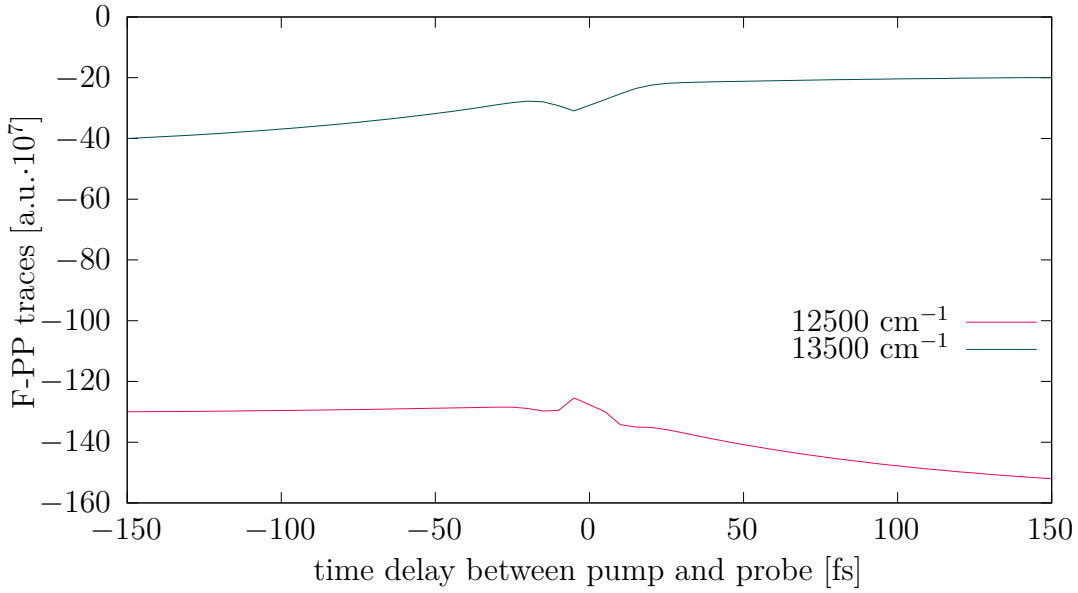

Figure A.17: F-PP traces for frequencies ϵ_A and ϵ_B, $\mu_B = 2\mu_A$, negligible EEA. Signal from molecule A, although weak, is in negative times increasing with $|T_{Pu}|$. Signal from molecule B is constant in negative times.

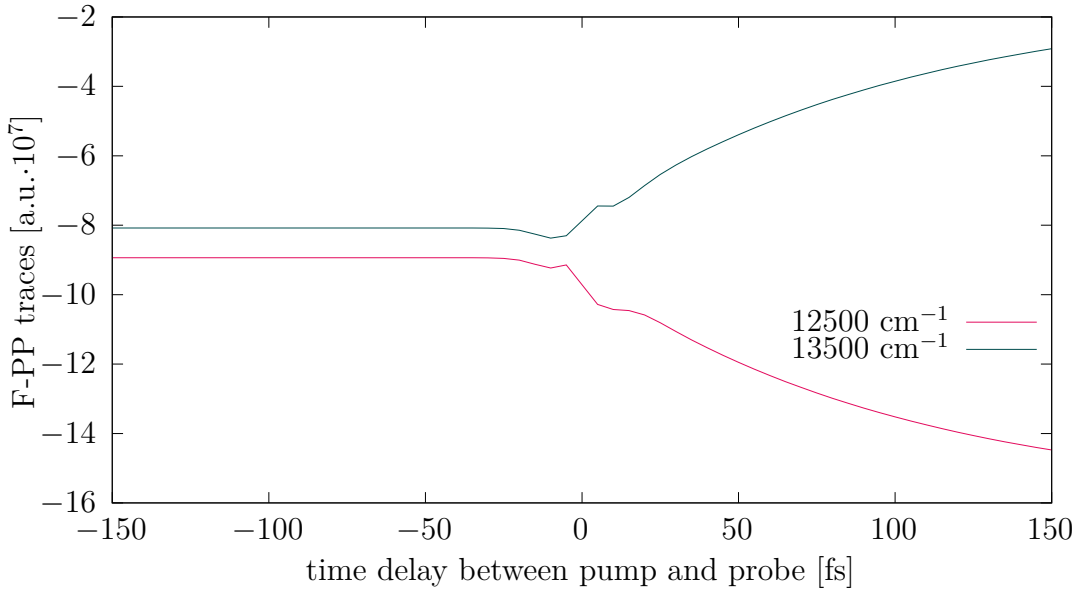

Figure A.18: F-PP traces for frequencies ϵ_A and ϵ_B, two molecules (one molecule A and one molecule B, $\mu_A = \mu_B$), negligible EEA. The signal from molecule A is decreasing in time, and the signal from molecule B is increasing. Signal in negative times is constant both for A and B.

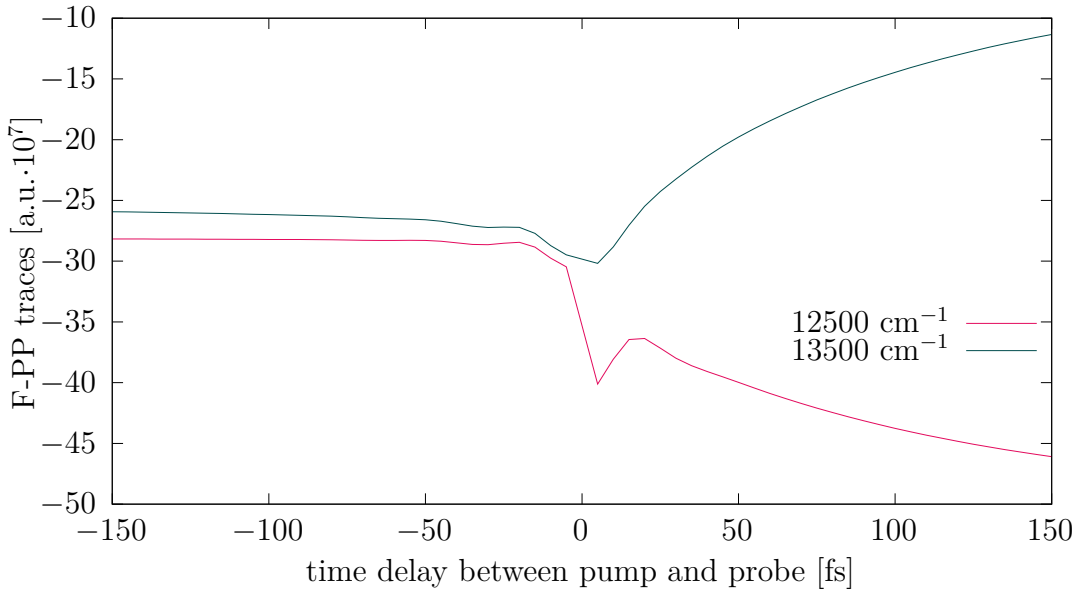

Figure A.19: F-PP traces for frequencies ϵ_A and ϵ_B for six molecules (three molecules A and three molecules B, $\mu_A = \mu_B$). Because EEA is negligible, the dynamics is as visible as for two molecules. However, the signal is three times stronger because there are six molecules instead of two.

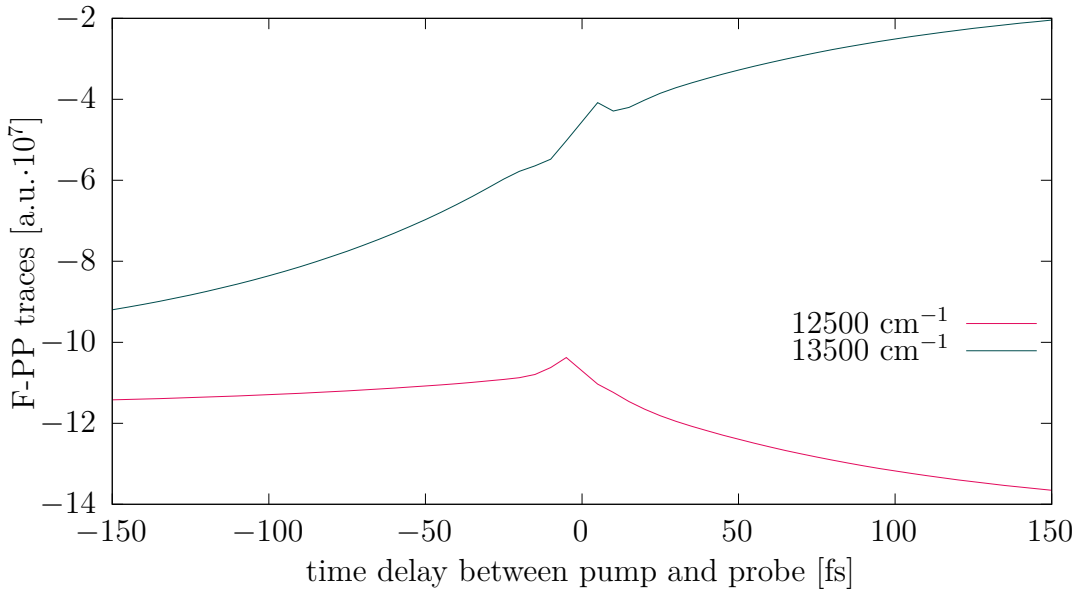

Figure A.20: F-PP traces for frequencies ϵ_A and ϵ_B, pump frequency 12500 cm^{-1} (selective excitation of molecule B), negligible EEA. For positive times, the signal from molecule A is decreasing and signal from B is increasing. Even for $\mu_A = \mu_B$, molecule A's signal is not constant in negative times, it is increasing with $|T_{Pu}|$.

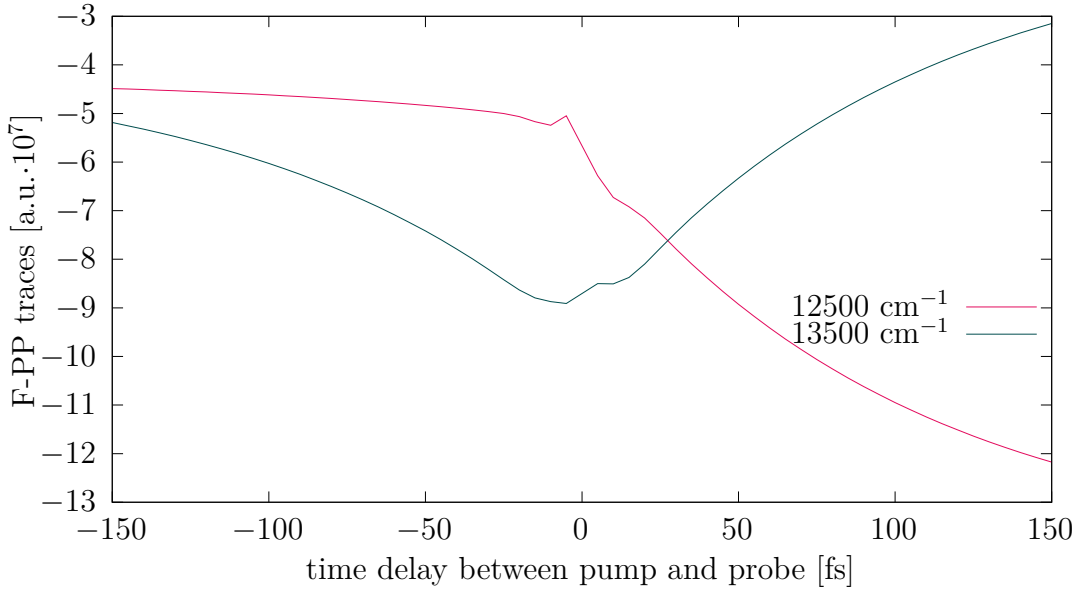

Figure A.21: F-PP traces for frequencies ϵ_A and ϵ_B, pump frequency 13500 cm^{-1} (selective excitation of molecule A), negligible EEA. For positive times, the signal from molecule A is decreasing and signal from B is increasing. Even for $\mu_A = \mu_B$, signal from molecule A is not constant in negative times, it is decreasing with increasing $|T_{Pu}|$, signal from B is again constant.

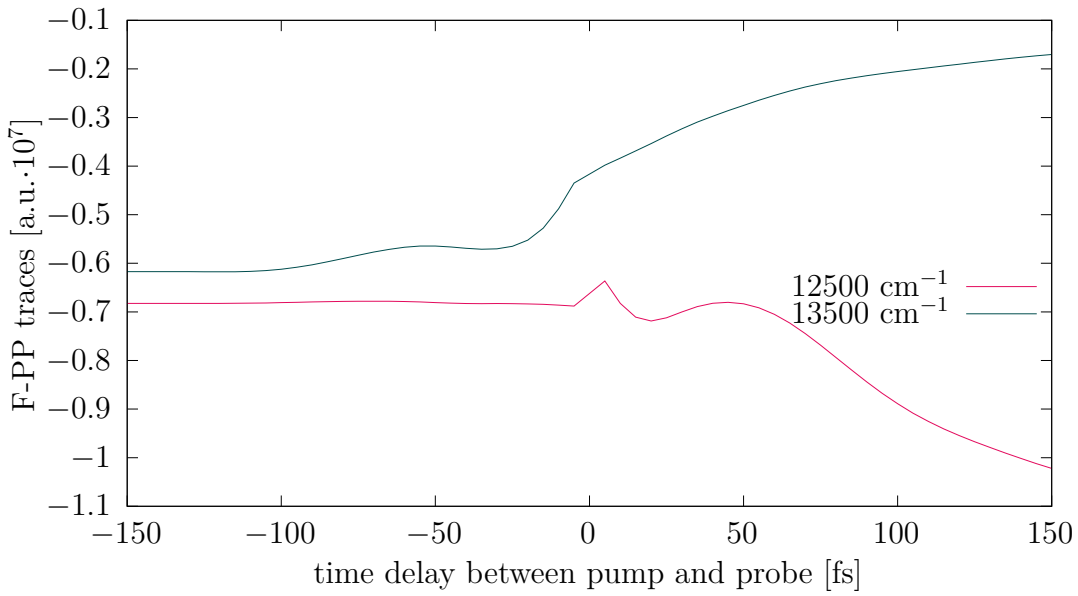

Figure A.22: F-PP traces for frequencies ϵ_A and ϵ_B for chirped probe, negligible EEA. The signal from molecule A is shifted to negative times; on the contrary, the signal from B is shifted to the right to positive times. A peak around zero for a particular frequency is broadened. Except for the behaviour around time zero, the dynamics is similar to the situation without chirp - in positive times, the signal from A decreases, and the signal from molecule B increases. In negative times, the signal remains constant.

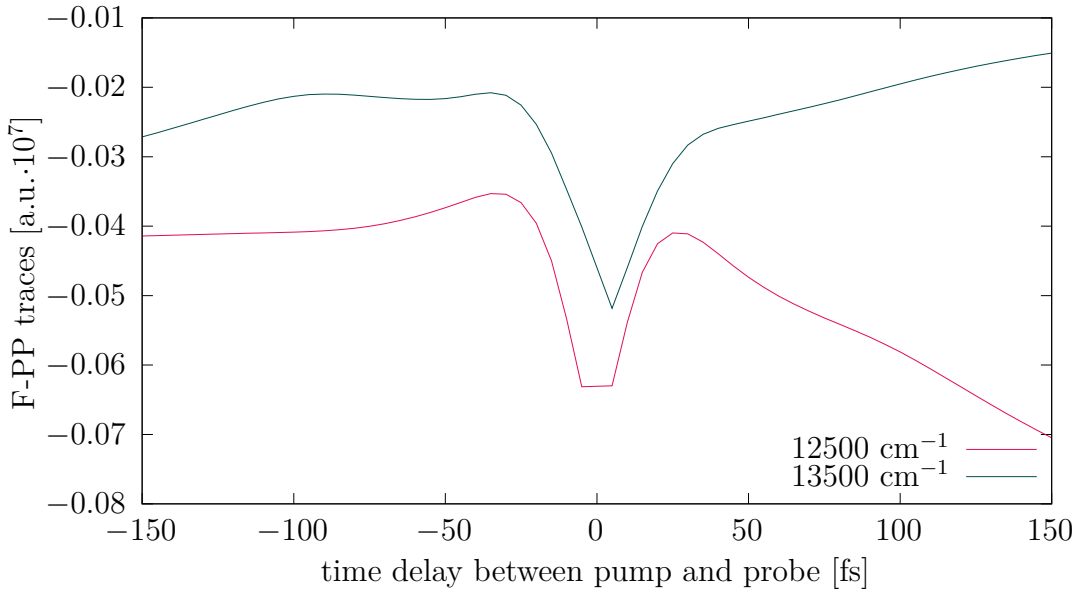

Figure A.23: F-PP traces for frequencies ϵ_A and ϵ_B, chirped probe and chirped pump, negligible EEA. There is no shift of time zero for any of the traces.

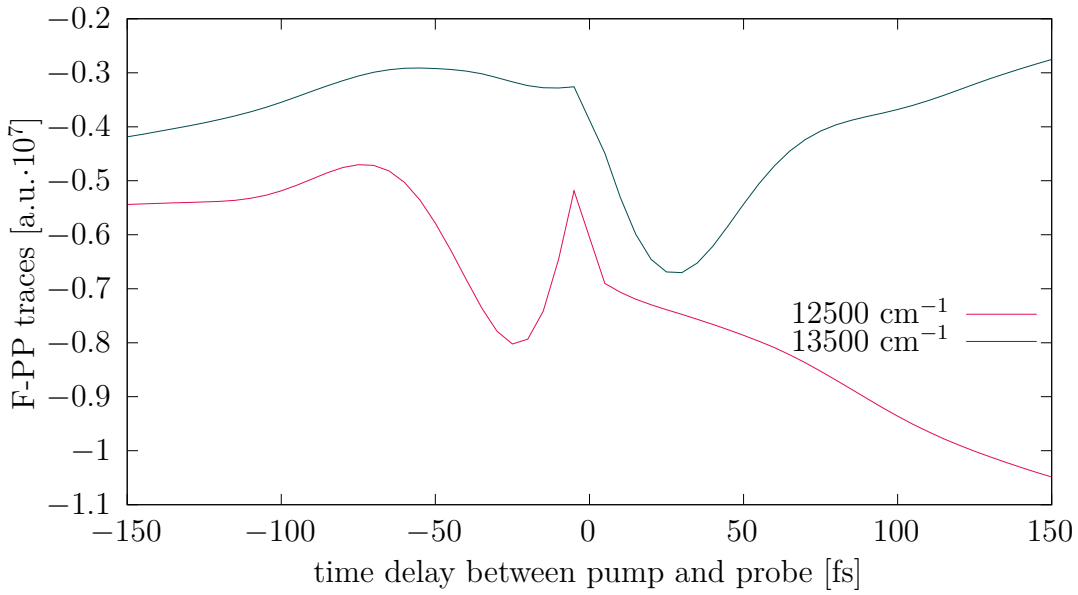

Figure A.24: F-PP traces for frequencies ϵ_A and ϵ_B, chirped pump, negligible EEA. The signal from molecule A is shifted right and the signal from B to the left (opposite to the situation with chirped probe in graph A.22). A peak around zero for a particular frequency is broadened. Except for the behaviour around time zero, the dynamics is similar to the situation without chirp - in positive times, the signal from A decreases, and the signal from molecule B increases. In negative times, the signal remains constant.

A.7 Traces for F-PP spectra with chirped pulse in longer times

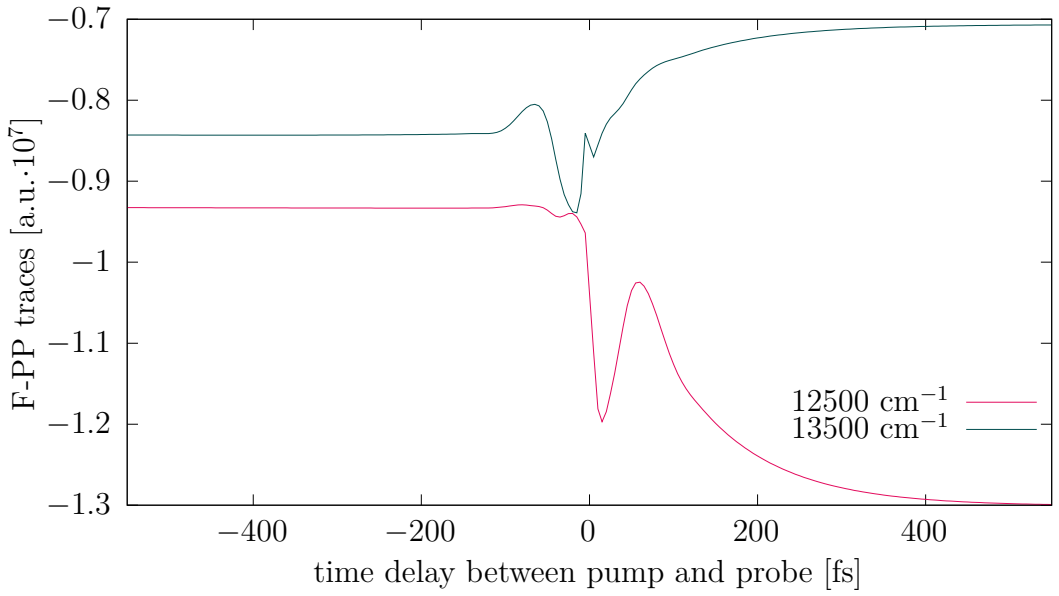

Figure A.25: F-PP traces for frequencies ϵ_A and ϵ_B, chirped probe, with EEA. The signal from molecule A is shifted to the left and the signal from B to the right. Except for the behaviour around time zero, the dynamics is similar to the situation without chirp - in positive times, the signal from A decreases, and the signal from molecule B increases. In negative times, the signal remains constant.